

Department of Mechanical Engineering

**PASSIVE CONTROL OF INSTABILITY OF
FLEXIBLE PANELS IN A MEAN FLOW**

Ben Hoes Tan

**This thesis is presented for the degree of
Master of Philosophy
of
Curtin University**

December 2017

DECLARATION OF ORIGINALITY

To the best of my knowledge and belief this thesis contains no material previously published by any other person except where due acknowledgement has been made. This thesis contains no material which has been accepted for the award of any other degree or diploma in any university. All investigations presented in this thesis are my own work except where specific reference has been made to the work of others. Some of the work presented in this thesis has been published in the following refereed publications:

Conference Articles (Research)

Tan, B.H., Lucey, A.D. and Pitman, M.W. 2010. Hydroelastic stability of flexible panel: eigen-analysis and time- domain response. In: *Proceedings of ASME 2010 3rd Joint US - European Fluids Engineering Summer Meeting*, 1-5 August 2010, Montreal, Canada, Paper no. FEDSM-ICNMM2010-30057.

Tan, B.H., Lucey, A.D. and Pitman, M.W. 2010. Hydroelastic stability of an inhomogeneous flexible panel in a uniform mean flow. In: *Engineers Australia - 6th Australasian Congress on Applied Mechanics, ACAM 6*, 12-15 December 2010, Perth, Australia, Paper no. 1130.

Tan, B.H., Lucey, A.D. and Pitman, M.W. 2011. Controlling hydroelastic instability of hull panels through structural inhomogeneity. In: *RINA, Royal Institution of Naval Architects - International Conference, High Speed Marine Vessels*, 2-3 March 2011, Fremantle, pp. 51-60.

Tan, B.H., Lucey, A.D. and Pitman, M.W. 2011. Controlling aero-elastic instability of curtain wall systems in high-rise buildings. In: *MODSIM2011, 19th International Congress on Modelling and Simulation*. Modelling and Simulation Society of Australia and New Zealand, December 2011, (Eds. F. Chan, D. Marinova & R.S. Andersen), pp. 601-607.

Tan, B.H., Lucey, A.D. and Pitman, M.W. 2012. Stability of a structurally inhomogeneous

geneous flexible plate in uniform axial flow. In: *Proceedings of the 10th International Conference on Flow Induced Vibration & Flow-Induced Noise*, 3-6 July 2012, Dublin, Ireland (Eds. C. Meskell & G. Bennett), pp. 203-210.

Tan, B.H., Lucey, A.D. and Howell, R.M. 2013. The effect of localised stiffening on the stability of a flexible panel in uniform flow. In: *2nd Symposium on Fluid-Structure-Sound Interactions and Control*, 20-23 May 2013, Hong Kong & Macau, pp. 86-87.

Tan, B.H., Lucey, A.D. and Howell, R.M. 2015. Application of a multi-objective genetic algorithm in a stabilisation strategy for flexible panels in a mean flow. In: *3rd Symposium on Fluid-Structure-Sound Interactions and Control*, 5-9 July 2015, Perth, Australia, pp. 195-196.

Journal Article (Research)

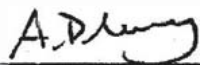
Tan, B.H., Lucey, A.D. and Howell, R.M. 2013. Aero-/hydro-elastic stability of flexible panels: Prediction and control using localised spring support. *Journal of Sound and Vibration*, Vol.332(26), pp.7033-7054.

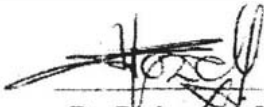
Signature: Tan Ben Hoe

Date: 10th Jan 2018

DECLARATION OF CONTRIBUTION OF OTHERS

We, the undersigned, attest that Research Higher Degree candidate, Ben Hoes Tan, has carried out the development of the methods, programmings, result analysis and writing of all papers included in this thesis.

Signature:  Date: 8th January 2018
Professor Anthony D. Lucey

Signature:  Date: 8/1/18
Dr. Richard M. Howell

DECLARATION OF AUTHORSHIP

I hereby certify that the work embodied in this thesis contains published papers of which I am a joint author. I have included as part of the thesis a written statement, endorsed by my supervisor, attesting to my significant contribution to the joint publications.

Signature:

Tan Bent Hoca

Date:

10th Jan 2018

ACKNOWLEDGEMENTS

I wish to express my gratitude to the people that I have to thank:

My supervisor, Prof A.D. Lucey

My associate supervisor, Dr Ramesh Narayanaswamy

Thesis Committee Chairperson, Prof Tilak Chandratilleke

My co-supervisor, Dr M.W. Pitman

Dr Andrew King and Dr Richard Howell for assisting me at thesis template preparation.

Kim Yap, Sucey Leong, Margaret Brown and the staff at the office of the department of mechanical engineering.

Dr. Tele Tan for providing me lab teaching job.

Naomi Mockford and Mary Thompson at the office of Engineering Foundation Years.

The authors acknowledge the support of the Australian Research Council through grant.

ABSTRACT

This thesis is motivated by the goal of controlling flow-induced unstable vibrations of flexible panels. The applications considered range from the hydro-elasticity of hull panels of high-speed ships to the aero-elasticity of glass panels in the curtain walls of high-rise buildings in very strong winds. The strategy investigated entails adding localised stiffness to panels in such a way that instabilities are postponed to higher flow speeds or modified to make them less destructive.

Firstly we study the effect of adding localised stiffness, via a spring support, on the stability of flexible panels subjected to axial uniform incompressible flow. A two-dimensional linear analysis is conducted using a hybrid of theoretical and computational methods that calculates the system eigen-states but can also be used to capture the transient behaviour that leads to the final state. We show that localised stiffening is a very effective means to increase the divergence-onset flow speed in both hydro- and aero-elastic applications. It is most effective when localised stiffness is located at the mid-chord of the panel and there exists an optimum value of added stiffness beyond that further increases to the divergence-onset flow speed which does not occur. For aero-elastic applications, localised stiffening can be used to replace the more dangerous flutter instability that follows divergence at higher flow speeds by an extended range of divergence. The difference in eigen-solution morphology between aero- and hydro-elastic applications is highlighted, showing that for the former coalescence of two non-oscillatory divergence modes is the mechanism for flutter onset. This variation in solution morphology is mapped out in terms of a non-dimensional mass ratio.

Secondly, we present the applicability of the stabilisation strategy in the full three-dimensional system. The three dimensional stability of a fluid-loaded flexible panel is studied to determine the effectiveness of adding localized stiffening strip to control or postpone instability.

Finally we extend the study of controlling instability to optimization of localised stiffness. Genetic algorithm is chosen to optimise the distribution of localised stiffness.

Table of Contents

ACKNOWLEDGEMENTS	v
ABSTRACT	vi
Table of Contents	vi
List of Figures	ix
1 Introduction	1
1.1 Research Background	2
1.2 Overview of Research	3
1.2.1 Research Problem	4
1.2.2 Methodology	4
1.2.3 Scope and Assumptions	4
1.2.4 Summary of Contributions	5
1.3 Thesis Structure	5
2 Control of Instability of 2-D Flexible Panel in a Mean Flow	8
3 Control Instability of 3-D Flexible Panel in a Mean Flow	31
NOMENCLATURE	31
3.1 Introduction	32
3.2 Plate mechanics	32
3.3 Flow dynamics	33
3.4 Coupled fluid-structure system	36
3.5 Modelling of transverse stiffening strip	38
3.6 Long-time responses of homogeneous and inhomogeneous system . .	38
3.6.1 2-D Homogenous system: high mass ratio and low mass ratio	39
3.6.2 3-D Homogenous system: high mass ratio and low mass ratio	40

3.6.3	2-D Inhomogeneous system: local stiffening by spring and high/low mass ratio	40
3.6.4	3-D Inhomogeneous system: local stiffening by transverse strip and high/low mass ratio	42
3.7	The effect of transverse and streamwise stiffening strips on a 3-D flexible panel	43
3.7.1	Equations for transverse and streamwise stiffening strips	43
3.7.2	Results of the effectiveness of streamwise and transverse stiffening strips	44
3.8	Conclusions	46
4	Optimization by a Multi-objective Genetic Algorithm	59
5	Conclusions and recommendations for further work	65
5.1	Conclusions	65
5.2	Recommendations for further work	65
	References	66
	Appendix	71
A	Statements of Contributions of Others	71

List of Figures

Note that figures and tables in reproduced published papers have their own self-contained numbering system and are therefore not listed here

1.1	(a) Schematics of a two-dimensional (side view) finite panel problem. (b) Schematics of a three-dimensional (isometric view) finite panel problem.	7
3.1	Schematics of the (a) two-dimensional (side view) and (b) three-dimensional (isometric view) problems.	48
3.2	Two-dimensional analysis: variation of system eigenvalues with non-dimensional flow speed for — high mass ratio = 38.5 (water over aluminum) and —o— low mass ratio = 0.049 (air over aluminum): (a) real part (growth/decay) and (b) imaginary part (oscillation frequency) of eigenvalues.	49
3.3	Three-dimensional analysis: variation of system eigenvalues with non-dimensional flow speed for a panel with aspect ratio unity. legend and sub-figure title as in fig. 2.	50
3.4	Two-dimensional analysis: the effect of an added support spring on divergence-onset, divergence-recovery / mode-2 divergence-onset, and modal-coalescence flutter-onset flow speeds for (a) high mass ratio = 92.3 (water over aluminum), and (b) low mass ratio = 0.226 (air over glass).	51
3.5	Three-dimensional analysis: the effect of a transverse stiffening strip at the panel mid-line on divergence-onset, divergence-recovery /mode-2 divergence-onset, and modal-coalescence flutter-onset flow speeds on a panel of aspect ratio unity for (a) high mass ratio = 38.5 (water over aluminum), and (b) low mass ratio = 0.049 (air over aluminum).	52

3.6	Neutrally-stable flexible-panel modes for high mass ratio (38.5) with a stiffening strip ($EI/B = 2$) across its midline at a pre-divergence non-dimensional flow speed, 380: (a) mode 1, (b) mode 2, and (c & d) centreline profiles of modes 1 and 2 over one cycle of oscillation respectively.	53
3.7	Flexible-panel divergence mode for high mass ratio (38.5) with a stiffening strip ($EI/B = 2$) across its midline at non-dimensional flow speed 450: (a) isometric view, and (b) centreline profiles over a sequence of time-steps from green to red lines.	54
3.8	Flexible-panel modal-coalescence flutter mode for high mass ratio (38.5) with a stiffening strip ($EI/B = 2$) across its mid-line at non-dimensional flow speed 600: (a) isometric view, and (b) centreline profiles over a sequence of time-steps from green to red lines.	55
3.9	Schematic of the problem studied: a fluid-loaded elastic plate has a localised stiffening strip, in either transverse or streamwise direction, bonded to the underside of the panel.	56
3.10	Variation of system eigenvalues with non-dimensional flow speed for — (thick) a homogenous panel, and a panel with each of $- \circ -$ transverse and $- \times -$ streamwise stiffening strips included, for (a) high, and (b) low mass ratios, respectively representing water and air flow applications.	57
3.11	Variation of critical speeds with stiffness of (a) and (c) transverse and (b) and (d) streamwise stiffening strips: (a) and (b) for a high mass-ratio system typical of water flow applications and (c) and (d) for a low mass-ratio system typical of air flow applications.	58

Chapter 1

Introduction

Fluid-structure interaction (FSI) phenomena can be observed in everyday life. There are many examples of FSI phenomena such as ancient sailing ships, modern aircraft, curtain walls and windows of high-rise buildings, high speed ships and the blood vessels in the human body. Flexible sails were used to allow the wind to provide the driving force for ancient sailing ships to travel for the purpose of trading amongst the ancient civilizations. The body of modern aircraft are made of thin aluminium alloy panels that can experience dangerous structural flutter problems at a certain critical speed and this phenomena has had a major effect on aircraft development during the last century. Similarly, curtain walls and windows of high-rise buildings, which are susceptible to strong wind on their higher level floors, can encounter the same dangerous structural flutter at a critical very strong wind speed. Modern high speed ships are made of lighter materials such as aluminium and glass fibre to save dead weight so that they can be propelled at a faster speed. As a result, thinner hull panels can have structural hydro-elastic instability problems in the same way. In the human body, small transmural pressure changes can be enough to cause blood-carrying vessel collapse during the compliant phase.

FSI includes the study of both solid mechanics and fluid mechanics, and their two governing equations are coupled together to investigate the behaviour of fluid and structure under the mutual interaction of the two systems. The interfacial force and deformation are the primary driving parameters to induce the response of the coupled systems. Recently more researchers have turned their focus to this field, and both the theoretical and experimental study of the interaction of the coupled fluid and structure dynamics behaviours hve been investigated. The contributions of new discoveries and new technologies will not impact only in engineering but can be extended to different fields of studies and applications. For example, there are many physiological phenom-

ena of blood circulation and respiration which are closely related to the FSI's interfacial flexible wall research. The better understanding of these physiological phenomena can be used to improve medical treatments and therapies.

In the field of FSI, there is the potential for some great discoveries in this century though the study of this thesis represents one portion of the entire fluid flow coupling flexible structure research. The complexity of coupling the wall equation and the fluid equation has made both the study-time and the computational-time of this type of research project longer. However, this time consuming situation is now changing because of the emergence of powerful computing workstations offering time savings that make these investigations more feasible; as a result, this will lead to more results and make a greater number of new discoveries possible.

1.1 Research Background

This thesis considers the FSI problem of the classical aero/hydro-elastic system comprising a flexible panel with one-side exposed to the incompressible uniform flow and the relevant linear studies include [1-5]. Figure 1.1a is the basic configuration of this problem. The system is representative of the high Reynolds number situations found in many engineering applications. Thus, for example, the panel could be: part of a ship's hull, the skin structure of an aircraft fuselage or wing, or a curtain wall or window of high-rise building. The hull panel of a high speed ship experiences the hydrodynamic loading due to seawater flow, but on the other hand the skin of an aircraft is affected by the aerodynamic loading. Additionally the glass panels of curtain walls, that have become a feature of contemporary high-rise buildings for both aesthetic and thermal-control reasons, have aerodynamic loading induced by strong axial wind. In such applications, the concern is that at some critical speed the panel loses stability, usually through divergence that can lead to a buckled nonlinearly saturated state [17, 26, 28, 29], or a highly destructive flutter instability at higher flow speeds. Investigation on how to control stability has become utmost important.

Strategies to postpone critical flow speeds to values beyond the speed for which a panel is designed are usually based upon material selection or uniform thickening of the panel that results in increased cost and dead weight. Other methods that have been studied their effect on controlling stability are material inhomogeneity and additional constraints. The effectiveness and applicability of those methods have been discussed at the papers [30-31]. On the contrary, the goal of the present thesis is to control instability through the judicious use of highly localised structural inhomogeneity (stiffening) based upon a full understanding of instability modes. Our previous work [32, 33] has demonstrated the utility of this stabilization strategy for a two-dimensional system of figure 1.1a where an isolated spring is included as an additional stiffening support.

Herein, we extend the hybrid of theoretical and computational methods of [15] to conduct an eigen-analysis of the three-dimensional model system depicted in figure 1.1b wherein a transverse stiffening strip replaces the spring-support of our two-dimensional studies; however, we also show that the much simpler two-dimensional spring-supported configuration does provide an excellent guide to the phenomenology of the more realistic three-dimensional model.

1.2 Overview of Research

The research in this thesis studies the passive control mechanisms to be added to the flexible panels for instability control. The types of flexible panels are shown in figure 1.1a for 2-dimensional panels and figure 1.1b for 3-dimensional panels. Such mechanisms can be applied in a form of damping effect, mass effect or stiffening effect. The main mechanism of this thesis mainly uses localised stiffening approaches. The investigation looks at instabilities and flow-phenomena that occur at high Reynolds number with the objective of investigating postponement of instability onset flow speed.

The investigation of the flexible panels instabilities can be divided into divergence and panel flutter. The major parts of this research are the study of this two kinds of wall-based instabilities by inviscid (potential flow) modelling coupled with the linear

structural systems. A new hybrid of theoretical and computational methods are developed in order to investigate this classical aero/hydro-elastic system.

The overview of research is outlined as follows: Research Problem, Methodology, Scope and Assumptions and Summary of Contributions.

1.2.1 Research Problem

The research problem is clearly defined as:

"To carry out a detailed study of aero/hydroelastic instability-control of flexible panels through the use of localised stiffening methods and the linear analysis by a new hybrid of theoretical and computational methods."

This research will focus on the development of localised stiffening methods to perform stability control. A new hybrid of theoretical and computational method is used to study the control methods and the stability envelope. The method will be extended to optimize the control method through the fine adjustment of different control variables.

1.2.2 Methodology

The Fluid-Structure Interaction (FSI) system is modelled by fully coupling a finite-difference representation of the structural mechanics with a boundary-element solution for the ideal-flow fluid mechanics. An Euler-Bernoulli beam is used for the 2-D model and classical thin-plate mechanics is used for the 3-D model. Our methods extend the hybrid of theoretical and computational methods to conduct an eigen-analysis of the wall-flow matrix equation for both 2-D and 3-D systems. A multi-objective genetic algorithm is used to optimize the different configurations of localised stiffening methods. By comparison, the best optimisation of configuration can be sorted out.

1.2.3 Scope and Assumptions

The high Reynolds number regime typical of many engineering applications makes the neglect of viscous effects on the flow of a good approximation. Potential flow is most

often assumed as the case in this study. Furthermore the finite-difference representation of a flexible panel is linear and small amplitude motion. The nonlinear part is the tension term which will not be considered in this thesis as its analysis is time-stepping numerical method. This research develops a linear stability control and optimisation by genetic algorithm.

1.2.4 Summary of Contributions

The major finding of the present work is that the addition of highly localised stiffening to the structural design of an otherwise homogeneous flexible panel can be a very effective means to postpone instability to a higher flow speed or beneficially modify the form of instability. A stiffer localised stiffening yields a greater postponement until an optimal value of localised stiffness is reached at which the critical mode switches from Mode 1 to Mode 2 and no further postponement of divergence occurs. This type of tailored stabilization strategy may be used in engineering that it can be far more effective than a 'brute force' approach to design that, for example, it thickens the entire panel to prevent aero-/hydro-elastic instability within the envelope of operational flow speeds.

1.3 Thesis Structure

This thesis consists of five chapters. Chapter 1 corresponds to the introduction and background. Chapter 2 to Chapter 4 make up the body/core of the thesis. Each core chapter has its own results and conclusions. The last chapter (Chapter 5) is the summary and future development. A brief description below of each chapter makes clear their roles in the thesis:

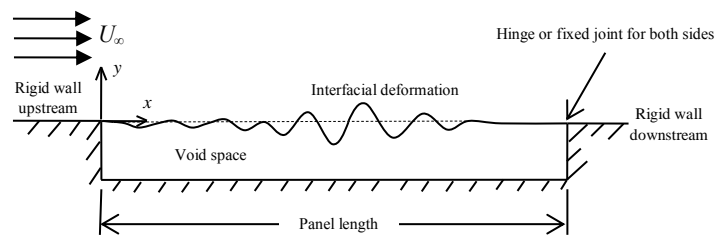
Chapter 1 explains the concerned problem of the thesis, the aims and scope, and the thesis layout. The thesis outlines the problem that has been investigated, explains the aim of the research and any limits on the scope of the work, and then provides an overview of findings.

Chapter 2 is a reproduction of a published journal paper: it gives a description of the 2-D formulation of a hybrid of theoretical and computational methods. This chapter explains the development and results of control instability of 2-D flexible panel in a mean flow.

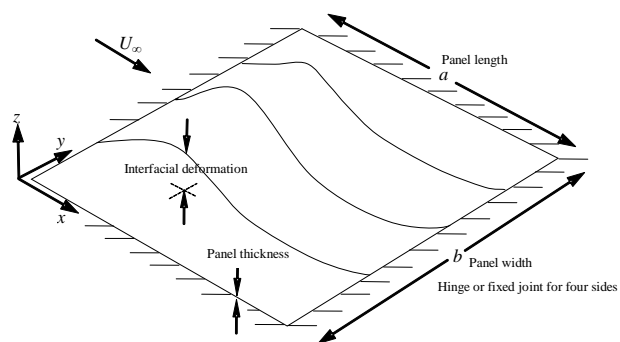
Chapter 3 is a combination of a published conference paper and a book chapter: it gives a description of the 3-D formulation of a hybrid of theoretical and computational methods. This chapter will explain the method of stabilisation strategy and results of control instability of a 3-D flexible panel in a mean flow. This chapter also highlights the results of two stabilisation strategies by either transverse stiffening strip or stream-wise stiffening strip.

Chapter 4 is a reproduction of a published book chapter: it explains how to optimise stabilisation methods by multi-objective genetic algorithm.

Chapter 5 gives a summary of research works and future development.



(a)



(b)

Figure 1.1: (a) Schematics of a two-dimensional (side view) finite panel problem. (b) Schematics of a three-dimensional (isometric view) finite panel problem.

Chapter 2

Control of Instability of 2-D Flexible Panel in a Mean Flow

Aero-/hydro-elastic stability of flexible panels: Prediction and control using localised spring support *Journal of Sound and Vibration*, Vol.332(26), pp.7033-7054. (2013)

B.H. Tan, A.D. Lucey & R.M. Howell

Contents lists available at [ScienceDirect](#)

Journal of Sound and Vibration

journal homepage: www.elsevier.com/locate/jsvi

Aero-/hydro-elastic stability of flexible panels: Prediction and control using localised spring support



B.H. Tan, A.D. Lucey*, R.M. Howell

Fluid Dynamics Research Group, Curtin University of Technology, P.O. Box U1987, Perth 6845, Australia

ARTICLE INFO

Article history:

Received 11 March 2013

Received in revised form

25 July 2013

Accepted 6 August 2013

Handling Editor: L. Huang

Available online 17 September 2013

ABSTRACT

We study the effect of adding localised stiffness, via a spring support, on the stability of flexible panels subjected to axial uniform incompressible flow. Applications are considered that range from the hydro-elasticity of hull panels of high-speed ships to the aero-elasticity of glass panels in the curtain walls of high-rise buildings in very strong winds. A two-dimensional linear analysis is conducted using a hybrid of theoretical and computational methods that calculates the system eigen-states but can also be used to capture the transient behaviour that precedes these. We show that localised stiffening is a very effective means to increase the divergence-onset flow speed in both hydro- and aero-elastic applications. It is most effective when located at the mid-chord of the panel and there exists an optimum value of added stiffness beyond which further increases to the divergence-onset flow speed do not occur. For aero-elastic applications, localised stiffening can be used to replace the more destructive flutter instability that follows divergence at higher flow speeds by an extended range of divergence. The difference in eigen-solution morphology between aero- and hydro-elastic applications is highlighted, showing that for the former coalescence of two non-oscillatory divergence modes is the mechanism for flutter onset. This variation in solution morphology is mapped out in terms of a non-dimensional mass ratio. Finally, we present a short discussion of the applicability of the stabilisation strategy in a full three-dimensional system.

© 2013 Elsevier Ltd. All rights reserved.

1. Introduction

This paper addresses and extends the classical fluid–structure interaction (FSI) problem wherein a flexible plate is destabilised by the action of a fluid flow parallel to the undisturbed panel. The modern capabilities of high-speed ships with cruise speeds in the range of 38–45 knots (19.5–23.1 m/s) – and up to 60 knots (30.1 m/s) when powered by gas-turbine engines – mean that hydroelastic instability increasingly needs to be accounted for in the design of hull panels. Recent architectural designs have seen the introduction of curtain walls comprising glass or perspex panels as an outer skin on high-rise buildings for a combination of aesthetic and passive temperature-control reasons. In addition to normal-loading effects, these may be susceptible to aeroelastic instability in storm or hurricane-force winds aligned with the main axis of the panel. In this paper we present an analytical study of panel stability into which localised stiffening is added and used to control aero-/hydro-elastic instability in the above and other applications of the basic configuration.

* Corresponding author. Tel.: +61 8 9266 7048; fax: +61 8 9266 2681.

E-mail address: A.Lucey@curtin.edu.au (A.D. Lucey).

The high Reynolds-number regime typical of the types of engineering applications cited above makes the neglect of viscous effects on the flow a good approximation. Accordingly, potential flow is most often assumed as is the case in this study. Given the importance and ubiquity of applications, this FSI system has generated a rich literature in which, most commonly, a Galerkin method is used to predict the system response with a particular focus on the parameters for which it becomes unstable. Thus, for example, [1–5] show that as the flow speed is increased for a given flexible plate, the panel first loses its stability to divergence. This buckling type of instability occurs because the fluid forces generated by a deformation exceed the restorative structural forces of that deformation. For a simple flexible plate held at both its ends, the fundamental mode is the critical mode for divergence. If the flow speed is increased further, divergence is replaced by modal-coalescence flutter that is best characterised as a Kelvin–Helmholtz type of resonance.

In parallel to these types of study, flexible compliant walls of infinite extent comprising more than one structural component (e.g. a spring-backed flexible plate) have been studied, e.g. [1,6,7] using an analytical approach wherein all system perturbations take a travelling-wave form, for example $\exp[i(\alpha x - \omega t)]$ wherein α and ω are respectively the perturbation wavenumber and angular frequency. The omission of end effects – that may be considered to be inhomogeneities in such modelling – is broadly acceptable provided that the length of the panel in any application is much longer than the wavelength of the critical modes being studied. However, under such conditions the travelling-wave analysis requires that some structural damping is present for the realisation of divergence instability although its predictions of divergence-onset flow speed agree with those of the Galerkin approach. This discrepancy was addressed in [8] wherein the role of end conditions, even for very long flexible walls was explained. More recently the rigorous analysis of [9] constructed a travelling-wave model that incorporated the fixed wall ends through a Weiner–Hopf technique and thereby reconciled the differences in findings between the two types of modelling.

Clearly, the aforementioned boundary-value studies predict the long-time response of the system after transients from some form of initial excitation have either been attenuated or convected away. The finite-time response can be of equal importance in that it links the original source and characteristics of an initial deformation to the long-time response through a process of response evolution. The ability to model the finite-time, or receptivity, problem may lead to engineering strategies that interrupt or modify this evolution and thereby prevent or postpone panel instability. Studies of system response to a source of initial or continuing localised excitation have been presented. For example, [10,11] respectively used initial impulse and oscillatory line excitation for the present system, while [12] tackled the closely related shell problem with oscillatory line excitation. Using a different analytical approach, [13] showed that absolute instability – that aligns with divergence – could exist in the system if structural damping were included. These analyses assumed an infinitely long flexible panel and focused on the long-time response. Nevertheless, they showed that the system could support a remarkable range of FSI wave types. Using numerical simulation, [14] showed that the effects of finiteness and transients led to globally unstable responses unseen in the analyses of infinitely long elastic panels.

In the present work, we use the hybrid of theoretical and computational modelling presented in [15] that casts the FSI system equation in state-space form after solving the coupled fluid and structure equations using boundary-element and finite-difference methods respectively. Like the purely analytical models discussed above, this approach is used to compute the system eigenmodes while its numerical-simulation aspects readily accommodate inhomogeneity in the base system. Thus we can evaluate the effect of an added localised spring support on the system eigenmodes with a particular focus on instability-onset flow speeds. We also extend the modelling of [15] in order to solve the initial-value problem and thereby simulate the transient response of finite flexible panels showing how its evolution from a source of initial excitation evolves into the infinite-time eigenmodes predicted by the boundary-value approach.

The paper is laid out as follows: We first extend the FSI system model of [15] to permit the inclusion of impulse line excitation and a supporting spring foundation that may either be uniform or comprise a discrete spring at a point along the flexible plate. We then present three sets of results that illustrate the system dynamics covering a range of applications. The first concerns a homogeneous Kramer-type compliant wall [7] comprising a flexible plate with a uniformly distributed spring foundation. In part, we use this case to validate the present modelling and its implementation. The second set of results addresses the classical case of a simple metal flexible panel subjected to water flow for which we show how the addition of a spring support can be used to modify hydroelastic instability onset. This case typifies the vast majority of incompressible flow studies for which the fluid-to-solid ratio is $O(1)$. In the third set of results we consider airflow over a glass or aluminium panel for which the fluid-to-solid ratio is $O(10^{-3})$, giving a system that has not hitherto been fully explored, presumably due to a lack of recognised applications until the emergence of curtain walls as an architectural feature. We show that this regime possesses some very different dynamics from the classical hydro-elastic case. We therefore map out the parameter space over which the differences occur as well as showing how adding a spring support can modify both divergence onset and the flutter characteristics in air-over-glass aero-elastic applications. Finally we unify our findings in the conclusions and explain how the present two-dimensional strategy for controlling aero-/hydro-elastic instability of panels can be carried across to real three-dimensional applications.

2. Methods

We first summarise the well-known governing equations for the fluid–structure systems depicted in Fig. 1. We then outline the hybrid theoretical–computational approach that permits either an eigen-analysis to be conducted for the

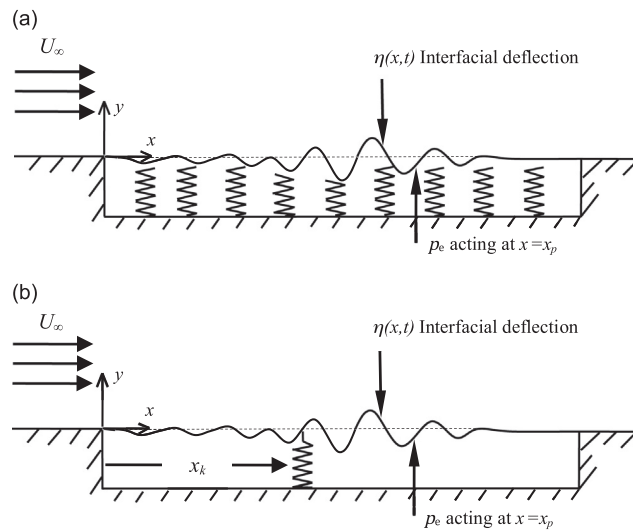


Fig. 1. Schematics of a uniform flow past a flexible panel with (a) uniformly distributed spring foundation and (b) localised added spring support.

long-time boundary-value problem or the time-evolution of disturbances to be constructed for the initial-value problem. Finally, we describe the non-dimensional framework adopted for the presentation of the results in this paper.

2.1. Governing equations

The small-amplitude behaviour of a thin plate, supported by either a uniformly distributed spring foundation with coefficient $K \neq 0$, and an added spring support with coefficient $k \neq 0$ localised at $x = x_k$, in the presence of a fluid flow and subjected to a localised initial pressure pulse of magnitude p_e at $x = x_p$ is governed by

$$\rho_m h \ddot{\eta} + d \dot{\eta} + B \eta_{,xxxx} + K \eta + k \delta(x - x_k) \eta = -p(x, 0, t) + p_e \delta(x - x_p) \delta(t), \quad (1)$$

where $\eta(x, t)$, ρ_m , h , d and B are, respectively, the plate's deflection, density, thickness, (dashpot-type) damping coefficient and flexural rigidity (evaluated using $B = Eh^3/[12(1-\nu^2)]$ where ν is the Poisson ratio of the plate material), δ is the Dirac delta function, and $p(x, 0, t)$ is the fluid-pressure perturbation that acts to deform the plate, noting that the mean transmural pressure is such that the plate's mean position lies in the plane $y=0$. The flexible plate of length L is hinged at its leading and trailing edges giving $\eta(0, t) = \eta_{,xx}(0, t) = \eta(L, t) = \eta_{,xx}(L, t) = 0$. We use overdot and suffix notations for temporal and spatial derivatives respectively.

The flow is assumed to be incompressible and irrotational, allowing the introduction of a velocity perturbation potential $\phi(x, y, t)$ that satisfies Laplace's equation

$$\phi_{,xx} + \phi_{,yy} = 0, \quad (2)$$

with the condition that $\phi \rightarrow 0$ as $y \rightarrow \infty$. The unsteady fluid pressure is determined using the linearised unsteady Bernoulli equation

$$p = -\rho_f \dot{\phi} - \rho_f U_\infty \phi_{,x}, \quad (3)$$

where ρ_f and U_∞ are, respectively, the fluid density and flow speed. The plate and fluid motions are coupled through the kinematic boundary condition

$$\phi_{,y} = \dot{\eta} + U_\infty \eta_{,x}, \quad (4)$$

which in the linearised system is enforced at $y=0$.

2.2. Solution methods

The governing equations are solved by combining a boundary-element method for the flow field, as developed in [16,17] for problems in FSI, with a finite-difference method for the wall motion. This reduces the two-dimensional field problem to a one-dimensional line problem at the interface of the fluid and structural components of the system. The resulting system equation, couched in the interfacial variable $\eta(x, t)$ and its differentials, is then cast in state-space form following the approach developed in [15]. In the present work, we make the straightforward extension of these methods to (i) incorporate spatial inhomogeneity in the form of an isolated spring support, and (ii) model the initial-value problem. Accordingly, we

provide herein only an outline and direct readers to the papers cited above for details of the contributing elements of the solution procedures.

The panel is discretised into N collocation points at which its mass is lumped and which provide the basis for writing Eq. (1) in the finite-difference form:

$$\rho_m h [I] \{\ddot{\eta}\} + d [I] \{\dot{\eta}\} + (B [D_4] + K [I] + [0_k]) \{\eta\} = -\{p\} + \delta(t) \{0_p\}, \quad (5)$$

where $[I]$ is the identity matrix and $[D_4]$ is the penta-diagonal fourth-order differentiation matrix operator. $[0_k]$ is a null matrix except for its element (m,m) which has the value k where $m = \text{int}[(x_k/L)N]$ is the collocation point closest to the location at which the spring has been added. Although we add only one isolated spring support in this study, clearly any number of such springs could be modelled using our approach. On the right-hand side of Eq. (5), the pressure pulse appears as the value p_e at location $n = \text{int}[(x_p/L)N]$ in the otherwise null vector $\{0_p\}$.

The pressure perturbation due to the motion of the wall is obtained by constructing a solution to the Laplace equation (2) using a source–sink singularity distribution, discretising this using a set of boundary-elements based upon the N collocation points, enforcing the no-flux condition, Eq. (4), at the N control points of the boundary elements to determine the required singularity strengths, and finally using the linearised Bernoulli equation (3) along a surface streamline; this gives the result

$$-\{p\} = 2\rho [\Phi] [D^+] \{\dot{\eta}\} + 2\rho U_\infty ([\Phi] [D_1] + [T] [D^+]) \{\eta\} + 2\rho U_\infty^2 [T] [D_1] \{\eta\}, \quad (6)$$

where $[\Phi]$ and $[T]$ are respectively the matrices of perturbation-potential and tangential-velocity influence coefficients, $[D_1]$ is the first-order differentiation finite-difference matrix operator and $[D^+]$ is a matrix operator for the interfacial vertical speed; expressions for the influence coefficients are listed in [17].

Substitution of Eq. (6) into Eq. (5) then yields the fluid–structure system equation

$$[A] \{\ddot{\eta}\} + [B] \{\dot{\eta}\} + [C] \{\eta\} = -\delta(t) \{0_p\}, \quad (7)$$

where

$$[A] = -\rho_m h [I] + 2\rho [\Phi] [D^+], \quad (8a)$$

$$[B] = -d [I] + 2\rho U_\infty ([\Phi] [D_1] + [T] [D^+]), \quad (8b)$$

$$[C] = -B [D_4] - K [I] - [0_k] + 2\rho U_\infty^2 [T] [D_1]. \quad (8c)$$

Introducing the $2 \times N$ vector of state variables $\{x\}^T = \{\eta\}, \{\dot{\eta}\}\}^T$ allows the system equation (7) to be re-written as

$$\{\dot{x}\} = [H] \{x\} + \delta(t) \{G\}, \quad (9)$$

in which

$$[H] = \begin{bmatrix} 0 & I \\ -[A]^{-1}[C] & -[A]^{-1}[B] \end{bmatrix} \quad \text{and} \quad \{G\} = \begin{Bmatrix} 0 \\ [A]^{-1}\{0_p\} \end{Bmatrix}. \quad (10a,b)$$

To determine the long-time response of the system we omit the initial excitation in Eq. (9), assume single-frequency response proportional to $\exp(i\omega t)$, and then solve the eigenvalue problem to determine the $2N$ values of $\omega = \omega_R + i\omega_I$. The real part, ω_R , gives the amplification/decay while the imaginary part ω_I is the angular frequency of the eigenmode.

To solve the initial-value problem we apply a zero-order hold on the input, $\{G\}$, of Eq. (9) to digitise the continuous system (H,G) . Time scaling is used to transform the state-space solution into a sampled system that is then solved using MATLAB functions to determine the transient response of the system.

2.3. Non-dimensional framework

For simple panels with length L characterising the wavelength of typical flow-induced deformations, it is common (e.g. [3,18,4,15]) to non-dimensionalise the FSI system using this lengthscale along with timescale defined as L/U_∞ . This yields the fluid-to-structure stiffness ratio $\Lambda = \rho_f U_\infty^2 L^3 / B$ as a control parameter for a system with a given (solid-to-fluid) mass ratio, $\mu = \rho_m h / (\rho_f L)$. In the present work that features spring supports, L does not necessarily represent the wavelength of critical modes in the destabilisation of a panel through divergence and flutter. Accordingly, we non-dimensionalise using a reference length-scale, l_{ref} and timescale t_{ref} defined by

$$l_{\text{ref}} = \frac{\rho_m h}{\rho_f} \quad \text{and} \quad t_{\text{ref}} = \frac{(\rho_m h)^{5/2}}{\rho_f^2 B^{1/2}}, \quad (11a,b)$$

thereby following the scheme used in [10,11,19] that reduces an infinitely long, unsupported elastic-plate problem to a system of equations with just one non-dimensional control parameter, namely the flow speed.

Using the forms in Eq. (11a,b) we define the non-dimensional terms

$$x', \eta' = \frac{x, \eta}{l_{\text{ref}}}, \quad t' = \frac{t}{t_{\text{ref}}}, \quad d' = d \left[\frac{(\rho_m h)^{3/2}}{\rho_f^2 B^{1/2}} \right], \quad K', k' = K, k \left[\frac{(\rho_m h)^4}{\rho_f^4 B} \right], \quad p' = p \left[\frac{(\rho_m h)^3}{\rho_f^3 B} \right], \quad (12a-e)$$

that give the non-dimensional form of the system equation as

$$\ddot{\eta}' + d' \dot{\eta}' + \eta'_{,x'x'x'x'} + K' \eta' + k' \delta(x' - x'_k) \eta = -p' + p'_e \delta(x' - x'_p) \delta(t'), \quad (13)$$

with panel length, often termed the mass ratio, and applied flow speed taking the non-dimensional forms

$$L' = \frac{\rho_f L}{\rho_m h} \quad \text{and} \quad U' = U \left[\frac{(\rho_m h)^{3/2}}{\rho_f B^{1/2}} \right]. \quad (14a,b)$$

This approach allows us to vary independently the key parameters of panel length and applied flow speed in the non-dimensional results. The relationship between the often-used stiffness ratio, $\Lambda = \rho_f U_\infty^2 L^3 / B$, and the two system variables used in this paper is

$$\Lambda = (U')^2 (L')^3. \quad (15)$$

Furthermore, for a panel with given geometric properties, L and h , variations to L' can be interpreted as changing the fluid-to-solid density ratio, ρ_f / ρ_m , thereby highlighting the differences between the aero- and hydro-elastic behaviour of a given panel.

3. Results

We present results for three related engineering systems. Although our results are presented in a non-dimensional form that spans the physical parameter space, each system aligns with a distinct engineering application, these being water flow over a rubber-like compliant wall (Section 3.1) with drag-reduction capabilities, water flow over a simple metal panel (Section 3.2) typical of that used for the hulls of high-speed ships, and air flow over simple glass panels (Section 3.3) typical of curtain walls in modern high-rise buildings. For the last two applications we close with a dimensional demonstration of how instability can be controlled by using a localised spring support for the applications cited. We do not present a separate validation of the present method because that has already been done for the base method in [15] while the validation of our extensions to the method is embedded in the new results upon which we focus.

3.1. Flexible panel with uniformly distributed spring foundation

We consider the spring-backed flexible-plate configuration of Fig. 1a, incorporating structural damping, that approximates a compliant coating of the type investigated in, for example, [7,15,17,20]. The physical properties of this wall have $h=0.01$ m, $\rho_m = 852$ kg/m³, $B = 4.44 \times 10^{-2}$ N m (having used $E = 4 \times 10^5$ N/m² and $\nu = 0.5$), $d = 2.0 \times 10^4$ N s/m³ and $K = 3.68 \times 10^7$ N/m³; the length, L , of the flexible panel is 0.6 m and the fluid is water with density $\rho = 10^3$ kg/m³. These data yield the non-dimensional parameter values $d' = 2.36$, $K' = 4.41$ and $k' = 0$ in the governing equation (13) and $L' = 70.4$ in Eq. (14a).

With $p'_e = 0$ in Eq. (13), the infinite-time behaviour of the system is represented by the variation of its eigenvalues with non-dimensional flow speed in Fig. 2a and b that respectively chart the real (positive denoting amplification and negative decay) and imaginary (oscillatory) parts of the non-dimensionalised eigenvalues using the reference time defined in Eq. (11b). Only the 40 eigenvalues having the lowest oscillatory frequencies are plotted although all 1600 were calculated having discretised the wall into $N=800$ elements. The onset of divergence instability is seen to occur at $U' = 2.326$ where the locus of the mode that yields this critical speed first crosses into the amplifying quadrant of Fig. 2a and its oscillatory frequency becomes zero in Fig. 2b; the latter feature has led to this instability often been termed static divergence in the very early studies of compliant walls such as [6,21].

The envelope formed by the closely spaced discrete modes seen in Fig. 2 suggests that the system can be modelled by a continuous spectrum of modes that is assumed in the normal-mode decomposition used to analyse walls of infinite extent. Using this approach, also referred to as a travelling-wave analysis wherein all system disturbances are proportional to $\exp[i(\alpha x - \omega t)]$, [7] derived analytical expressions for the critical, or lowest, flow speed for divergence-onset and determined the wavelength ($\lambda = 2\pi/\alpha$) of the critical mode that has $\omega = 0$ at divergence onset; these were respectively given by

$$U_D = 2 \left(\frac{BK^3}{27\rho_f} \right)^{1/8} \quad \text{and} \quad \lambda_D = 2\pi \left(\frac{3B}{K} \right)^{1/4}. \quad (16a,b)$$

Using the present wall properties Eq. (16a) gives the critical flow speed $U_D = 19.51$ m/s that when non-dimensionalised yields $U'_D = 2.303$. This is approximately 1 percent lower than our prediction of 2.326 from Fig. 2. Exact agreement could only be expected in the limit of infinite plate length and the present prediction for a plate of finite length is expected to be higher, as found, because of the structural restraints at its leading and trailing edges. This correlation supports the integrity of our approach and its implementation.

Using our transient analysis, we now solve an initial-value problem to map out the system behaviour that would lead to the establishment of the infinite-time behaviour predicted by Fig. 2. This type of analysis also serves to distinguish valid modes from physically unachievable, or spurious, system states that can be predicted in an eigen-solution. A line impulse is applied at the centre of the undisturbed compliant-wall panel to initiate motion. The time sequence of profiles in Fig. 3a shows wall

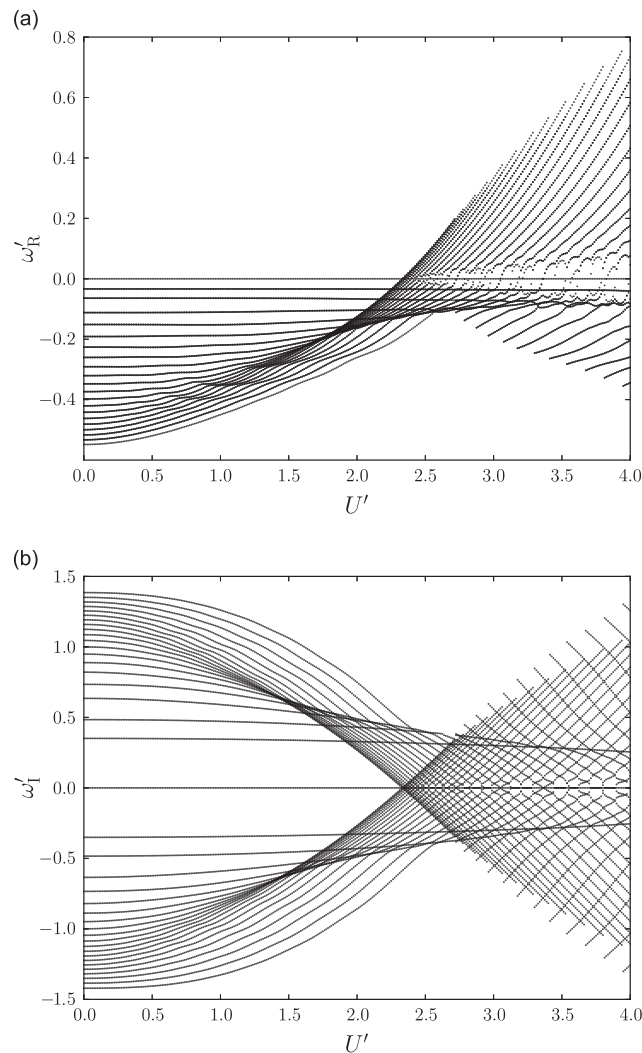


Fig. 2. Variation of system eigenvalues with non-dimensional flow speed for a (plate-spring) compliant-wall panel with $L' = 70.4$, $d' = 2.36$ and $K' = 4.41$: (a) is the real (positive, growth; negative, decay) part and (b) is the imaginary (oscillatory) part of the eigenvalues.

deformations at $U' = 2.320$, incrementally below the predicted divergence-onset speed, so as to simulate the marginally stable state that exists just before divergence onset. At early times flow-modified flexural waves propagate outwards from the impulse while at later times the wall settles into a nearly uniform mode across the entire wall in which fit approximately 12 wavelengths. This mode would be almost identical to the critical mode of divergence onset at a marginally higher flow speed. However, in the present simulation, amplitude decay occurs through the action of the structural damping. The wall would therefore return to its undisturbed state in the long-time limit when all of the energy initially input by the excitation has been dissipated. Again, good agreement is found with the travelling-wave based predictions of [7]; for the present physical data, Eq. (16b) predicts a critical wavelength of 0.049 m that would yield close to 12 disturbance wavelengths on the present finite wall of length 0.6 m. A much higher flow speed, $U' = 3.867$, than that of divergence onset is used to generate Fig. 3b to illustrate unstable behaviour. Rapid amplitude growth of system disturbances is seen to propagate in both upstream and downstream directions from the point of initial excitation. This is characteristic of absolute instability as defined in [22]. For the present fluid–structure system it is discussed and demonstrated theoretically and numerically in [23] and for a cylindrical shell in [12] that has a similar solution morphology to that of a spring-backed flexible plate. In [12,23] it is shown that the addition of a further structural component – a spring backing to a flexible plate or hoop stress in a cylindrical shell – causes a very significant increase to Crighton and Oswell's [11] flow speed of $U' = 0.074$ for the onset of absolute instability. This is reflected by the critical flow speeds, $U'_D = 2.303$ and 2.326 for infinitely long and the present finite walls respectively, of instability-onset determined herein; we return to this point in Section 3.2 where the flexible wall is similar to that studied by Crighton and Oswell. The importance of absolute instability owes itself to the fact that it can spread to all locations of the compliant wall irrespective of the location of the initial, or a continuing [14], excitation.

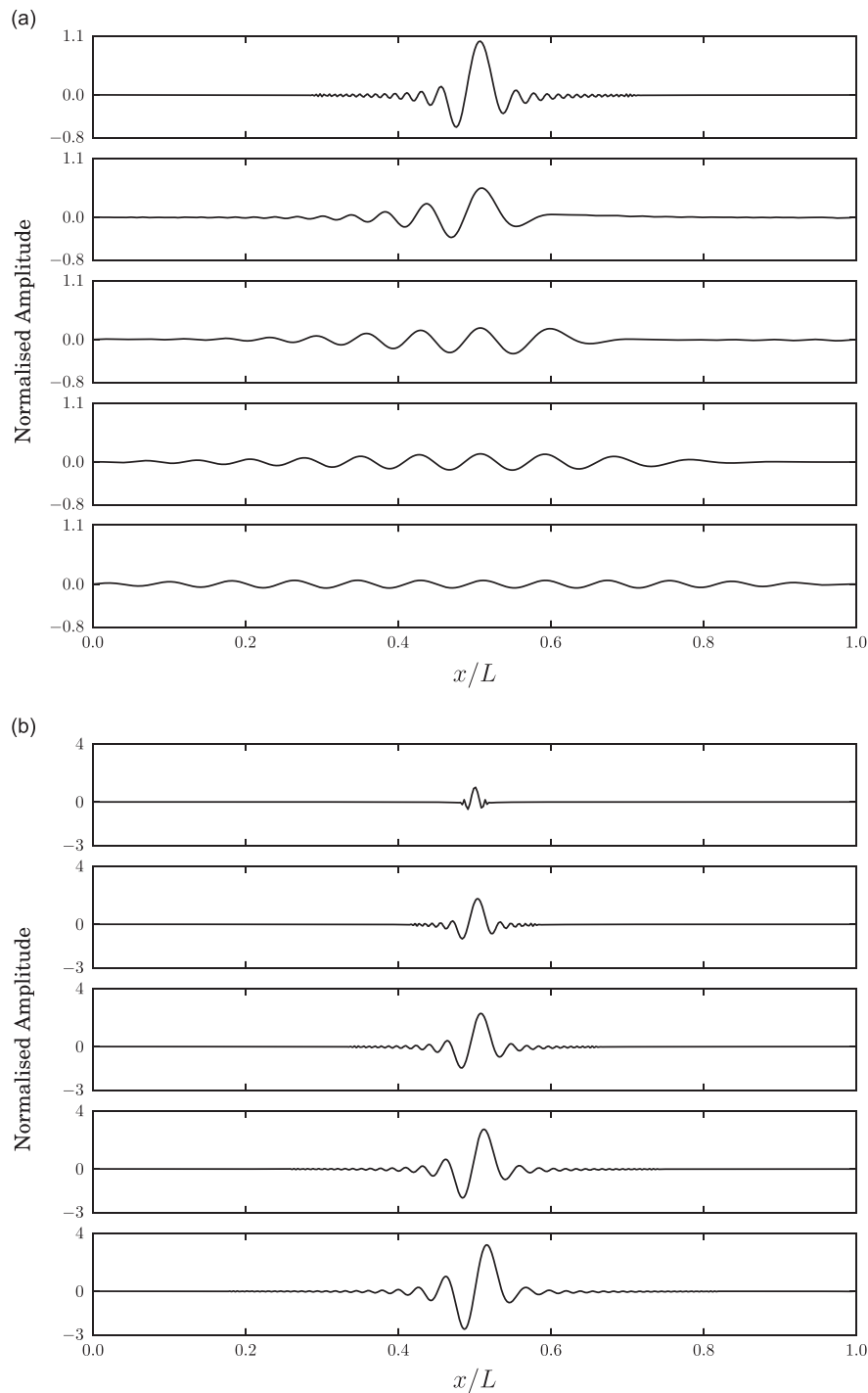


Fig. 3. Sequence of instantaneous panel profiles developing (top to bottom) from a line impulse applied at the mid-point for the compliant-wall panel of Fig. 1 at: (a) a marginally pre-divergence flow speed, $U' = 2.320$, at time steps $1\Delta T'$, $5\Delta T'$, $20\Delta T'$, $50\Delta T'$, and $300\Delta T'$ and (b) a post-instability-onset flow speed, $U' = 3.867$, at time steps $125\Delta T'$, $625\Delta T'$, $1,250\Delta T'$, $1,875\Delta T'$, and $2,500\Delta T'$, where $\Delta T' = 2.53$.

3.2. Flexible panel with a single-spring support: hydroelastic applications

The investigation of this paper now focuses on the hydro-elasticity of a simple elastic panel held at its ends. The purpose here is to show that the addition of an isolated spring support between the two ends, as shown in Fig. 1b, can control the onset and form of instability. The dimensional properties used correspond to those of an aluminium panel with

$h=0.0025$ m, $\rho_m=2600$ kg/m³, and $B=76.62$ N m (having used $E=5.52 \times 10^{10}$ N/m² and $\nu=0.25$). The spring-stiffness coefficient is $k_s = \int k\delta(x-x_k) dx$ and initially explored in multiples, n , of $k_+ = 6.0 \times 10^3$ N/m², hence $k_s = nk_+$. The length, L , of panel is 0.6 m (although we close this sub-section with results that show the dependence of divergence instability upon L/h) and the fluid is water with density $\rho = 10^3$ kg/m³. The non-dimensional parameter values in the governing equation (13) are therefore $d' = 0$, $K' = 0$, k' selected so that $k'_+ = 2.15 \times 10^{-5}$, and with $L' = 92.3$ in Eq. (14a).

Fig. 4a and b respectively show the variation of the real and imaginary parts of the two lowest-frequency system eigenmodes with flow speed; however, all $2N = 400$ eigenmodes are included in the solution of the FSI system. Three sets of data, $k'_s = nk'_+$ with $n=0, 6$ and 15 for a spring support added at the panel mid-point $x/L = 0.5$, are presented, the first giving the result for the standard panel studied many times before, for example [2,3,18,24] and the homogeneous results of [15]. At low flow speeds, the fluid-loaded panel undergoes neutrally stable oscillations. Fig. 4b shows that the oscillation frequency in the first mode is increased by the inclusion of the spring but that the second mode is almost unaffected because the spring has been placed at the nodal point of this mode. As the flow speed is increased a bifurcation is seen to occur at $U' = 0.00714$ for the homogeneous case. This is the onset of divergence instability at which the flow speed is sufficiently high that the hydrodynamic stiffness – the last term on the right-hand side of Eq. (6) – exactly balances the panel’s structural restorative forces. Combining the present critical flow speed $U' = 0.00714$ with the present length of the panel, $L' = 92.31$, through Eq. (15) gives the non-dimensional stiffness ratio $\Lambda = 40.1$ for divergence-onset. This is in excellent agreement with the predictions of the aforementioned studies of homogeneous plates. Beyond this threshold a positive real part of the eigenvalue appears in Fig. 4a that commences the divergence loop of instability. As the added-spring constant is increased the divergence-onset flow speed, for a panel of given flexural rigidity, is seen to increase to 0.0123 for $6k'_+$ and

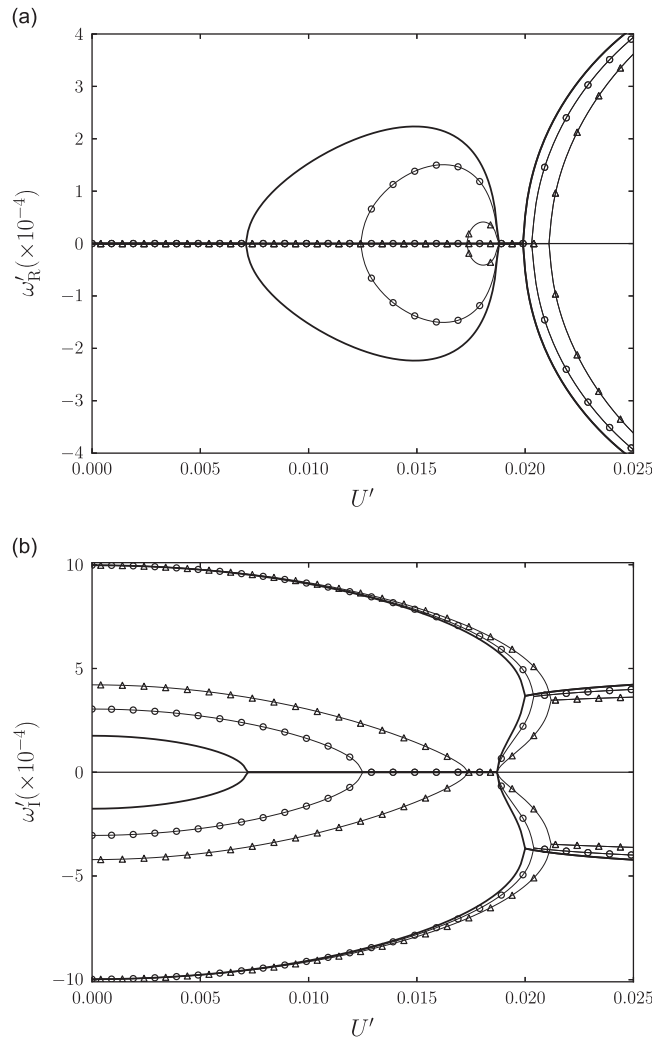


Fig. 4. Variation of the two lowest system eigenvalues: (a) real (positive, growth; negative, decay) part, and (b) imaginary (oscillatory) part, with non-dimensional flow speed for an elastic flexible panel with $L' = 92.31$ for different values of a spring support at the panel mid-point: —, $0k'_+$ (homogeneous case); $-\circ-$, $6k'_+$, $-\triangle-$, $15k'_+$, where $k'_+ = 2.15 \times 10^{-5}$.

0.0174 for $15k'_+$. At higher flow speeds there is a recovery from divergence but soon after modal-coalescence (of the first two modes) flutter occurs at a flow speed of 0.0199 for the standard case ($0k'_+$), at 0.0203 for $6k'_+$ and 0.0210 for $15k'_+$. The very significant increase in divergence-onset flow speed as k'_s is increased, together with the lesser postponement of flutter, suggest a simple strategy for extending the envelope of stable operation of fluid-loaded panels in engineering applications.

We now show how the added spring contributes to the postponement of divergence in terms of energy budgets. The dimensional wall energy comprises three parts, namely plate strain energy E_S , plate kinetic energy E_K and the stored energy of the added spring E_{SP} , respectively defined as

$$E_S = \frac{1}{2}B \int_0^L \eta_{xx}^2 dx, \quad E_K = \frac{1}{2}\rho_m h \int_0^L \eta_t^2 dx \quad \text{and} \quad E_{SP} = \frac{1}{2}k_s \eta^2|_{x=x_p}. \quad (17a,b,c)$$

Ref. [14] also introduced a term called the virtual work done by the hydrodynamic stiffness component, p_s – the part of the pressure that is dependent upon the interfacial displacement (the final term on the right-hand side of Eq. (6)) – in the establishment of a wall deformation. This is defined as

$$E_{VW} = -\frac{1}{2} \int_0^L \eta p_s dx. \quad (18)$$

Each of the terms in Eqs. (17) and (18) is non-dimensionalised through multiplication by $(\rho_m h)/(\rho_f B)$, consistent with the scheme outlined in Section 2.3. The eigenmodes, $\eta(x, t)$, corresponding to the eigenvalues of Fig. 4 are normalised and thus the non-dimensional energy terms are scaled for an amplitude of unity. It was shown in [14] that divergence onset can be defined as the flow speed for which E_{VW} exactly balances the mechanical energy of the wall. To show how this occurs, both without and with an added spring, we present Fig. 5. Fig. 5a corresponds to the standard result in Fig. 4 and is a time-stepping numerical evaluation of the Mode-1 energy terms for a flow speed marginally lower than that of divergence onset at $U' = 0.00710$. Because the flow speed is so close to that of divergence onset, where structural and hydrodynamic forces nearly balance each other, the wall acceleration and velocity are very small, hence the insignificant values of E_K in the plot and the slow oscillation of the wall. The key feature is that E_{VW} is almost exactly balanced with the plate's strain energy, E_S . Fig. 5b is the equivalent result with a spring added at the panel mid-point and corresponds to the result of Fig. 4 for $k'_s = 6k'_+$. The evaluation is conducted at $U' = 0.0120$ slightly lower than that of divergence onset. It is now seen that both the strain energy of the plate and the spring energy contribute to the total value of mechanical energy that balances E_{VW} and the proportions in which they do so. In this particular case, it is evident that most of the wall's restorative force is provided by the added spring in the stabilisation strategy.

To illustrate the effect of the added spring support on the key fluid–structure modes that would be most evident in the system response, we present Figs. 6–8, obtained using $k'_s = 6k'_+$. Fig. 6 shows the neutrally stable oscillations at $U' = 0.00378$ as a set of panel profiles over one cycle corresponding to the eigenvalues of Modes 1, 2 and 3 calculated using the analysis that generated Fig. 4. The thick lines show the initial and final positions of the panel. While superficially Mode 1 appears similar to the fundamental mode for a standard panel (see [15] for comparisons), the effect of the spring added at the mid-point has clearly introduced the next higher harmonic. Similarly Mode 2 can be seen to contain an element of the fourth harmonic albeit at a lower intensity. This progression continues with Mode 3 for which the higher sixth higher harmonic is perceptible upon very close inspection. Further results (not presented here) for example at $k'_s = 15k'_+$ serve to increase the contribution of these ‘wavelength-doubling’ harmonics; this phenomenon could be expected given that in the limit of infinite added-spring stiffness the flexible panel effectively becomes two separate panels. Fig. 7, obtained at $U' = 0.0151$ in the divergence loop of Fig. 4 ($6k'_+$ result), shows the amplifying and accompanying decaying modes of the instability over a sequence of equal time-steps. Growth is seen to occur as a quasi-downstream-travelling wave while the attenuating wave that would not be evident in the physical system (demonstrated in the initial-value problem presented below) is a quasi-upstream-travelling wave. Further results show that increasing k'_s from the value used in Fig. 7a causes greater downstream distortion of the wave so as to increase the ratio of the peak amplitude to the deflection of the panel mid-point where the spring has been located. Fig. 8 shows the amplifying mode of the complex-conjugate pair at $U' = 0.0227$ in the regime of flow speeds of Fig. 4 for which Modes 1 and 2 have coalesced to give a powerful flutter instability. Fig. 8a shows the actual sequence of deformations while in Fig. 8b amplitude growth has been (artificially) suppressed so as to give a clearer picture of the mode shape. Animations show that the flutter effectively occurs as a travelling wave that ‘sloshes’ between the leading- and trailing-edge constraints as demonstrated theoretically by [4]. The mode shape principally comprises a natural Mode 2 shape whereas the standard unsupported case features significant Mode 3 content [15]. This is because the presence of the added spring predisposes the panel to a reduction of the mid-point deflection for which Mode 2 has a lower energy intensity in the combined plate-plus-spring system.

The foregoing results of this sub-section predict the infinite-time response of the system – the boundary-value problem. We now investigate how such responses might come into being from a source of localised initial excitation in finite time by a time-stepping solution of the initial-value problem. The merit of such an enquiry is that understanding the mechanism through which panel instability comes into being might lead to the development of intervention strategies by which it can be forestalled. The undeformed plate is subjected to a line impulse at $t' = 0$ modelled as non-zero p'_e applied at the plate's mid-point in Eq. (13) for the same case, $k'_s = 6k'_+$ as Figs. 7 and 8. Fig. 9 shows the development of divergence instability at a flow speed $U' = 0.0151$ for the case modelled in Fig. 7. Immediately after the applied excitation Fig. 9a shows that the plate response is characterised by very high frequency low-wavelength waves that travel outwards from the point of initial

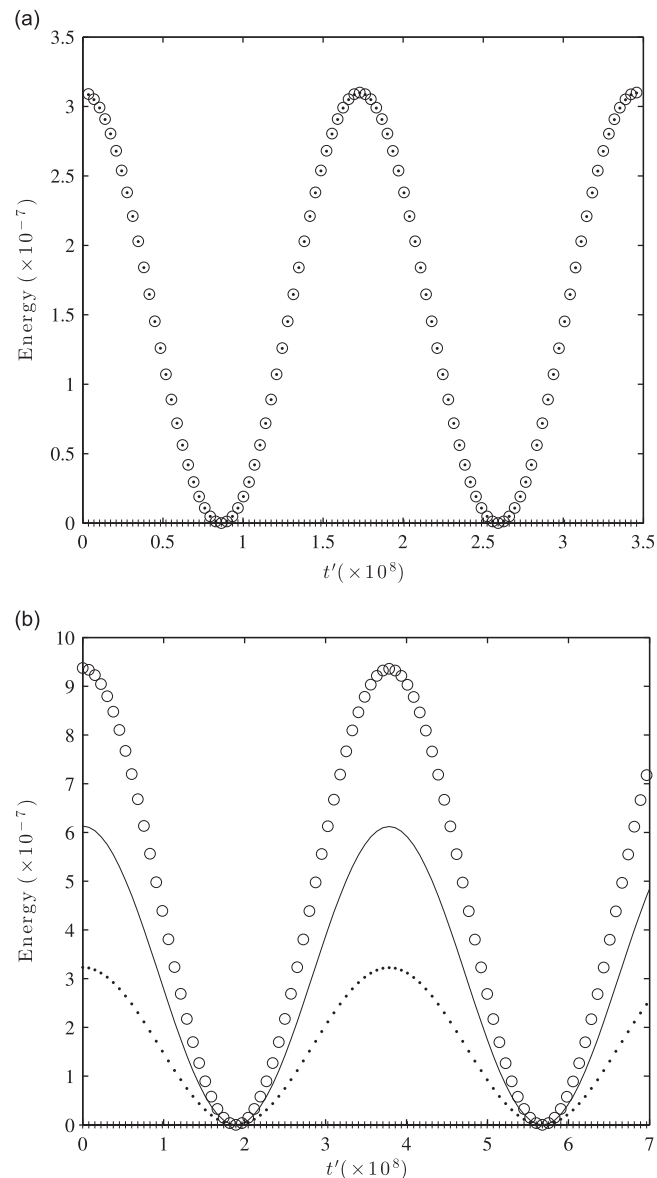


Fig. 5. Variation of flexible-panel strain energy, E_s (\cdots), kinetic energy, E_k ($+$), spring energy, E_{sp} (—) and virtual work done by the hydrodynamic stiffness, E_{vw} (\circ) with time for neutrally stable oscillatory motion at a flow speed incrementally below that of divergence onset for the system of Fig. 4: (a) $0k_+$ (homogeneous case), and (b) added spring support with coefficient $6k_+$ added at the panel mid-point.

excitation. These are essentially flexural waves of the plate – the structural-force intensity far outweighs the pressure loading – possessing a range of frequencies because the input impulse is a wide-spectrum excitation. These waves are neutrally stable and serve to propagate disturbance energy upstream and downstream of the original input source. The evident amplitude growth over this sequence of time-steps might suggest instability. However, what occurs is that the quantum of energy input first transfers to very short wavelength disturbances that have a high spatial energy intensity. The energy is then re-distributed to waves of lower spatial energy intensity with an accompanying amplitude growth that maintains constant total mechanical energy of the panel. This type of amplitude adjustment for neutrally stable linear waves on flexible surfaces has been demonstrated and explained in [19]. In the later sequence of time-steps of Fig. 9b these disturbances rapidly evolve into the dominant low-frequency divergence-instability mode predicted by the eigenvalue analysis of Fig. 7a as the infinite-time response.

Crighton and Oswell [11] studied a similar problem comprising a fluid-loaded, infinitely long, elastic plate subjected to continuous line excitation. Their theoretical analysis predicted the existence of an absolute instability at $U' = 0.074$, a much higher speed than that (0.0151) used to generate the instability that evolves through Fig. 9. However, Crighton and Oswell remarked that in an unpublished report by D. Atkins (cited by [7,10]) the presence of some structural damping precipitated

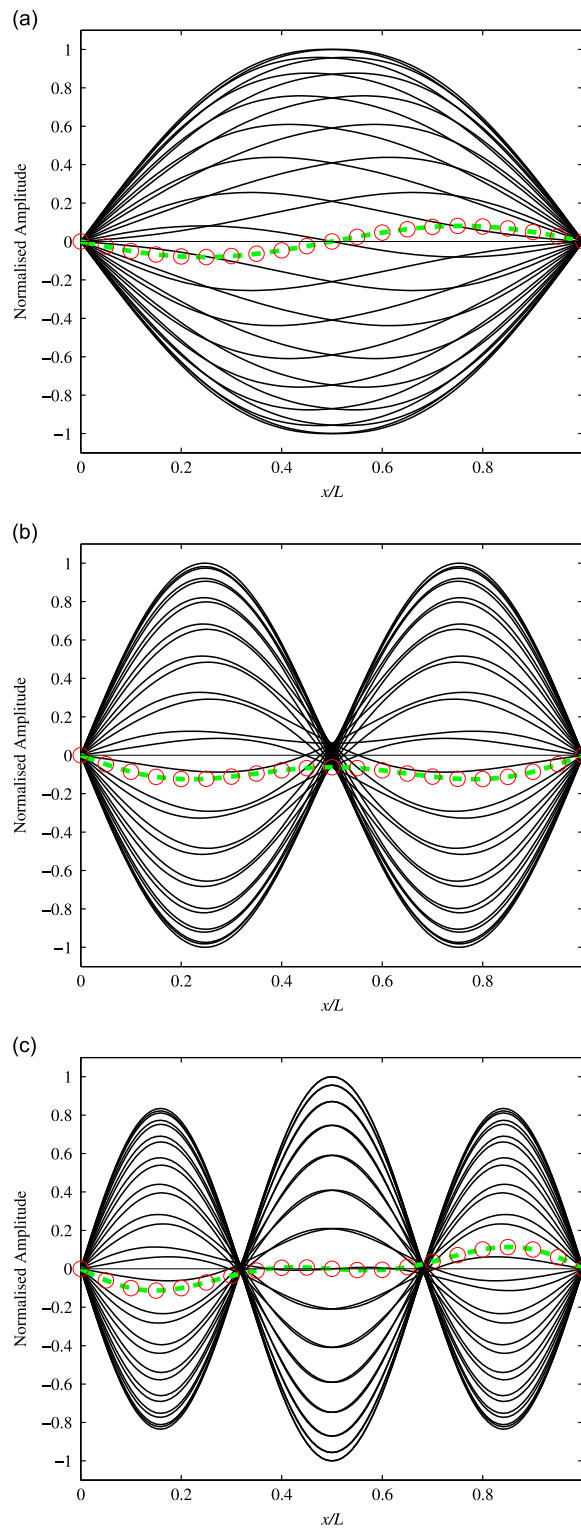


Fig. 6. Snapshots of panel deformation illustrating the neutrally stable oscillatory motion corresponding to the flexible-panel eigenmodes of Fig. 4 for the case of a spring support with $6k_+$ at $U = 0.00378$: (a) Mode 1, (b) Mode 2, and (c) Mode 3. The thick broken line and circle symbols respectively indicate the starting and finishing deformations over the time period of the evaluation.

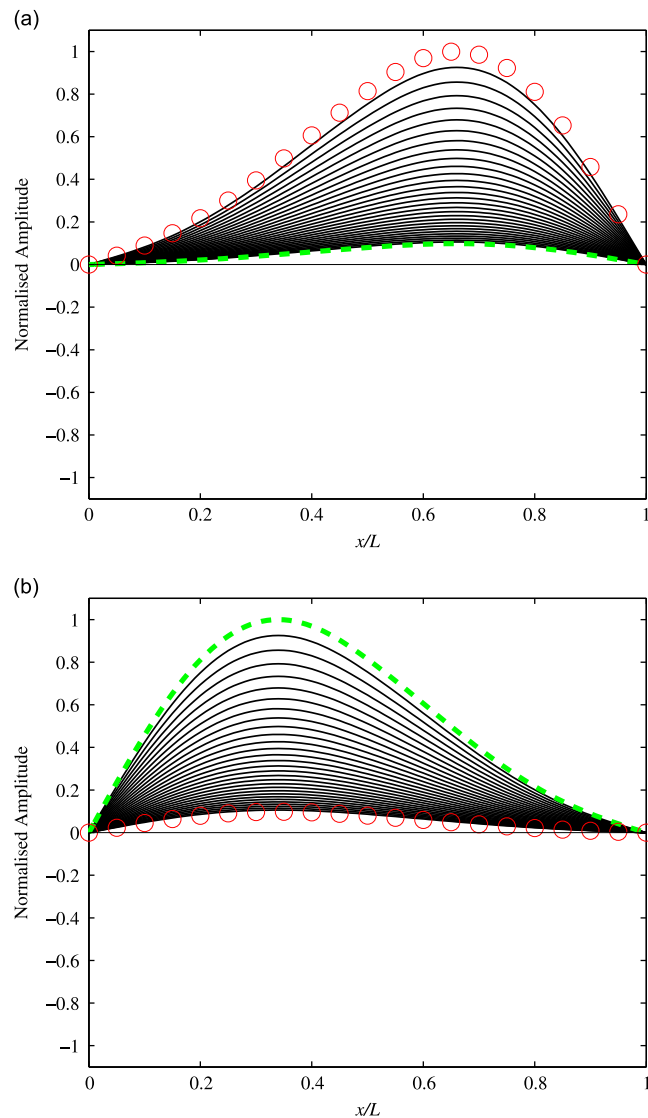


Fig. 7. Snapshots of panel deformation illustrating motion in the divergence range of flow speeds of the flexible-panel eigenmodes of Fig. 4 for the case of a spring support with $6k_s$ at $U' = 0.0151$: (a) amplifying, and (b) decaying solutions of the divergence mode. The thick broken line and circle symbols respectively indicate the starting and finishing deformations over the time period of the evaluation.

an absolute instability that persisted down to zero flow speed for a plate of infinite length. Lucey [14] and Abrahams and Wickham [13] subsequently demonstrated, for a long but finite elastic plate and an infinitely long damped plate respectively, that the Atkins absolute instability existed at the maxima turning point on the lower branch of the wavenumber-frequency dispersion curve and was therefore different to Crighton and Oswell's 'triple-point' absolute instability. The divergence instability in the present work aligns better with the Atkins instability of an infinitely long flexible plate but does not persist down to a zero critical flow speed because, as demonstrated in Fig. 9, it is the finite length of the panel that determines the longest permissible disturbance wavelength and thus the non-zero value of critical flow speed.

Fig. 10 shows the transient response at flow speed $U' = 0.0227$ that is predicted to give the modal-coalescence flutter instability of Fig. 8. Fig. 10a and b show the early response to the initial excitation as a sequence of wall-deformation plots within the time ranges $1\Delta T'$ to $50\Delta T'$ and $50\Delta T'$ to $2500\Delta T'$ respectively where $\Delta T' = 0.813$. At later times in the evolution Fig. 10c shows superimposed panel profiles as time progresses for the time range $2500\Delta T'$ to $125,000\Delta T'$, in equal time steps of $2500\Delta T'$, that follow immediately from that of Fig. 10b. Fig. 10a shows that essentially flexural waves of the plate carry disturbance energy away from the source of excitation in both upstream and downstream directions with a similar phenomenology to that in the establishment of divergence instability described in the preceding paragraph. After reflection from the end points wave superposition occurs and longer wavelength disturbances start to dominate the response as seen in Fig. 10b. Finally, in Fig. 10c, the highly unstable flutter mode becomes established and rapid deformation growth is

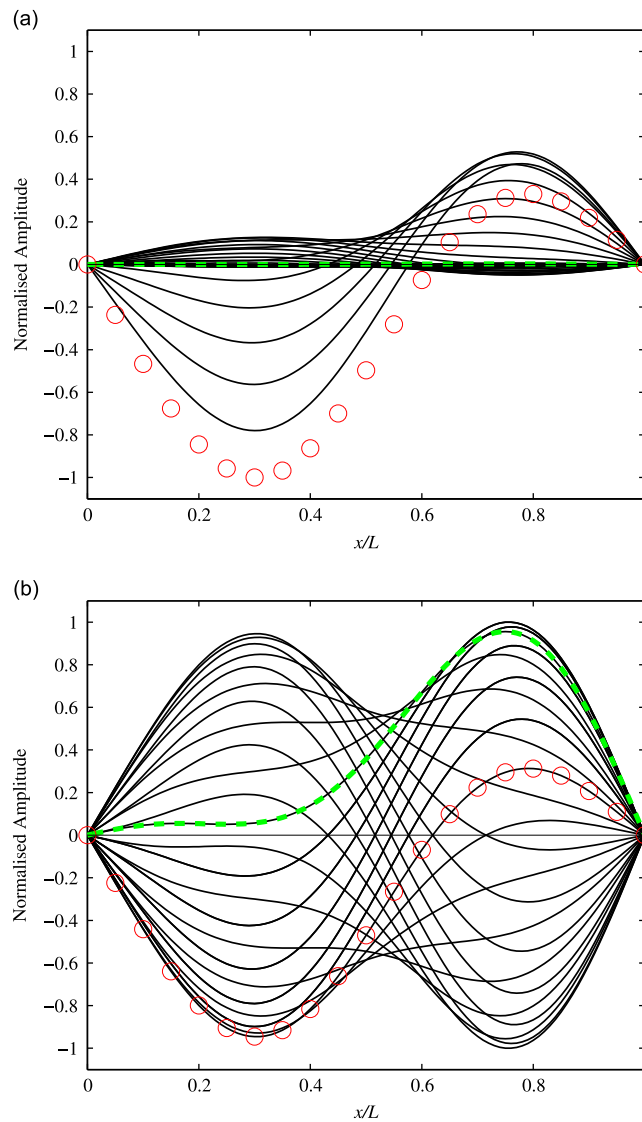


Fig. 8. Snapshots of panel deformation illustrating motion in modal-coalescence-flutter of the flexible-panel eigenmodes of Fig. 4 for the case of a spring support with $6k_s$ at $U^* = 0.0227$: (a) showing modal amplification, and (b) with the modal growth suppressed to illustrate the mode shape. The thick broken line and circle symbols respectively indicate the starting and finishing deformations over the time period of the evaluation.

evidenced. For even later times of the same simulation, Fig. 10d shows a sequence of responses over one cycle of oscillation ($200,000\Delta T^*$ to $220,000\Delta T^*$, in equal time steps of $730\Delta T^*$) to highlight the mode shape of the instability; this is seen to be exactly the same as the infinite-time prediction of Fig. 8a.

Thus, we have mapped out the entire evolution history of divergence instability and modal-coalescence flutter when initiated by a line impulse. The mechanism for disturbance spread at early times means that a similar process of panel destabilisation would occur if the initial excitation were applied at a position on the panel other than its mid-point. Overall, the route to instability closely resembles that termed ‘from waves to modes’ in the studies of [25] for fluid-conveying flexible pipes. Given that high-frequency (lightly loaded) flexural waves feature significantly in the early development of both divergence and flutter instabilities, the effects of dissipation in the structure and/or designing-in structural damping, for example through doping the panel, could serve to inhibit the development of instability at post-critical flow speeds.

We now show the extent to which the strategy of divergence postponement by an added spring support can be taken. Fig. 11a and b show the variation of flow speeds of divergence onset, divergence recovery and modal-coalescence flutter onset with the magnitude of the added spring support, k_s , for two cases of spring location $x_k/L = 0.5$ and 0.25 . For ease of interpretation it is more convenient to non-dimensionalise distance of the added-spring location from the leading edge by the panel length. For each figure $L^* = 92.31$, the same used throughout this sub-section and we note that the critical speeds

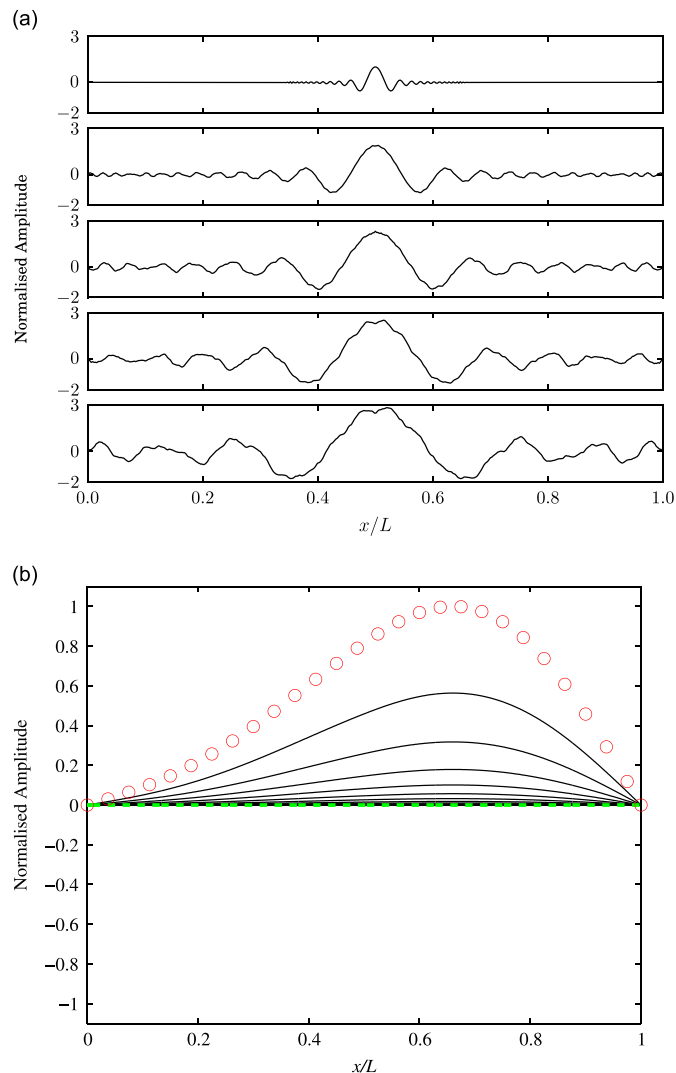


Fig. 9. Development of divergence instability from a line impulse applied at the mid-point of a flexible panel with spring support for the case of Fig. 4 (at $U' = 0.0151$ and with $6k'_s$) and Fig. 7: (a) sequence of instantaneous panel profiles (from top to bottom) at time steps $1\Delta T'$, $10\Delta T'$, $20\Delta T'$, $30\Delta T'$, and $50\Delta T'$, and (b) sequence of superimposed panel profiles for times $0\Delta T'$ to $250,000\Delta T'$ plotted at time increments of $2,500\Delta T'$, where $\Delta T' = 0.813$. In (b) the thick broken line and circle symbols respectively indicate the starting and finishing deformations over the time period of the evaluation.

plotted take the functional form

$$U'_c = f(L', k'_s, x_k/L). \quad (19)$$

These results clearly show that the addition of a single localised spring support can significantly increase the divergence-onset flow speed. As could be expected on physical grounds, this strategy is more effective when the spring is placed at the panel mid-point. When placing it here, it is noted that there is a threshold of approximately $k'_s = 0.4 \times 10^{-3}$ for which further stabilisation of the system ceases. This is because the second system mode replaces the first as the critical mode for divergence onset, the spring support being so stiff that it effectively divides the original panel into two separate panels of equal length. Accordingly, this value may be regarded as optimal for the design of divergence-free flexible panels.

The results presented herein show that the addition of an isolated spring support to the structure can yield a very significant extension to the flow-speed range of a simple flexible panel before divergence instability sets in. To give an engineering feel for this benefit, we provide the following dimensional examples that arise from the non-dimensional results. For aluminium panels subjected to a water flow (*i.e.* defining the properties of the two media) with the single spring added at the panel mid-point, the functional relation of Eq. (19) with divergence onset as the critical speed takes the dimensional form $U_D = f(L/h, k_s, 0.5)$. We consider three aluminium panels typically used for the hulls of high-speed ships. These have lengths and thicknesses: (i) $L = 0.6$ m, $h = 2.5$ mm giving $L/h = 240$, (ii) $L = 1.2$ m, $h = 8.0$ mm giving $L/h = 150$, and (iii) $L = 0.9144$ m, $h = 6.35$ mm giving $L/h = 144$. Table 1 shows the predicted divergence-onset flow speed for each of these

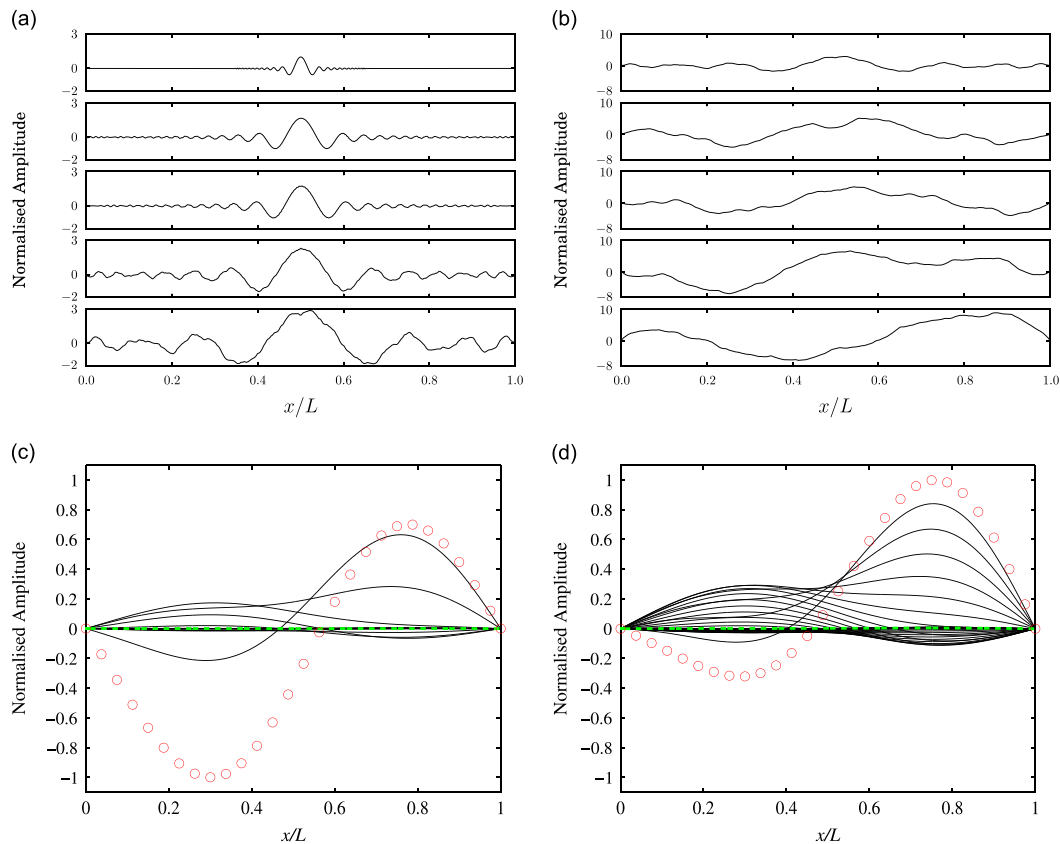


Fig. 10. Development of modal-coalescence flutter from a line impulse applied at the mid-point of a flexible panel with spring support for the case of Fig. 4 (at $U^* = 0.0227$ and with $6k_+$) and Fig. 8: (a) and (b) respectively show sequences $1\Delta T^*$, $6\Delta T^*$, $7\Delta T^*$, $20\Delta T^*$, $50\Delta T^*$ and $50\Delta T^*$, $300\Delta T^*$, $350\Delta T^*$, $1000\Delta T^*$, $2500\Delta T^*$ of instantaneous panel profiles (from top to bottom in each and noting the different scales on the vertical axes), while thereafter (c) shows sequences of superimposed panel profiles for times $2500\Delta T^*$ to $125,000\Delta T^*$ plotted at time increments of $2500\Delta T^*$, and (d) shows motion in the established mode for later times $200,000\Delta T^*$ to $220,000\Delta T^*$ plotted at time increments of $730\Delta T^*$, where $\Delta T^* = 0.813$. In (c) and (d) the thick broken line and circle symbols respectively indicate the starting and finishing deformations over the time period of the evaluation.

panels and how this increases with the addition and stiffening of an added spring support. Note that these predictions from our two-dimensional analysis are lower than those for a truly finite panel held along all four of its edges. For example, [4] shows that a panel with an aspect ratio 1 (width divided by length) has a divergence-onset flow speed that is approximately twice that predicted by the two-dimensional (infinite aspect ratio) analysis herein, whereas at aspect ratio 5 the difference is approximately 5 percent. However, the relative increases to onset flow speeds achieved by adding a single spring support would also be expected for truly finite panels. The data of Table 1 shows how the addition of a spring support can increase the operational speed of a craft. Alternatively, the operational flow-speed limit imposed by hydroelastic instability can be kept constant and a spring support added to permit a thinner panel to be used. Table 2 therefore shows how the thicknesses of the three panels could be reduced if a spring support were to be introduced to keep the divergence-onset flow speed unchanged. While these results indicate material, hence mass, savings, the addition of a transverse array of springs imposes a mass penalty. To quantify this balance, we consider Panel (ii) in Table 2. The panel mass saved, per transverse metre, by reducing its thickness is 3.12 and 5.93 kg/m respectively when introducing added spring support at $6k_+$ and $15k_+$. Suitable transverse arrays of springs would respectively have masses 0.425 kg/m (18 springs per metre with maximum load capacity 1321 N/m) and 1.062 kg/m (45 springs per metre with maximum load capacity 3301 N/m). Thus, the net mass savings, relative to an unsupported panel, when adding spring support at $6k_+$ and $15k_+$, would then respectively be 11 percent and 19 percent which remain a significant engineering benefit.

3.3. Flexible panel with a single-spring support: aeroelastic applications

When considering the non-dimensional FSI system defined by Eqs. (12)–(14) it is evident that the flow speeds of divergence onset, divergence recovery and modal-coalescence flutter onset are, for a simple unsupported elastic panel, functions of the non-dimensional length, L' that is the inverse of the solid-to-fluid mass ratio. Sections 3.1 and 3.2 have primarily used $L' = 70.4$ and 92.3 respectively. We now present the FSI phenomenology of a panel with the much lower value of $L' = 0.225$ that we will show is markedly different from that prevailing at the higher value used in Section 3.2. This finding is of practical

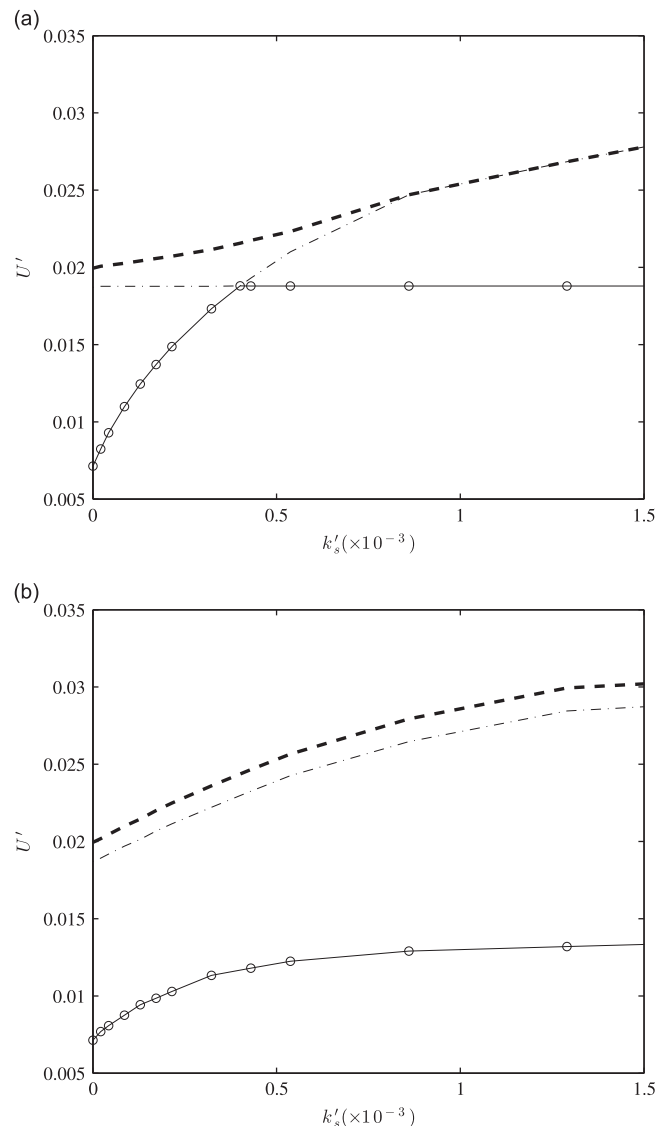


Fig. 11. Variation of divergence-onset (—○—), divergence recovery (---) and modal-coalescence flutter (- · -) onset flow speeds with the coefficient of an added spring support for a flexible panel with $L' = 92.31$: spring added at (a) panel mid-point ($x_c/L = 0.5$), and (b) $x_c/L = 0.25$.

relevance because such results appertain to the aero-elasticity of a typical glass panel of a curtain wall subjected to an axial-flow wind loading with air density $\rho = 1.27 \text{ kg/m}^3$. To illustrate how this non-dimensional data could be constituted, the glass panel would have $h = 0.004 \text{ m}$, $L = 1.7 \text{ m}$, $\rho_m = 2400 \text{ kg/m}^3$, and $B = 381 \text{ N m}$ (having used $E = 6.85 \times 10^{10} \text{ N/m}^2$ and $\nu = 0.2025$). When we investigate the same stabilisation strategy used in Section 3.2, the added spring has stiffness $k_s = nk_+$ given in multiples, n , of $k_+ = 8.5 \times 10^3 \text{ N/m}^2$ that when non-dimensionalised gives $k'_+ = 9.64 \times 10^3$.

Fig. 12 shows the variation of the two lowest system eigenvalues with flow speed for the standard panel and two cases of a panel with an additional spring support, $k'_s = 1k'_+$ and $2k'_+$, located at its centre. We first focus upon the standard case, comparing the solution morphology with Fig. 4 for which the fluid was water. As the air speed is increased divergence-onset is first encountered at $U' = 59.35$; combining this with the present $L' = 0.225$ through Eq. (15) gives the non-dimensional stiffness ratio $\Lambda = 40.1$ for divergence-onset, again in excellent agreement with the previous works as discussed in Section 3.2. Beyond this critical speed the panel undergoes Mode-1 divergence. Further increases to U' then cause Mode 2 to succumb to divergence instability at $U' = 155.0$. In a physical situation Mode-1 divergence would be seen to dominate the panel behaviour because it has a higher amplification rate. The hydroelastic result of Fig. 4 shows Mode-1 divergence recovery with neutral stability of Mode 2 until a further increase to flow speed causes these two oscillatory modes to coalesce into flutter. In contrast, the airflow case features the coalescence of the two unstable non-oscillatory divergence Modes 1 and 2 to create the oscillatory flutter instability. The fact that two non-oscillatory modes can merge to give an oscillatory instability is highly

Table 1

Examples of the increase to divergence-onset flow speed for typical aluminum panels forming the hull of a high-speed ship through the addition of a single spring support at the panel mid point. The length and thickness of the panels are respectively: (i) $L=0.6$ m, $h=2.5$ mm giving $L/h = 240$, (ii) $L=1.2$ m, $h=8.0$ mm giving $L/h = 150$, and (iii) $L=0.9144$ m, $h=6.35$ mm giving $L/h = 144$.

Spring constant ($k_+ = 6 \times 10^3$ N/m ²)	L/h		
	240 Panel (i)	150 Panel (ii)	144 Panel (iii)
$0k_+$	3.7 m/s (7.2 knots)	7.6 m/s (14.7 knots)	8.1 m/s (15.7 knots)
$6k_+$	6.5 m/s (12.6 knots)	9.3 m/s (18.0 knots)	9.8 m/s (19.0 knots)
$15k_+$	9.2 m/s (17.8 knots)	11.4 m/s (22.1 knots)	11.8 m/s (22.9 knots)

Table 2

Examples of material savings (by decreasing panel thickness) keeping the divergence-onset flow speed unchanged for typical aluminium panels forming the hull of a high-speed ship through the addition of a spring support at the panel mid point. Panels (i)–(iii) as described in Table 1.

Spring constant ($k_+ = 6 \times 10^3$ N/m ²)	L		
	0.6 m Panel (i)	1.2 m Panel (ii)	0.9144 m Panel (iii)
$0k_+$	2.5 mm (standard)	8.0 mm (standard)	6.35 mm (standard)
$6k_+$	1.7 mm (31%)	7.0 mm (13%)	5.6 mm (12%)
$15k_+$	1.4 mm (46%)	6.1 mm (24%)	4.9 mm (22%)

unusual, although we have shown earlier in Fig. 7a that, although a divergence eigenmode has zero oscillatory component, its form of amplification gives it the character of a travelling wave; this was first proposed in [16]. The explanation for the unusual overall behaviour is that for airflow the FSI is dominated by fluid-stiffness effects due to the third term (ρU_∞^2 -dependent) of the fluid-pressure loading in Eq. (6). To generate equivalent hydrodynamic-stiffness effects between air (with density ρ_A) and water (with density ρ_W) flows, the fluid-damping and fluid inertia effects, respectively given by the second and first terms on the right-hand side of Eq. (6), are factors of $\sqrt{\rho_A/\rho_W}$ and ρ_A/ρ_W smaller for air than water. When water is the fluid medium the magnitude of these terms is principally responsible for the coupling of Modes 1 and 2 that leads to the far-better known sequence of divergence recovery followed by modal-coalescence flutter.

The foregoing discussion shows that the fluid density and, in particular, its value relative to that of the solid medium is responsible for the solution morphology remarked upon in the standard case of Fig. 12. In the non-dimensional scheme, the panel length L , defined in Eq. (14a), may be interpreted as the fluid-to-solid density ratio for a panel of given dimensional length and thickness. We therefore show how the key flow-speeds of Mode-1 divergence onset, Mode-1 divergence recovery or Mode-2 divergence onset, and modal-coalescence flutter vary with L in Fig. 13. Rather than flow speed, we plot $(U')^2(L')^3$ which is the fluid-to-solid stiffness, Λ , on the vertical axis against the logarithm of $1/L'$ on the horizontal axis because the domain covers a number of decades. First we remark that Fig. 12 indicates that the value of Λ for Mode-1 divergence onset is independent of L' taking the value 40.1. This is to be expected because exactly at divergence onset the panel is static and the solid inertia (and thus density) can play no part in its determination. For post-Mode-1 divergence behaviour, Fig. 13 shows that the system solution follows the pattern typical of water over a metal panel for $1/L'$, inversely proportional to the fluid density, up to a threshold value of approximately 0.57 (noting that $\ln(0.57) = -0.57$ on the horizontal scale). For higher values than this, the fluid density is sufficiently low, relative to that of the solid, that both Modes 1 and 2 concurrently succumb to divergence instability and then coalesce at higher flow speeds to create the flutter instability. This interpretation is based upon density differences between fluid and solid media. The alternative interpretation of Fig. 13 is that, for given solid and fluid media, a panel with low h/L (long panel for a given thickness) has the well-known solution morphology following the sequence of Mode-1 divergence-onset, Mode-1 divergence recovery, modal-coalescence flutter typified by Fig. 4, whereas a panel with high h/L (short panel for a given thickness) evinces the unusual two-mode divergence and then coalescence route to flutter typified by Fig. 12.

We now return to Fig. 12 to consider the effect of adding a spring support to the panel as a stabilisation strategy. It is seen that the added spring postpones Mode-1 divergence onset to higher flow speeds. It does not affect Mode-2 divergence onset because the spring has been added at the panel mid-point where there is a quasi-node for this mode. With regard to post-divergence modal-coalescence flutter, Fig. 12 shows that increasing the spring-stiffness coefficient reduces the flutter-onset

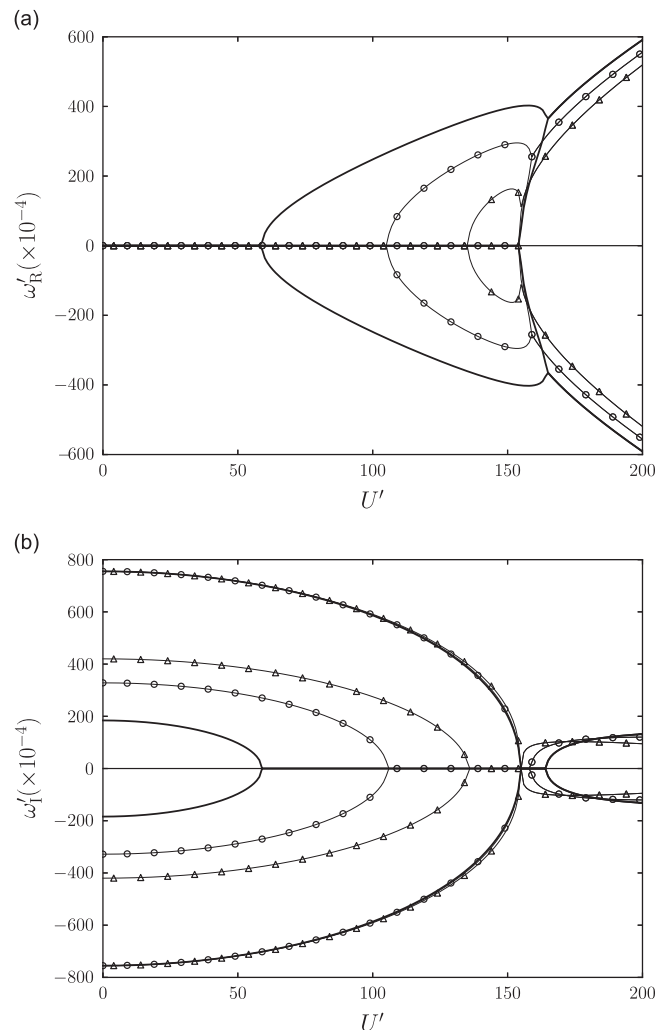


Fig. 12. Variation of the two lowest system eigenvalues, (a) real (positive, growth; negative, decay) part, and (b) imaginary (oscillatory) part, with non-dimensional flow speed for an elastic flexible panel with $L' = 0.225$ for different values of a spring support at the panel mid-point: —, $0k_+$ (homogenous case); $-\circ-$, $1k_+$, $-\triangle-$, $2k_+$, where $k_+ = 9.64 \times 10^3$.

speed slightly and causes the envelope of the amplifying part of its eigenvalue to narrow with increasing flow speed. In Fig. 14 we show the effect of further increases to the spring-stiffness coefficient on the solution morphology. Fig. 14a and d is obtained when $k'_s = 1.5k'_+$ and shows results similar to those shown in Fig. 12. When $k'_s = 2.5k'_+$, Fig. 14b and e shows a clear difference. At flow speeds higher than the range that gives modal-coalescence flutter, the system decouples and returns to Mode-1 and Mode-2 divergence at $U' \approx 240$. Fig. 14c and f shows that when $k'_s = 3.5k'_+$ the modal-coalescence flutter disappears entirely and the system stability for the range of flow speeds shown is dominated by Mode-2 divergence. The continuous variation of divergence- and flutter-onset flow speeds with the spring-stiffness coefficient, k'_s is shown in Fig. 15a and b with the spring located at $x_k/L = 0.5$ and 0.25 respectively. The critical speeds are the loci of the function written as Eq. (19) with $L' = 0.225$ for the present data. With the spring located at the panel mid-point it is seen that the change of solution morphology occurs at $k'_s = 2.69 \times 10^4 (= 2.75k'_+)$ with the replacement of modal-coalescence flutter by two-mode divergence illustrated by the sequence in Fig. 14. Thus, the inclusion of an isolated spring can be used to replace a more damaging dynamic instability such as flutter with divergence buckling of the panel that would become static due to nonlinear saturation if even a marginal level of structural damping were present [17,26]. It is also noted that both Fig. 15a and b indicate that the onset of divergence can be postponed to significantly higher flow speeds through the addition of an isolated spring. Clearly the postponement is greatest when the spring is located at the panel mid-point because it is Mode 1 that gives the onset of divergence below the threshold value of $k'_s = 2.69 \times 10^4$ in Fig. 15a and throughout the range of k'_s for Fig. 15b.

To give an engineering feel for the potential benefits of stabilisation through an added spring support, Table 3 provides dimensional examples of critical wind speeds for glass panels of different lengths and thicknesses. The glass panel has

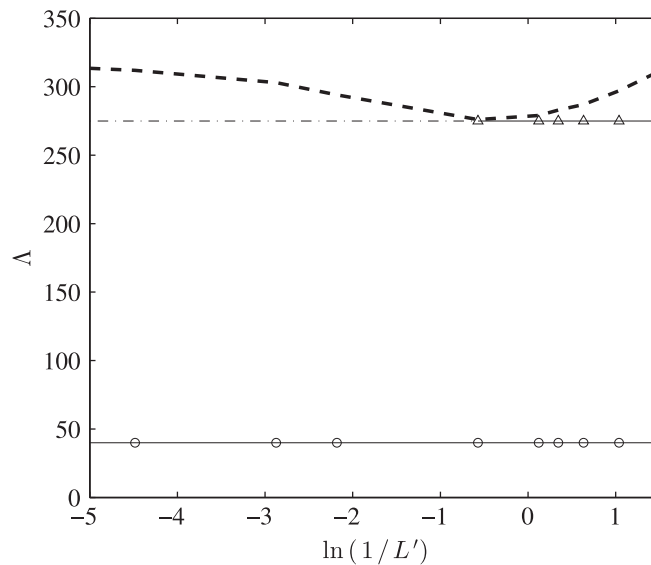


Fig. 13. Variation of Mode-1 divergence-onset (—○—), Mode-1 divergence recovery (---), Mode-2 divergence-onset (—△—) and modal-coalescence flutter (- · -) onset flow speeds ($\Lambda = (U')^2(L')^3$) with the logarithm of the inverse of the mass ratio L' for a simple unsupported elastic panel.

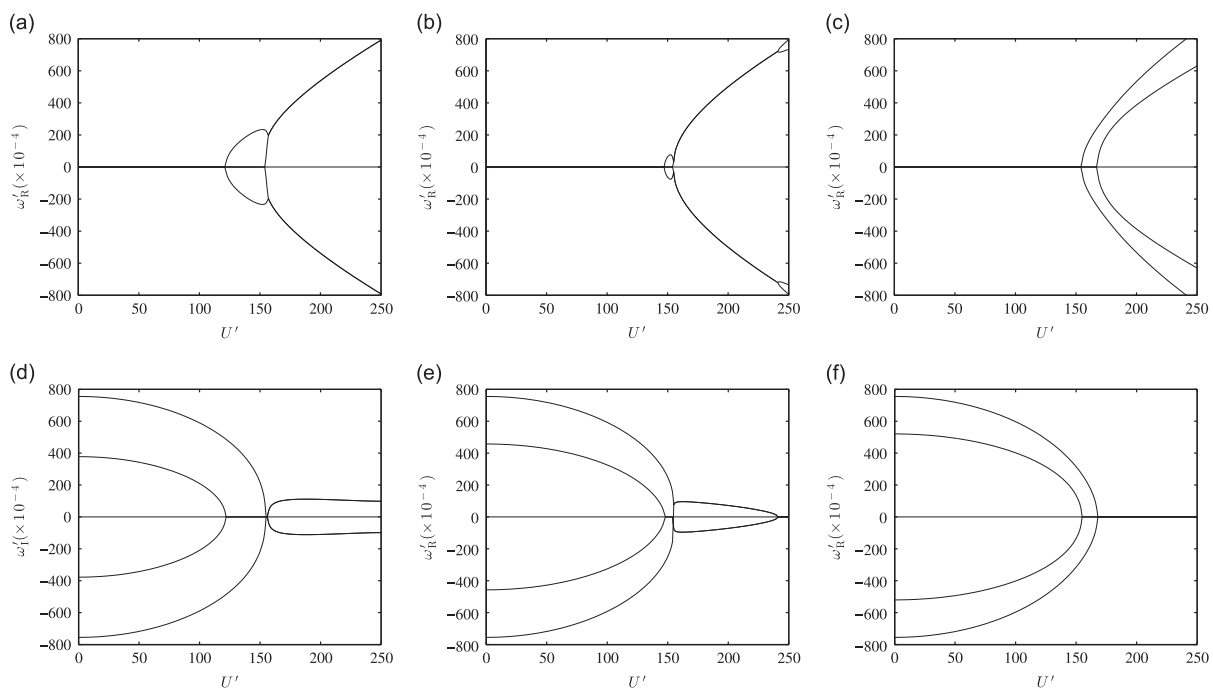


Fig. 14. Variation of the two lowest system eigenvalues, (a), (b) and (c) real (positive, growth; negative, decay) part, and (d), (e) and (f) imaginary (oscillatory) part, with non-dimensional flow speed for an elastic flexible panel with $L' = 0.225$ for different values of a spring support at the panel midpoint: (a) and (d) $1.5k_+$, (b) and (e) $2.5k_+$, and (c) and (f) $3.5k_+$, where $k_+ = 9.64 \times 10^3$.

a single spring added at its mid-point and, with the two media defined, the critical-speed function of Eq. (19) for divergence-onset becomes $U_D = f(L/h, k_s, 0.5)$. Table 3 lists the predicted divergence-onset flow speeds (in km/h) for each of three typical flat tempered-glass panels for different values of the stiffness coefficient of the added spring. Further increases to spring-stiffness would yield even higher divergence-onset wind speeds because, for example, the results for the panel with $L/h = 406$ that has a mass ratio similar to that used to generate Fig. 15a approximately correspond to data points on the rising divergence-onset curve between $k_s = 0$ and 0.5×10^4 . Given that Category 1 cyclones have wind speeds in the range 119–153 km/h, while Category 4 and 5 cyclones respectively generate wind-speeds in the ranges 210–249 km/h and over 250 km, the value of this stabilisation strategy for the panels of curtain walls is clearly evident.

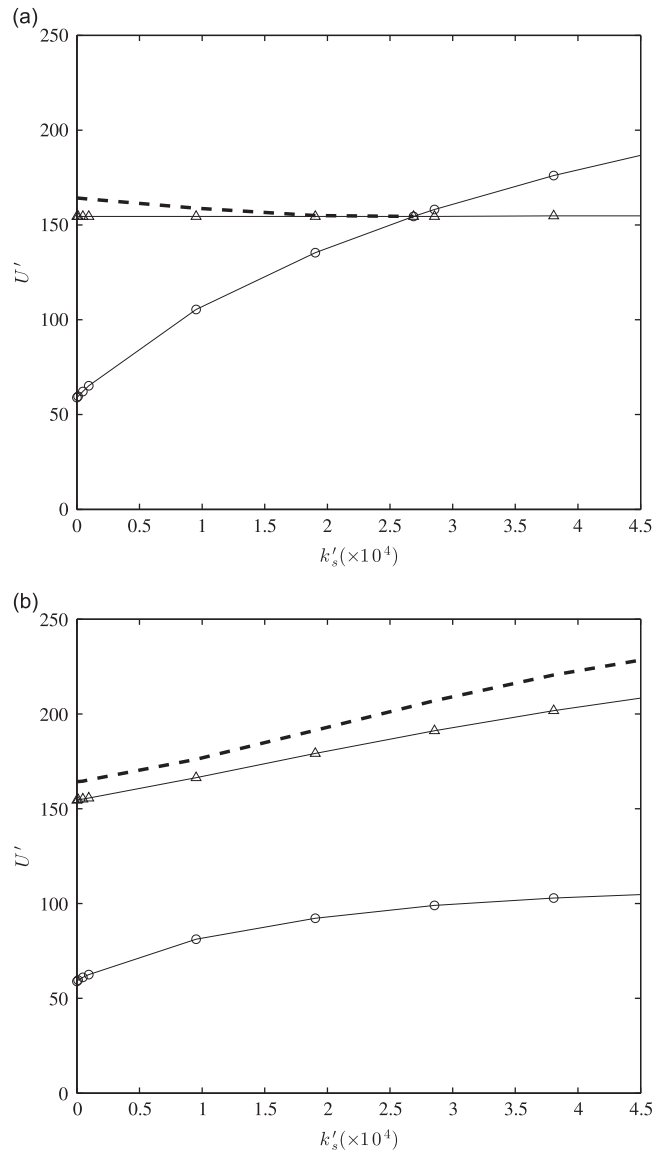


Fig. 15. Variation of Mode-1 divergence-onset (—○—), Mode-2 divergence-onset (—△—) and modal-coalescence flutter (---) onset flow speeds with the coefficient of an added spring support for a flexible panel with $L' = 0.225$: spring added at (a) panel mid-point ($x_k/L = 0.5$) and (b) $x_k/L = 0.25$.

Table 3

Examples of the increase to divergence-onset flow speed for typical flat tempered-glass panels subjected to axial wind-flow through the addition of a single spring-support at the panel mid-point.

Spring constant ($k_+ = 8500 \text{ N/m}^2$)	L/h		
	533 ($L = 2.135 \text{ m}, h = 4 \text{ mm}$)	406 ($L = 2.440 \text{ m}, h = 6 \text{ mm}$)	366 ($L = 3.66 \text{ m}, h = 10 \text{ mm}$)
$0k_+$	126 km/h	189 km/h	219 km/h
$0.05k_+$	139 km/h	200 km/h	230 km/h
$0.5k_+$	224 km/h	266 km/h	287 km/h

4. Conclusions

We have extended the methods of [15] to study the initial-value problem of a finite flexible panel or compliant wall interacting with an inviscid flow for small (linear) disturbance amplitudes. Our results show that waves propagate in both

downstream and upstream directions from a highly localised source of excitation so that with the passage of time instability comes to occupy all locations of the flexible panel. Thus, at applied flow speeds greater than those of divergence and modal-coalescence flutter, destabilisation is global and ultimately leads to the establishment of the system eigenmodes that are predicted by the boundary-value problem. This elucidation of the transients that lead to system instability may permit the design of intervention strategies to postpone, either in developmental time or to a higher critical flow speed, the onset of instability.

By investigating the solution space over a range of non-dimensional mass ratios, we have shown that different eigen-system morphologies can exist. Of particular note is that, when the fluid density is much lower than that of the solid for given panel dimensions (e.g. a wind flow over a realistic glass panel), flutter instability occurs through the coalescence of two non-oscillatory divergence modes. This counter-intuitive behaviour can be understood by recognising that at post-divergence flow speeds, divergence modes evidence a form of downstream wave travel more usually identified with conventional oscillatory travelling waves. A similar phenomenology can occur for denser fluids when the panel is very short for which high flow speeds are required for its destabilisation. The instability phase space has been mapped out to identify quantitatively the value of mass ratio at which the flutter-onset mechanism switches between divergence-mode coalescence and oscillatory-mode coalescence.

The major finding of the present work is that the addition of highly localised stiffening to the structural design of an otherwise homogeneous flexible panel can be a very effective means to postpone instability to a higher flow speed or beneficially modify the form of instability. Divergence postponement can be achieved across the full range of mass ratios, most effectively through the addition of an isolated spring support at the panel mid-chord. A stiffer spring yields a greater postponement until an optimal value of spring stiffness is reached at which the critical mode switches from Mode 1 to Mode 2 and no further postponement of divergence occurs. This type of tailored stabilisation strategy may find engineering use in that it can be far more effective than a 'brute force' approach to design that, for example, thickens the entire panel to prevent aero-/hydro-elastic instability within the envelope of operational flow speeds. For applications with low values of mass ratio, the addition of an isolated spring has also been shown to change the eigen-system morphology so that modal-coalescence flutter instability is replaced by two-mode divergence. This can be advantageous because flutter is a dynamic instability leading to material fatigue whereas divergence instability grows into a static nonlinear buckled state.

Stabilisation by means of an added spring is more effective than including an additional fixed (zero-displacement) restraint within the panel streamwise extent as investigated in [15]. A fixed restraint may be considered an added spring of infinite stiffness in the context of the present work and this exceeds the optimal value of spring-stiffness for divergence postponement. Moreover, [15] showed that a fixed restraint modifies the spatial energy balance of the panel and can introduce a new low-speed form of mild panel flutter. This does not occur in the present work that permits motion of the spring's attachment point to the panel.

Finally, for real engineering applications, the use of an added spring in the present two-dimensional work is questionable because the lower end of the spring must be attached to a rigid structure that could equally be used as a support to replace the panel with two shorter, more stable, flexible panels. However, in the three-dimensional application of localised stiffening, the spring would be replaced by a transverse stiffening strip adhered to the under-surface of the panel and attached to the side edges of the ribbed bay or baffle that the panel encloses. Our preliminary work on this extension, [27], shows that the stabilising benefits demonstrated in the present paper carry across into the full three-dimensional problem thereby making the localised stiffening strategy a practicable technology. Moreover, in the full problem multiple combinations of both transverse and streamwise stiffening strips could be used to optimise instability postponement for a given overall – plate plus stiffening strips – structural mass.

Acknowledgements

The authors gratefully acknowledge the many valuable discussions with Dr. M.W. Pitman that have contributed to the work of this paper and the Australian Research Council through the Grant DP1096376 supporting the project of which the present work forms a part.

References

- [1] J. Dugundji, E. Dowell, B. Perkin, Subsonic flutter of panels on a continuous elastic foundation, *AIAA Journal* 1 (1963) 1146–1154.
- [2] D.S. Weaver, T.S. Unny, The hydroelastic stability of a flat plate, *ASME: Journal of Applied Mechanics* 37 (1971) 823–827.
- [3] C.H. Ellen, The stability of simply supported rectangular surfaces in uniform subsonic flow, *ASME: Journal of Applied Mechanics* 95 (1973) 68–72.
- [4] A.D. Lucey, P.W. Carpenter, The hydroelastic stability of three-dimensional disturbances of a finite compliant panel, *Journal of Sound and Vibration* 165 (1993) 527–552.
- [5] C.Q. Guo, M.P. Paidoussis, Stability of rectangular plates with free side-edges in two-dimensional inviscid channel flow, *Journal of Applied Mechanics* 67 (2000) 171–176.
- [6] T.B. Benjamin, The threefold classification of unstable disturbances in flexible surfaces bounding inviscid flows, *Journal of Fluid Mechanics* 16 (1963) 436–450.
- [7] P.W. Carpenter, A.D. Garrad, The hydrodynamic stability of flows over Kramer-type compliant surfaces. Part: 2. Flow-induced surface instabilities, *Journal of Fluid Mechanics* 170 (1986) 199–232.

- [8] A.D. Lucey, P.W. Carpenter, On the difference between the hydroelastic instability of infinite and very long compliant panels, *Journal of Sound and Vibration* 163 (1) (1993) 176–181.
- [9] N. Peake, On the unsteady motion of a long fluid-loaded elastic plate with mean flow, *Journal of Fluid Mechanics* 507 (2004) 335–366.
- [10] P.R. Brazier-Smith, J.F. Scott, Stability of fluid flow in the presence of a compliant surface, *Wave Motion* 6 (1984) 436–450.
- [11] D.G. Crighton, J.E. Oswell, Fluid loading with mean flow. I. Response of an elastic plate to localized excitation, *Philosophical Transactions of the Royal Society of London A* 335 (1991) 557–592.
- [12] N. Peake, On the behaviour of a fluid-loaded cylindrical shell with mean flow, *Journal of Fluid Mechanics* 338 (1997) 387–410.
- [13] I.D. Abrahams, G.R. Wickham, On transient oscillations of plates in moving fluids, *Wave Motion* 33 (2001) 7–23.
- [14] A.D. Lucey, The excitation of waves on a flexible panel in a uniform flow, *Philosophical Transactions of the Royal Society of London A* 356 (1998) 2999–3039.
- [15] M.W. Pitman, A.D. Lucey, On the direct determination of the eigenmodes of finite flow-structure systems, *Proceedings of the Royal Society A* 465 (2009) 257–281.
- [16] A.D. Lucey, P.W. Carpenter, A numerical simulation of the interaction of a compliant wall and inviscid flow, *Journal of Fluid Mechanics* 234 (1992) 121–146.
- [17] A.D. Lucey, G.J. Cafolla, P.W. Carpenter, M. Yang, The nonlinear hydroelastic behaviour of flexible walls, *Journal of Fluids and Structures* 11 (1997) 717–744.
- [18] A.D. Garrad, P.W. Carpenter, A theoretical investigation of flow-induced instabilities in compliant coatings, *Journal of Sound and Vibration* 84 (4) (1982) 483–500.
- [19] A.D. Lucey, P.K. Sen, P.W. Carpenter, Excitation and evolution of waves on an inhomogeneous flexible wall in a mean flow, *Journal of Fluids and Structures* 18 (2003) 251–267.
- [20] P.W. Carpenter, A.D. Garrad, The hydrodynamic stability of flows over Kramer-type compliant surfaces. Part 1. Flow instabilities, *Journal of Fluid Mechanics* 155 (1985) 465–510.
- [21] M.T. Landahl, On the stability of a laminar incompressible boundary-layer over a flexible surface, *Journal of Fluid Mechanics* 13 (1962) 609–632.
- [22] P. Huerre, P.A. Monkewitz, Local and global instabilities in spatially developing flows, *Annual Review of Fluid Mechanics* 22 (1) (1990) 473–537.
- [23] A.D. Lucey, N. Peake, Wave excitation on flexible walls in the presence of a fluid flow, in: P.W. Carpenter, T.J. Pedley (Eds.), *IUTAM: Flow Through Collapsible Tubes and Past Other Highly Compliant Boundaries*, Kluwer Academic Publishers, 2003, pp. 118–145.
- [24] T. Ishii, Aeroelastic instabilities of simply supported panels in subsonic flow, *Meeting of the American Institute of Aeronautics and Astronautics*, Los Angeles, Paper AIAA-65-752, 1965.
- [25] O. Doaré, E. DeLangre, Local and global instability of fluid-conveying pipes on elastic foundations, *Journal of Fluids and Structures* 16 (1) (2002) 1–14.
- [26] C.H. Ellen, The non-linear stability of panels in incompressible flow, *Journal of Sound and Vibration* 54 (1) (1977) 117–121.
- [27] B.H. Tan, A.D. Lucey, M.W. Pitman, Stability of a structurally inhomogeneous flexible plate in uniform axial flow, in: C. Meskell, G. Bennett (Eds.), *Proceedings of the 10th International Conference on Flow Induced Vibration and Flow-Induced Noise*, 2012, pp. 203–210.

Chapter 3

Control Instability of 3-D Flexible Panel in a Mean Flow

This chapter investigates long-time responses of a 3-D flexible panel and compares with its 2-D counterpart.

NOMENCLATURE

Flexible Panel variables:

K	Spring foundation coefficient	N/m^3
k	Localized added spring coefficient	N/m^2
	Spring is defined as localized added spring support throughout this thesis otherwise stated in the text.	
ν	Poisson ratio of panel material	
L	Length of flexible panel	m
h	Thickness of panel material	m
E	Youngs Modulus	N/m^2
B	Flexural rigidity ($= \frac{Eh^3}{12(1-\nu^2)}$)	Nm
ρ_m	Material density	kg/m^3
η	Interfacial deflection	m

Fluid flow variables:

ϕ	Velocity potential function	
U_∞	Mean-stream velocity	m/s
ρ_f	Fluid density	kg/m^3
μ	Fluid viscosity	Ns/m^2

3.1 Introduction

The previous chapter of a two-dimensional system is depicted in Figure 3.1a and its modelling [15] has been explained and utilized in [32-34]. This 2-D system can be stabilized by adding a single spring support as a local stiffening. It is logical that someone may ask what kind of local stiffening should be added for a real 3-D flexible panel. This chapter is to answer the question. The first objective of the present chapter is to model and solve the three-dimensional system shown in Figure 3.1b, so that system eigenvalues can be extracted to determine and predict the behavior of the plate and, in particular, identify parameter values that result in its instability. The second objective is to determine the effect of localized structural inhomogeneity introduced as a stiffening strip (or rib on the underside of the panel) on the stability of the panel.

The development of the model is broken into three main sections. An overview of the plate mechanics is presented, and then the potential-flow solution methodology and pressure determination is described. Finally, the coupling that yields the fully interactive three-dimensional FSI system is presented, and the resulting governing equation is cast in state-space form so that eigenmodes describing the system at an infinite time after some form initial excitation can be calculated.

3.2 Plate mechanics

The small-amplitude motion of a homogeneous thin flexible plate as shown in Figure =3.1b, fixed along all of its four edges, in the presence of a fluid flow is

$$\rho_m h \frac{\partial^2 \eta}{\partial t^2} + d \frac{\partial \eta}{\partial t} + B \nabla^2 \nabla^2 \eta = -\Delta p(x, y, 0, t), \quad (3.1)$$

where $\eta(x, y, t)$, ρ_m , h , d and B are respectively, the plate's deflection, density, thickness, damping coefficient and flexural rigidity of the flexible panel. $\nabla^2 \nabla^2$ is the biharmonic operator. On the right-hand side, $\Delta p(x, y, z, t)$ is the unsteady perturbation fluid pressure.

The plate is discretised into $M \times N$ equidistantly spaced points at which the mass is lumped. Equation 3.1 is then written in finite-difference form to yield the plate-motion equation

$$\rho_m h [I] \{\ddot{\eta}\} + d [I] \{\dot{\eta}\} + B [D_4] \{\eta\} = -\{\Delta p\}, \quad (3.2)$$

where $[I]$ and $[D_4]$ are the identity and fourth-order biharmonic spatial differentiation matrices respectively with order $P = M \times N$. $\ddot{\eta}$, $\dot{\eta}$, η are column vectors of size P of the acceleration, velocity and deflection of plate respectively, while $\{\Delta p\}$ is the pressure column vector with size P . The boundary conditions for Equations 3.1 and 3.2 used herein are that the plate has four hinged edges enforced as zero deflection and bending moment.

3.3 Flow dynamics

The fluid is assumed to be incompressible and its flow is irrotational and unsteady. A velocity potential can therefore be introduced as a linear combination of uniform flow and a perturbation due to the plate motion. The total velocity potential ψ is the sum of velocity-perturbation potential ϕ and uniform velocity potential with mean flow U_∞ in x -direction

$$\psi(\mathbf{r}, t) = \phi(\mathbf{r}, t) + U_\infty x, \quad (3.3)$$

where $\mathbf{r} = (x, y, z)$. Each of the total velocity potential ψ and the velocity-perturbation potential ϕ satisfy the Laplace equation that incorporates the irrotationality of the flow and enforces mass conservation

$$\nabla^2 \psi = 0, \quad (3.4)$$

$$\nabla^2 \phi = 0. \quad (3.5)$$

The flow field can be written as

$$\mathbf{u}(\mathbf{r}, t) = \nabla\phi(\mathbf{r}, t) + U_\infty\mathbf{i}. \quad (3.6)$$

The perturbation potential ϕ is generated by integrating a distribution of sources of intensity σ over the wall-flow interface S , thereby giving

$$\phi(\mathbf{r}_Q, t) = \int \int_S \frac{\sigma(\mathbf{r})}{|\mathbf{r}_Q - \mathbf{r}|} ds. \quad (3.7)$$

The solution of the Laplace equation must satisfy the kinematic boundary condition that enforces no flow through the impermeable boundary. Accordingly, the velocity of fluid normal to the flexible-plate must equal the flexible-plate velocity in that direction

$$(U_\infty\mathbf{i} + \nabla\phi(x, y, z, t)) \cdot \mathbf{n} = u^p. \quad (3.8)$$

Here \mathbf{n} and u^p are the unit vector and wall speed in the direction of outward normal of the wall-flow interface respectively.

The solution of the Laplace equation can then be used to determine the pressure on the panel through the unsteady Bernoulli equation

$$\rho \frac{\partial \psi}{\partial t} + \frac{1}{2} \rho \vec{U} \cdot \vec{U} + p = \frac{1}{2} \rho U_\infty^2 + p_\infty, \quad (3.9)$$

in which ρ and \vec{U} are the fluid density and velocity vector respectively. By assuming that the wall motion is of small amplitude, Equation 3.9 can be linearised to give

$$\Delta p = -\rho \frac{\partial \phi}{\partial t} - \rho U_\infty \frac{\partial \phi}{\partial x}, \quad (3.10)$$

having substituted for the velocity perturbations using the derivatives of their velocity potential.

As in the structure discretization of Equation 3.2, the solid-fluid interface is discretised into an array of panels numbered $i : 1 \rightarrow M$ and $j : 1 \rightarrow N$. These panels form the

basis for the application of a zero-order boundary-element method using source(-sink) singularities. By applying standard panel-method techniques [35] and their adaptation to numerical simulations of the present problem [36], the disturbance normal velocity, velocity-perturbation potential and tangential velocity induced at each panel can be obtained. Consistent with the foregoing linearization, the source-strength distribution remains in the undisturbed plane, $z = 0$. We then have the straightforward determination of source strengths on any panel i, j through

$$\sigma_{ij} = \frac{1}{2\pi}(U_\infty \alpha_{ij} + u_{ij}^V), \quad (3.11)$$

where α_{ij} and u_{ij}^V are the slope in x-direction and the vertical velocity of the control point respectively. By expressing α_{ij} and u_{ij}^V in terms of wall deflection and wall velocity respectively, the source strength on each panel is related to wall motion only by

$$\sigma_{ij} = \frac{1}{2\pi}(U_\infty [D'_1]\{\eta_{ij}\} + [D^{+'}]\{\dot{\eta}_{ij}\}), \quad (3.12)$$

where $[D^{+'}]$ is a matrix operator for the interfacial vertical speed and $[D'_1]$ is the first order spatial differentiation finite-difference matrix operator. Furthermore, the perturbation potential ϕ_{ij} and tangential perturbation velocity in the x -direction u_{ij} can be derived and are related to the source strength σ_{ij} through

$$\phi_{ij} = [\Phi']\{\sigma_{ij}\}, \quad (3.13)$$

$$u_{ij} = [T']\{\sigma_{ij}\}, \quad (3.14)$$

where $[\Phi']$ and $[T']$ are the potential influence coefficient and the tangential velocity influence matrices.

The pressure perturbation at any panel's control point can now be found using a

discretized form of the linearized unsteady Bernoulli equation

$$\{\Delta p_{ij}\} = -\rho \dot{\phi}_{ij} - \rho U_{\infty} u_{ij}. \quad (3.15)$$

By substituting Equations 3.12, 3.13, and 3.14 into Equation 3.15, the perturbation pressure is found and seen to be related to wall deflection. $[D'_1]$, $[D^{+'}]$, $[\Phi']$ and $[T']$ are transformed into their corresponding square coefficient matrices $[D_1]$, $[D^+]$, $[\Phi]$ and $[T]$ of size P . The matrices of system variables are transformed into variable column vectors of size P . Thus the interfacial pressure can be written as

$$-\{\Delta p\} = \frac{\rho}{2\pi} [\Phi][D^+]\{\dot{\eta}\} + \frac{\rho}{2\pi} U_{\infty} ([\Phi][D_1] + [T][D^+])\{\dot{\eta}\} + \frac{\rho}{2\pi} U_{\infty}^2 [T][D_1]\{\eta\} . \quad (3.16)$$

3.4 Coupled fluid-structure system

We now assemble the coupled FSI system equation. The interfacial fluid pressure of Equation 3.16 is substituted into the plate-motion equation 3.2 and re-arranging, we obtain

$$[A]\{\ddot{\eta}\} + [B]\{\dot{\eta}\} + [C]\{\eta\} = 0 , \quad (3.17)$$

where

$$\begin{aligned} [A] &= -\rho_m h [I] + \frac{\rho}{2\pi} [\Phi][D^+], \\ [B] &= -d [I] + \frac{\rho}{2\pi} U_{\infty} ([\Phi][D_1] + [T][D^+]), \\ [C] &= -B [D_4] + \frac{\rho}{2\pi} U_{\infty}^2 [T][D_1]. \end{aligned}$$

Re-arranging Equation 3.17 so that the left-hand side is the acceleration term gives

$$\{\ddot{\eta}\} = -[A]^{-1}[B]\{\dot{\eta}\} - [A]^{-1}[C]\{\eta\}. \quad (3.18)$$

We now define $[E] = -[A]^{-1}[B]$ and $[F] = -[A]^{-1}[C]$, so that Equation 3.18 becomes

$$\{\dot{\eta}\} = [E]\{\dot{\eta}\} + [F]\{\eta\}. \quad (3.19)$$

Introducing state variables $x_i = \eta_i$ and $x_{P+i} = \dot{\eta}_i$ for i from 1st to the P^{th} point, the $2P$ output vector for the state-space model is

$$\begin{Bmatrix} \{\eta\} \\ \{\dot{\eta}\} \end{Bmatrix} = \{x\}. \quad (3.20)$$

Using these definitions, equation 3.18 is then converted into the state differential equation

$$\{\dot{x}\} = \begin{bmatrix} 0 & I \\ [F] & [E] \end{bmatrix} \{x\}, \quad (3.21)$$

and letting

$$[H] = \begin{bmatrix} 0 & I \\ [F] & [E] \end{bmatrix},$$

noting that matrix H is $2P \times 2P$, the final form of the state differential equation 3.21 is

$$\{\dot{x}\} = [H]\{x\}. \quad (3.22)$$

The long-time response is found by first assuming single-frequency response in the time domain, and then extracting the resulting eigenvalues of $[H]$. The single-frequency response is proportional to e^{st} where s is a complex variable; the imaginary part is the vibration frequency while the real part indicates growth or decay of the system disturbance. Finally, the system eigenvectors can then be used to assemble the deflection, $\eta(x,t)$, of the panel.

3.5 Modelling of transverse stiffening strip

To incorporate the effect of a stiffening strip notionally attached to the underside to the panel a transverse (thin) beam is conceived, straddling the panel, as depicted in Figure 1b. The beam has second moment of area I and elastic modulus E ; in this paper it is aligned with the y -direction and thus contributes an additional restoring force (per unit area) of

$$(EI) \frac{\partial^4 \eta}{\partial y^4} \quad (3.23)$$

that acts over a single line of boundary-element panels, $j : 1 \rightarrow N$, and which, when discretised, generates a further, η -dependent term in the left-hand side Equation 3.2. Clearly a similar approach could be used to incorporate one or more stiffeners in a combination of either the x - and/or y -directions. In the present investigation, only a transverse stiffener located at the plate mid-line, $x = a/2$, is used and we neglect its inertial effects. In support of the latter assumption, it was shown in [36] that significant added mass - of the order of the plate mass - is necessary to modify the flutter behaviour in the related problem of a cantilevered-free flexible plate.

3.6 Long-time responses of homogeneous and inhomogeneous system

The results presented in this paper serve first to demonstrate the integrity of the new modelling for the case of a homogeneous plate and show how its phenomenology is similar to that of the antecedent two-dimensional model. Thereafter, the stabilization of the flexible plate through the addition of a stiffener is addressed.

The homogeneous-plate system can be shown [3, 4, 31, 32] to be governed by two non-dimensional control parameters, the fluid-to-solid mass ratio (or non-dimensional plate length) and the fluid-to-solid stiffness ratio (or non-dimensional flow speed), respectively defined by

$$L' = \frac{\rho_f a}{\rho_m h} \quad \text{and} \quad \Lambda^F = \frac{\rho_f U_\infty^2 a^3}{B}, \quad (3.24a,b)$$

in addition to which the aspect ratio (b/a) needs to be defined. Hereinafter we will, for convenience, to the terms in Equation 3.24a,b as the mass ratio and flow speed. Consistency with these non-dimensional parameters requires that time be non-dimensionalised using a/U_∞ . In the results that follow, we also provide physical examples to give an engineering feel for types of systems to which the results are applicable. Throughout this paper we consider only elastic plates, hence $d = 0$ in Equation 3.1; the effect of energy dissipation in the structure has been addressed in [15].

3.6.1 2-D Homogenous system: high mass ratio and low mass ratio

As a reference, Figure 3.2 shows the computed variation of eigenvalues with flow speed for the well-known two-dimensional analysis (e.g. [2,3,15]). Although all 400 system eigenvalues are calculated, only the two with the lowest frequencies have been plotted for clarity. Two distinct values of mass ratio are presented that, for a plate of given length and thickness, could represent water ($\rho_f = 1000\text{kg}/\text{m}^3$) and air ($\rho_f = 1.27\text{kg}/\text{m}^3$) flow over an aluminum panel of length 1 m and thickness 1 cm. These two cases respectively yield mass ratios of 38.5 and 0.049. For both water and air flows, divergence sets in at a non-dimensional flow speed of 40.1; this is in excellent agreement with the Galerkin-method based analyses of [2,3]. As the flow speed is increased, the high-mass ratio results (water) evince divergence recovery and then modal-coalesce flutter occurs. This solution morphology, and the flow-speed values at which these events occur, agree well with previous studies [2,3,15]. For the mass-ratio case (air) this sequence is very different: instead of first-mode divergence recovery, the second mode also undergoes divergence instability and at higher flow speeds, these two non-oscillatory modes coalesce to give flutter. This somewhat surprising result -

that could also occur for very short panels with a water flow having the same mass ratio as the present air case - arises from the dominance of the aero-/hydro-dynamic stiffness in the fluid pressure loading; it is explained in more detail in [34].

3.6.2 3-D Homogenous system: high mass ratio and low mass ratio

Results of the corresponding (to Figure 3.2) three-dimensional analysis are shown in Figure 3.3 for a panel of aspect ratio unity; i.e. a 1 m \times 1 m aluminum panel (for which 3,200 system eigenvalues are calculated). The non-dimensional divergence-onset flow speed is seen to be much higher than that of the two-dimensional analysis. This is because the fixed side edges contribute additional structural restraint to the system as well as contributing to a transverse scaling of the flow pressure that is responsible for destabilization; the latter also features in the destabilisation of cantilevered-free plates of finite width [37]. The present value of divergence-onset flow speed and the solution morphology for the high mass-ratio case (water) agrees well with that of the Galerkin analysis for the same system [4] and serves to validate the present methods. What these results show is that the sequence of destabilisation events - from divergence through to flutter - is the same as for the two-dimensional analysis. Qualitatively, a two-dimensional analysis can be used to predict the physics of the FSI system, while the three-dimensional analysis must be used for the quantification of divergence and flutter instability onset flow speeds.

3.6.3 2-D Inhomogeneous system: local stiffening by spring and high/low mass ratio

We now present results for a strategy of stabilization by adding additional localized stiffness to the flexible plate. For the two-dimensional analysis, additional stiffnesses are incorporated by the inclusion of a localized spring support at the panel mid-point as shown in Figure 3.1a. Figure 3.4a shows the variation of divergence-onset, divergence-recovery and modal-coalescence flutter-onset flow speeds with the coefficient of the

added spring support for a high value of mass-ratio, 92.3, representing water flow over an aluminum panel of length 0.6 m and thickness 2.5 mm (hence $B = 76.6Nm$). The spring coefficient, k , is non-dimensionalised through division by $(\rho_m h)^3 / (\rho_f^3 B)$. Figure 3.4b shows the same variations for a low mass ratio 0.226, representing air flow over a glass panel of length 1.7 m and thickness 4 mm (hence $B = 381 Nm$) typical of that found in curtain walls of high-rise buildings.

In both high and low mass-ratio cases, the addition of a spring support is seen to be very effective in increasing the critical flow speed of (Mode 1) divergence-onset. However, there is a limit to this strategy because at a threshold value of spring stiffness, Mode 2 takes over as being critical. This is understandable because Mode 2 has a (quasi) node at the panel mid-point where the spring has been located. At higher values of spring stiffness than this threshold the solution morphologies between the high and low mass-ratio cases differ. For the former, the standard sequence of divergence recovery followed by modal-coalescence flutter (seen in Figure 3.2) continues to hold although the neutral-stability flow-speed range between divergence recovery and flutter onset reduces to zero for a very stiff spring. However, for low mass ratio, values of spring stiffness above the threshold value yield concurrent Mode 1 and Mode 2 divergence that replaces modal-coalescence flutter. For glass panels this may be advantageous as it is flutter that is the most destructive instability.

Clearly the introduction of an isolated spring support would require some form of additional structure on which to mount its base; as such, it can only be regarded as an idealization of panel stiffening for two-dimensional analyses. The practicable way to stiffen a flexible panel is to introduce a stiffening rib that straddles the panel in the transverse direction as shown in Figure 3.1b to which we now turn in the three-dimensional analysis.

3.6.4 3-D Inhomogeneous system: local stiffening by transverse strip and high/low mass ratio

Figures 3.5a and 3.5b respectively show the variation of divergence-onset, divergence-recovery or Mode-2 divergence onset, and modal-coalescence flutter-onset flow speeds with the flexural rigidity, EI (non-dimensionalised using the plate flexural rigidity B) of the stiffener located at the panel mid-line for the two cases of high (water) and low (air) mass ratio that generated the results in Figure 3.3 for an aluminum panel of aspect ratio unity. Comparing these with the results in Figures 3.4a and 3.4b - the two-dimensional analysis of added stiffness - indicates that the qualitative effects are almost identical. Thus the discussions of the phenomenology for each of Figures 3.4a and 3.4b respectively carry across to the three-dimensional systems of Figures 3.5a and 3.5b. Most importantly, it is shown how and why even a single stiffening rib can be used very effectively to control the hydro-/aero-elastic stability of a flexible panel.

To give qualitative feel for the types of deformation that would result when a transverse stiffening strip (or rib) is added to the mid-line of an otherwise homogeneous flexible plate, we present a series of mode shapes in Figures 3.6 - 3.8. Each of these is for the case of high mass ratio (water over aluminum) and with the stiffener having $EI/B = 2$; the sequence of results pertains to points in the stability map of Figure 3.5a at different flow speeds on the vertical line $EI/B = 2$.

Figure 3.6 illustrates panel behaviour typical in the neutrally stable pre-divergence range of flow speeds. The effect of the stiffening strip can especially be seen in the shape of Mode 1 that features a strong (in vacuo) Mode-2 type content.

Figure 3.7 illustrates panel behaviour typical in the divergence range of flow speeds. The effect of the stiffening strip is to reduce the mid-point deflection and thereby introduce a second-mode content to the unstable mode. Finally, Figure 3.8 shows a typical modal-coalescence flutter. While the modal coalescence has occurred between systems Modes 1 and 2 (see Figure 3.3), non-negligible elements of (in vacuo) Modes 3 and 4 are seen; the stiffening strip tends to advance the order of basis modes that contribute

to the panel's behaviour.

3.7 The effect of transverse and streamwise stiffening strips on a 3-D flexible panel

We study the three-dimensional stability of a fluid-loaded flexible panel to determine the effectiveness of adding localized stiffening to control or postpone instability. A hybrid of computational and theoretical modelling is used to cast an eigenvalue problem for the fluid-structure system. It is shown that the addition of each of transverse and streamwise stiffening strips postpones divergence onset but for the former there is a threshold strip stiffness above which no further postponement is possible. Streamwise stiffening is additionally shown to be effective for increasing post-divergence flutter-onset flow speeds while in aero-elastic applications a transverse stiffening strip can be used to replace flutter instability with divergence. The present results suggest a relatively economical and practicable way to ameliorate panel instability in both hydro- and aero-elastic applications.

3.7.1 Equations for transverse and streamwise stiffening strips

This section restates the modelling of the two stiffening strips. Details of the modelling are provided in the section 1, 2, & 3 or [15, 27]; for the results of this chapter the modelling has been extended to incorporate a streamwise stiffening strip.

A streamwise or transverse (thin) beam is conceived to incorporate the effect of a stiffening strip notionally attached to the underside to the panel as depicted in Figure 3.9. The beam has second moment of area I and elastic modulus E ; in this chapter it can be aligned with the x - or y - direction and thus contributes an additional restoring force (per unit area) as in the following equations,

$$(EI_x) \frac{\partial^4 \eta}{\partial x^4} , \quad (3.24)$$

$$(EI_y) \frac{\partial^4 \eta}{\partial y^4} . \quad (3.25)$$

The homogeneous fluid-structure is controlled by three parameters, namely the fluid-to-solid mass and stiffness ratios, respectively defined by $L' = \rho a / (\rho_m h)$ and $\Lambda^F = \rho U_\infty^2 a^3 / B$, and the aspect ratio of the plate, $A = b/a$, in which a , b and h are respectively the length (in the flow direction), width and thickness of the plate that has density and flexural rigidity ρ_m and B ; the fluid has density ρ and speed U_∞ . In the structurally inhomogeneous system, the stiffness of the added strip is described relative to the flexural rigidity of the plate; i.e. EI/B . For each of the transverse and streamwise cases studied in this paper, the stiffening strip is respectively located at the mid-chord and mid-width of the panel although our methods can be used for its addition at any position. For the results of this paper, we use a plate that is hinged along its edges and throughout has aspect ratio $A = 1$ discretised into 1600 square panels

3.7.2 Results of the effectiveness of streamwise and transverse stiffening strips

Figures 3.10a and 3.10b show the variation of system eigenvalues with applied flow speed for two very different values of mass ratio, $L' = 38.5$ and 0.049 , that respectively typify water flow over the aluminium panel of a high-speed ship and airflow over the glass panel of a curtain wall of a high-rise building. The upper and lower panels show the real (Ω_R) and imaginary (Ω_I) parts of the system eigenvalues (frequencies), non-dimensionalised with respect to the frequency of fundamental mode of the corresponding two-dimensional system, that respectively indicate the growth(+ve)/decay(-ve) and oscillatory motion of the mode. In each of Figures 3.10a and 3.10b, we plot the eigen-values for the homogeneous case and when each of a transverse and streamwise stiffening strip with $EI/B = 1$ has been added to the panel. For both the homogeneous cases, Mode-1 divergence is first seen to occur when $\Lambda^F = 202$ because exactly at onset the panel is static through the balance of flow and structural stiffnesses; this

critical value, along with the post-divergence features of the eigen-plot, is in excellent agreement with the results of [4] obtained using a Galerkin analysis and serves to validate the present modelling. Both transverse and streamwise stiffening strips are seen to increase the value of divergence-onset flow speed (Λ^F for a given panel geometry and material properties) in both water- and air-flow applications. However, it is seen that the streamwise stiffening strip also confers a marked postponement to modal-coalescence flutter. This is because streamwise stiffening beneficially affects both of the coalescing (streamwise) Modes 1 and 2 whereas a mid-chord transverse stiffening strip has little effect on Mode 2 because it is located at that mode's nodal line. Note that these figures also feature eigenstates of the second transverse mode but these have much higher divergence- and flutter-onset flow speeds than those with the fundamental transverse mode discussed above.

Clearly, Figures 3.10a and 3.10b indicate that the addition of a localised stiffening strip is a very effective way to postpone divergence onset and, for a streamwise orientation, the modal coalescence flutter that replaces divergence instability at higher flow speeds. Figure 3.11 serves to quantify these benefits for the addition of transverse and streamwise stiffening strips for the two cases of applications to high (water) mass-ratio - Figures 3.11a and 3.11b - and low (air) mass-ratio - Figures 3.11c and 3.11d. Accordingly, the variations of the critical flow speeds (as Λ^F) for each of divergence onset, divergence-recovery or two-mode divergence, and modal-coalescence flutter onset are plotted against EI/B , the stiffness of the added strip.

For the typical high mass-ratio case, the results of Figures 3.11a and 3.11b show that while both types of stiffening strip can be used to increase the divergence-onset flow speed, there exists a maximum value of stiffness for which this strategy can be used when a transverse strip is used. This is because further increases to its stiffness sees Mode 2 become the critical mode for divergence as the stiffener is effectively located at the (transverse) nodal line of Mode 2. The typical low mass-ratio case summarised by Figures 3.11c and 3.11d feature a different sequence of (increasing) critical speeds wherein initial Mode-1 divergence onset is then followed by Mode 2

divergence onset and finally by flutter due to the coalescence of the two divergence modes. Both transverse and streamwise stiffening strips are seen to be effective for the postponement of Mode-1 divergence while a streamwise strip is also effective in the postponement of modal-coalescence flutter. Higher values of transverse stiffening (results not shown here) also evidence a limit beyond which Mode 2 becomes the critical mode and no further postponement is obtained. However, beyond this threshold value of EI/B modal-coalescence flutter no longer exists and this may be advantageous for glass panels that have little ductility and are therefore readily damaged by a vibrational instability over even a short duration of loading.

3.8 Conclusions

A hybrid of theoretical and computational methods has been developed to study the linear three-dimensional hydro-/aero-elasticity of a flexible panel held along all four of its edges. The main merit of this method is that it can be used to analyse the FSI of panels having arbitrary structural inhomogeneity.

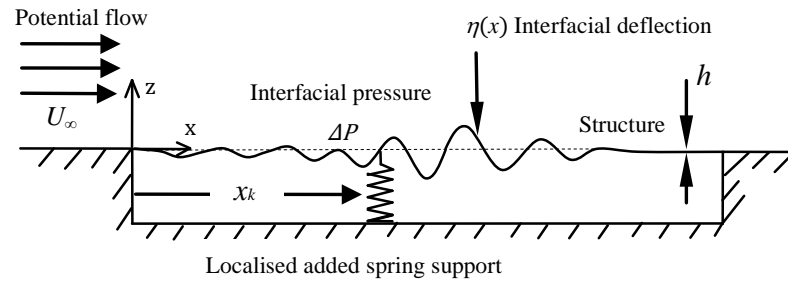
The investigations of this paper has used the method to determine the effect of localized added stiffness on a panel's behaviour, in particular the instability boundaries of divergence and modal-coalescence flutter. It has shown that a transverse stiffening rib can yield significant increases to the divergence-onset flow speed up to a certain threshold value of rib stiffness. This finding would be of engineering benefit in such applications as the panels of high-speed ship hulls.

For low fluid-to-solid density ratios (the mass ratio for given panel length and thickness), sufficiently high stiffness of the added rib eliminates the coalescence of the first two modes, replacing flutter with divergence of both of these modes. This effect would be of benefit in applications such as wind-loaded glass panels of curtain walls of high-rise buildings given that divergence, which would statically saturate at finite amplitude, is far less destructive than flutter.

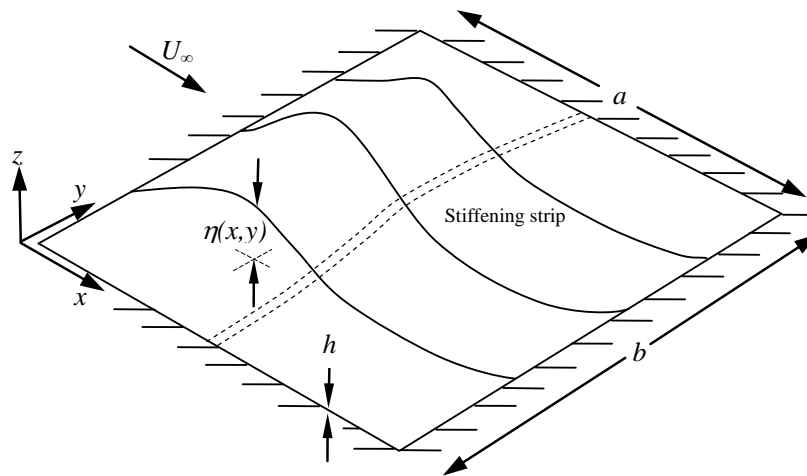
The present study has shown that a two-dimensional analysis of the system using

an isolated spring to represent the transverse rib of a flexible panel is able to capture qualitatively all of the phenomenology of the full three-dimensional FSI system.

The hybrid methods has been developed and deployed to compare and contrast the effectiveness of transverse and streamwise stiffening strip for the control of hydro- and aero-elastic instabilities of an otherwise homogeneous elastic panel. It is shown that both forms of stiffening can be used to postpone divergence onset flow speeds. However, there is a threshold stiffness above which no further gains are obtained when a transverse strip is used. For high mass-ratio systems typical in hydro-elasticity, the use of streamwise stiffening strip also gives substantial increases to the onset flow speed of post-divergence flutter while for low mass ratios typical in aero-elasticity a transverse orientation is able to suppress flutter. These findings set the basis for the study and optimization of more complex arrangements of stiffening strips as a strategy for the control of flow-induced panel instability.

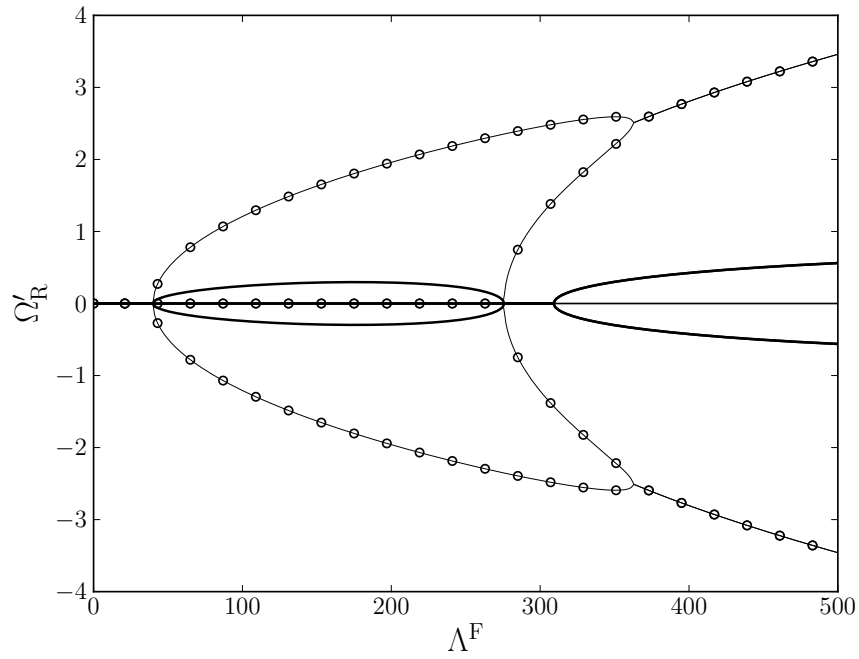


(a)

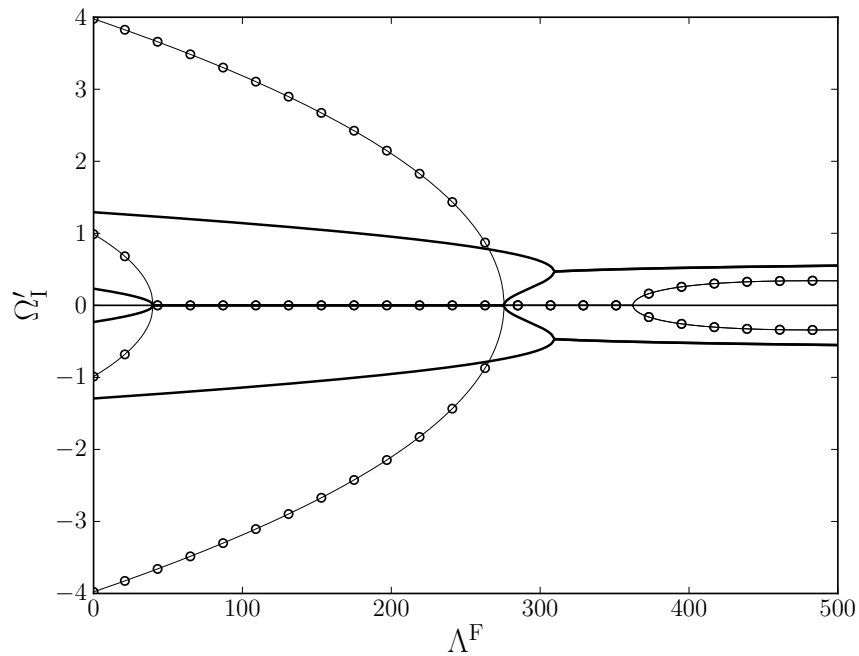


(b)

Figure 3.1: Schematics of the (a) two-dimensional (side view) and (b) three-dimensional (isometric view) problems.

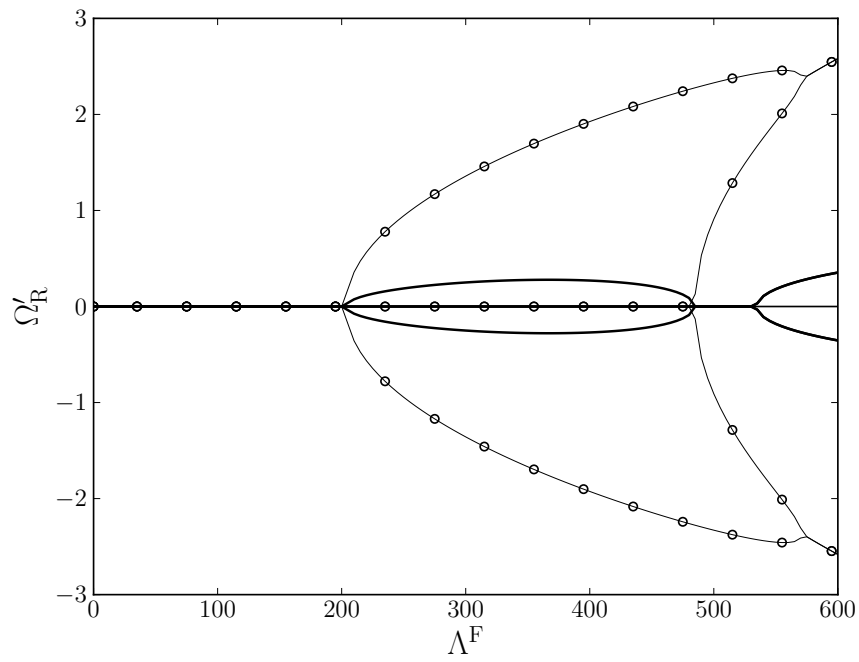


(a)

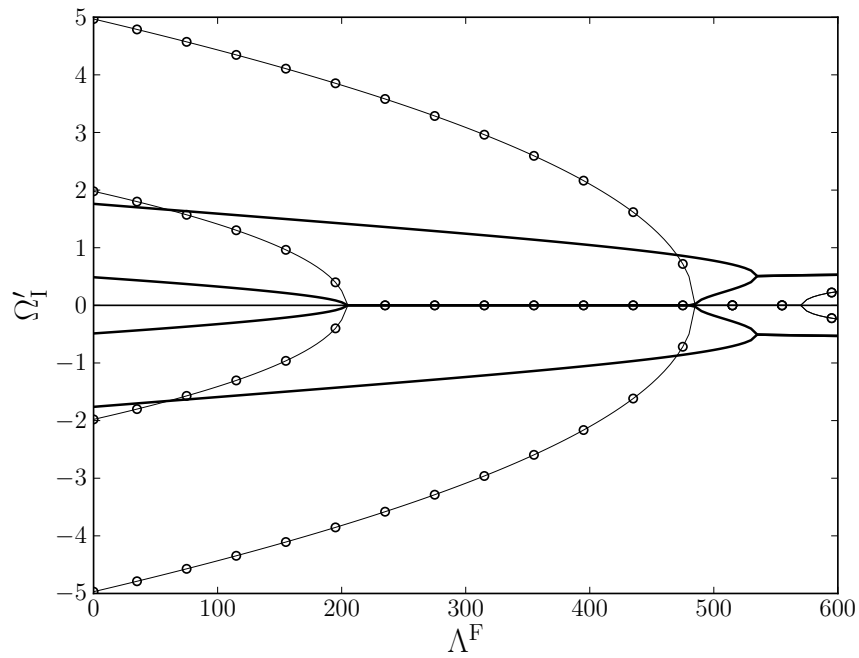


(b)

Figure 3.2: Two-dimensional analysis: variation of system eigenvalues with non-dimensional flow speed for — high mass ratio = 38.5 (water over aluminum) and —o— low mass ratio = 0.049 (air over aluminum): (a) real part (growth/decay) and (b) imaginary part (oscillation frequency) of eigenvalues.

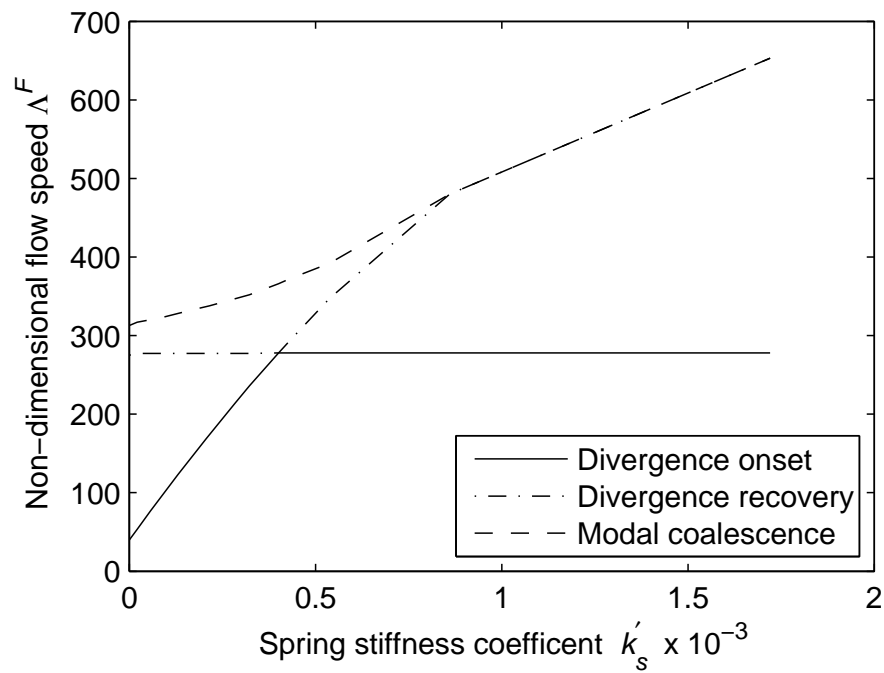


(a)

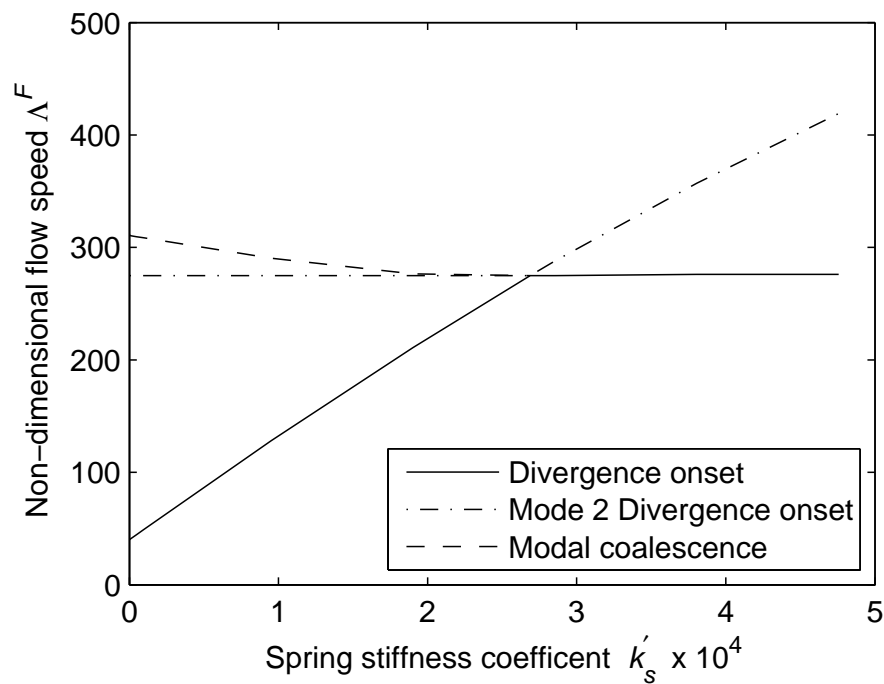


(b)

Figure 3.3: Three-dimensional analysis: variation of system eigenvalues with non-dimensional flow speed for a panel with aspect ratio unit. legend and sub-figure title as in fig. 2.

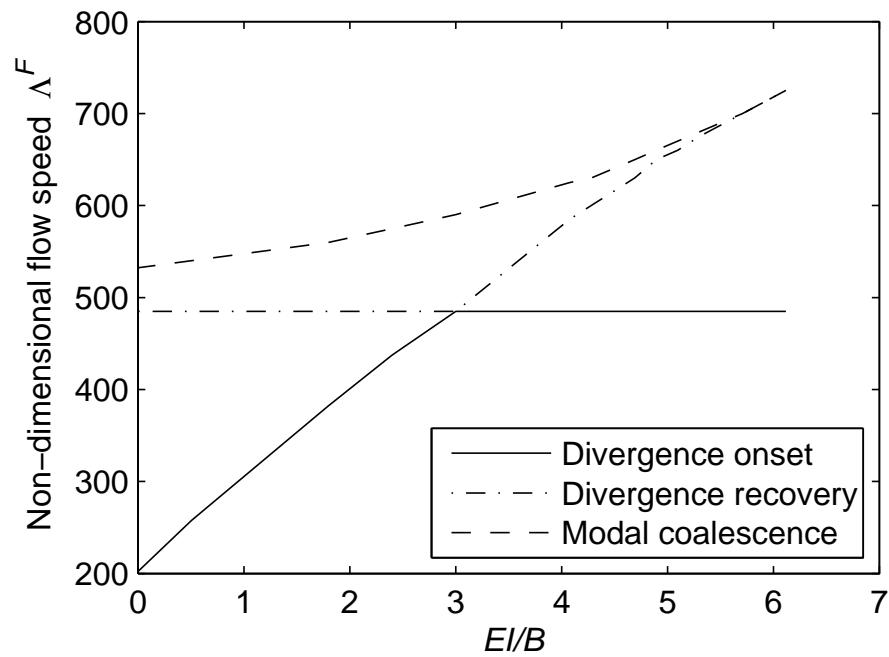


(a)

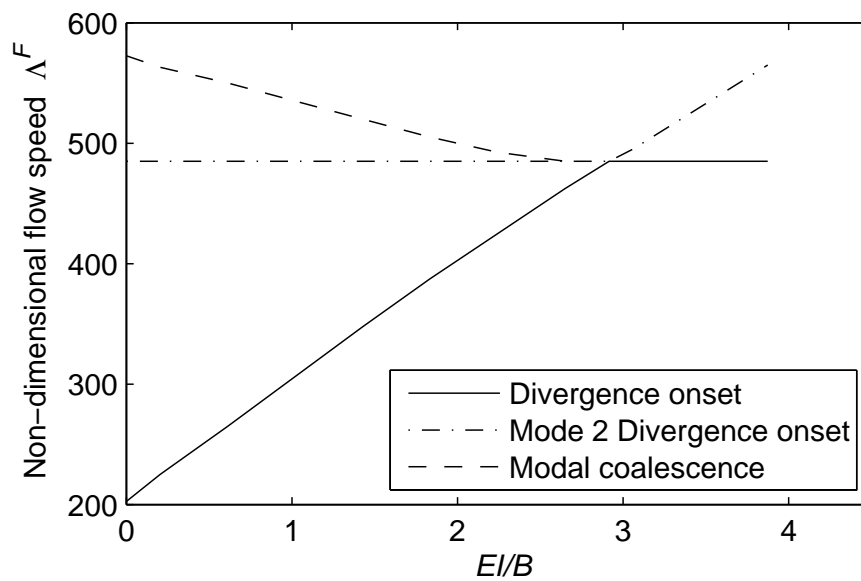


(b)

Figure 3.4: Two-dimensional analysis: the effect of an added support spring on divergence-onset, divergence-recovery / mode-2 divergence-onset, and modal-coalescence flutter-onset flow speeds for (a) high mass ratio = 92.3 (water over aluminum), and (b) low mass ratio = 0.226 (air over glass).



(a)



(b)

Figure 3.5: Three-dimensional analysis: the effect of a transverse stiffening strip at the panel mid-line on divergence-onset, divergence-recovery /mode-2 divergence-onset, and modal-coalescence flutter-onset flow speeds on a panel of aspect ratio unity for (a) high mass ratio = 38.5 (water over aluminum), and (b) low mass ratio = 0.049 (air over aluminum).

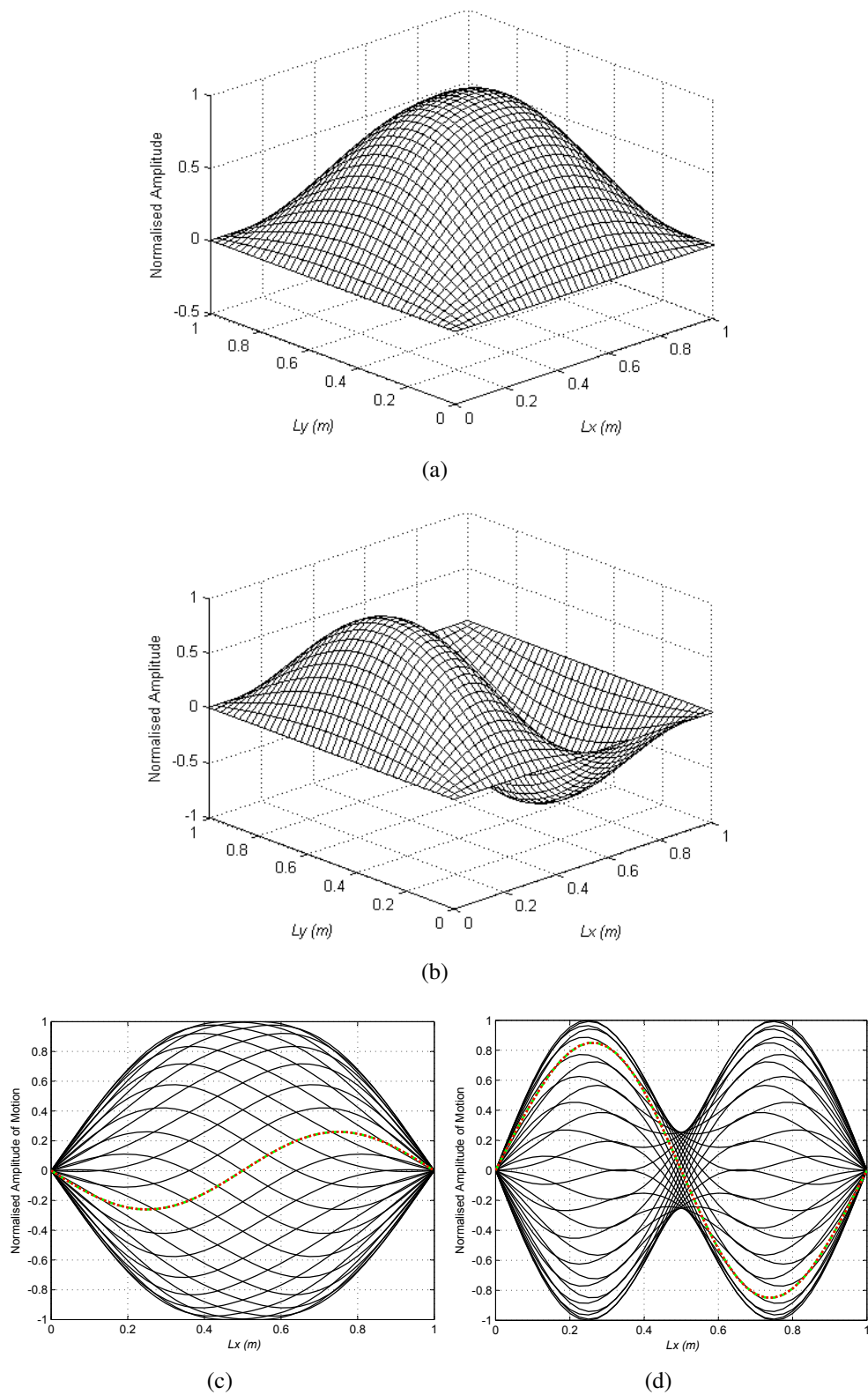
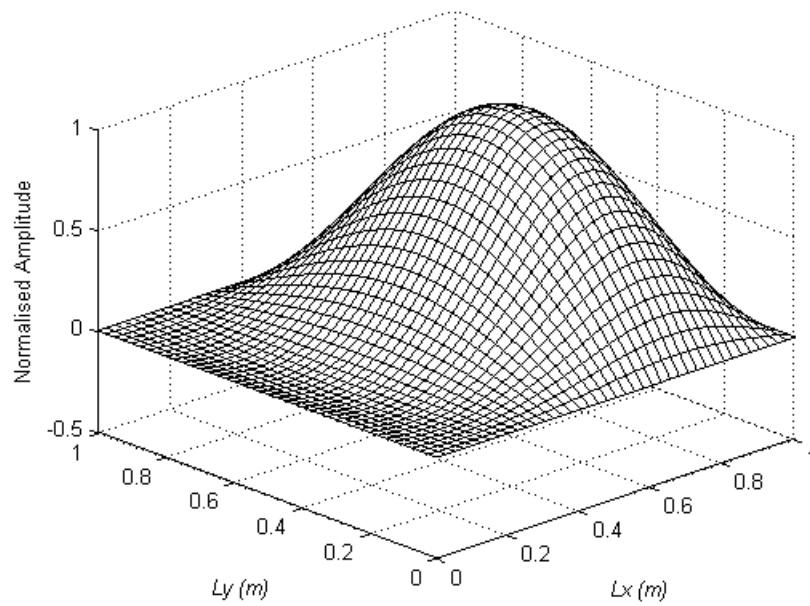
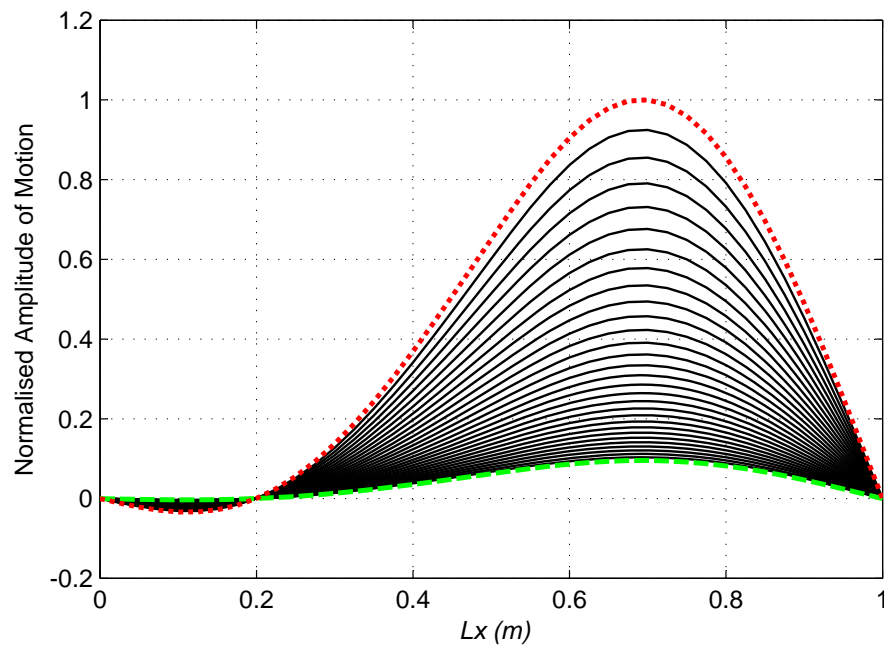


Figure 3.6: Neutrally-stable flexible-panel modes for high mass ratio (38.5) with a stiffening strip ($EI/B = 2$) across its midline at a pre-divergence non-dimensional flow speed, 380: (a) mode 1, (b) mode 2, and (c & d) centreline profiles of modes 1 and 2 over one cycle of oscillation respectively.

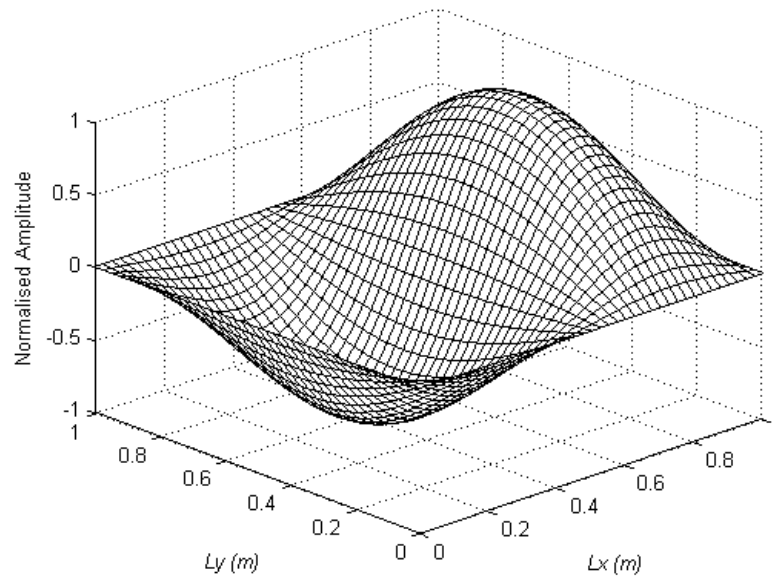


(a)

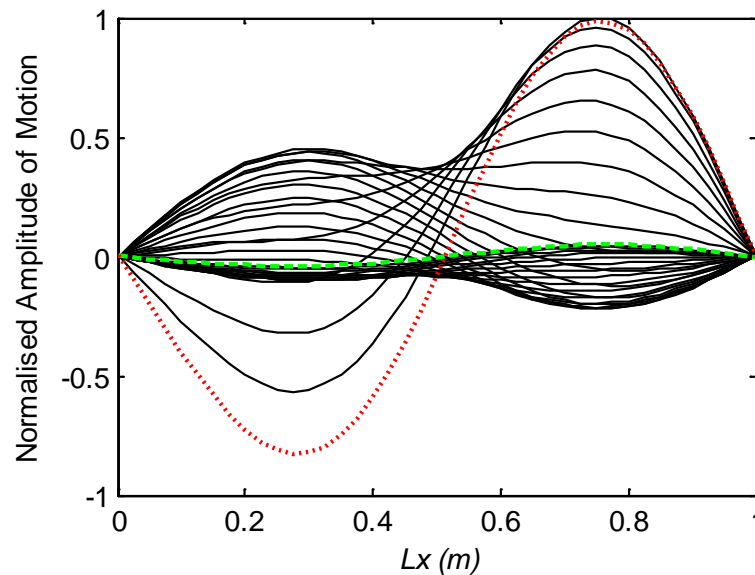


(b)

Figure 3.7: Flexible-panel divergence mode for high mass ratio (38.5) with a stiffening strip ($EI/B = 2$) across its midline at non-dimensional flow speed 450: (a) isometric view, and (b) centreline profiles over a sequence of time-steps from green to red lines.



(a)



(b)

Figure 3.8: Flexible-panel modal-coalescence flutter mode for high mass ratio (38.5) with a stiffening strip ($EI/B = 2$) across its mid-line at non-dimensional flow speed 600: (a) isometric view, and (b) centreline profiles over a sequence of time-steps from green to red lines.

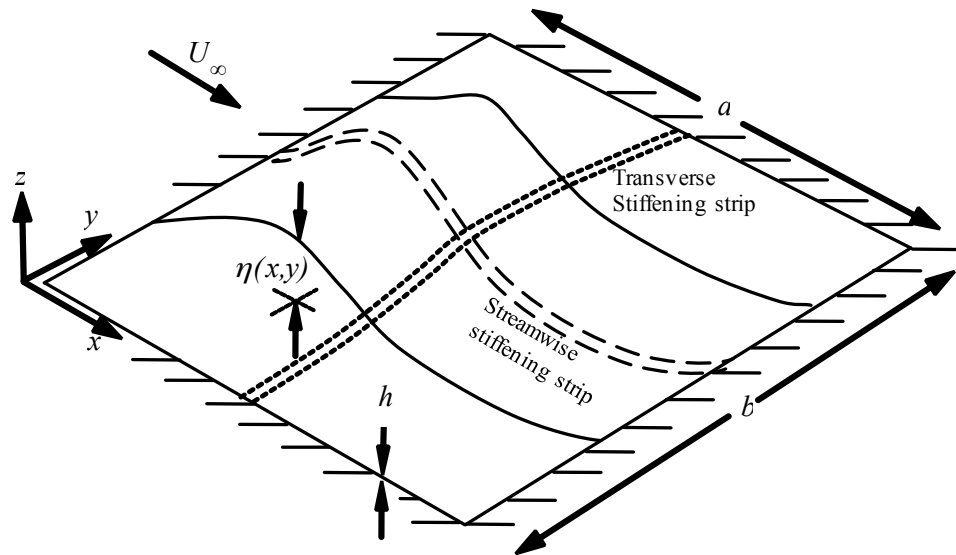


Figure 3.9: Schematic of the problem studied: a fluid-loaded elastic plate has a localised stiffening strip, in either transverse or streamwise direction, bonded to the underside of the panel.

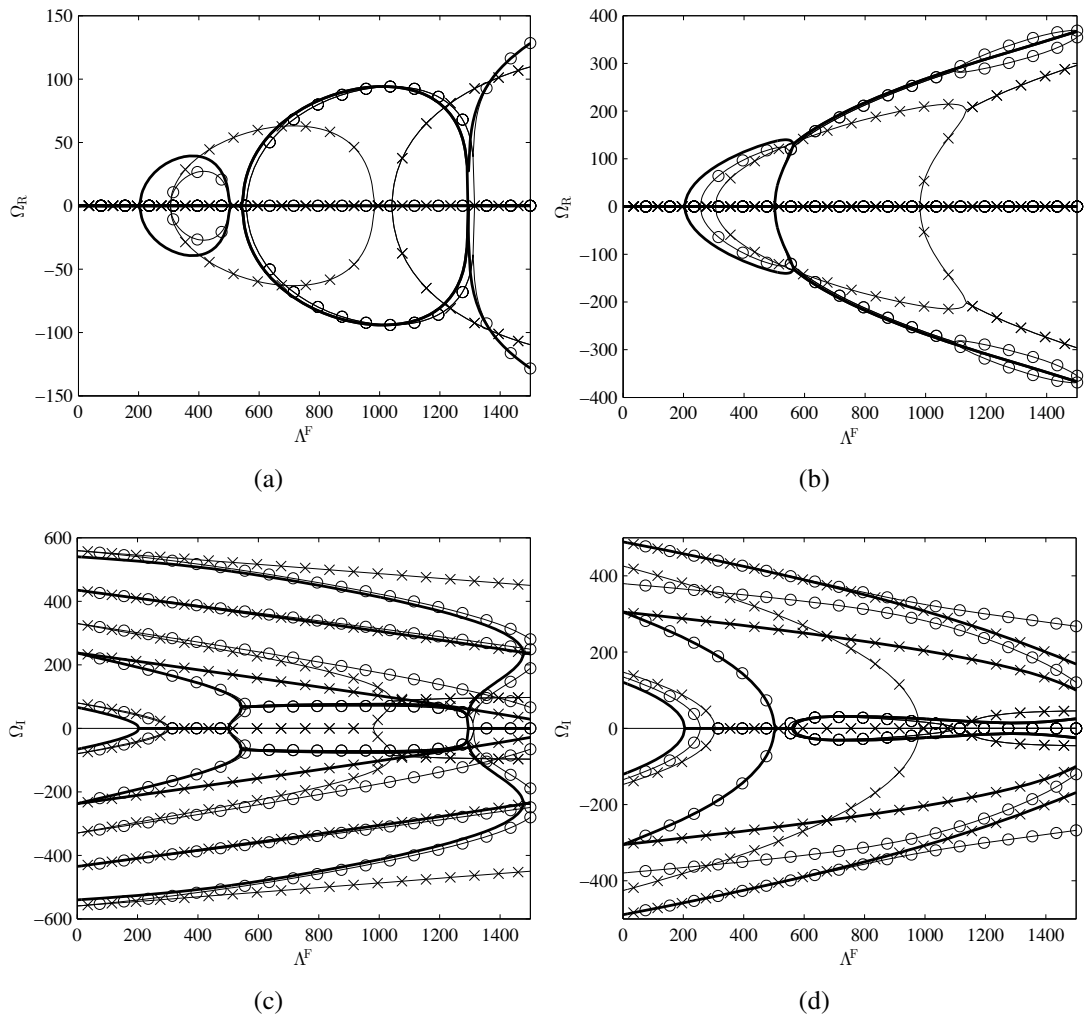


Figure 3.10: Variation of system eigenvalues with non-dimensional flow speed for — (thick) a homogenous panel, and a panel with each of - o - transverse and - x - streamwise stiffening strips included, for (a) high, and (b) low mass ratios, respectively representing water and air flow applications.

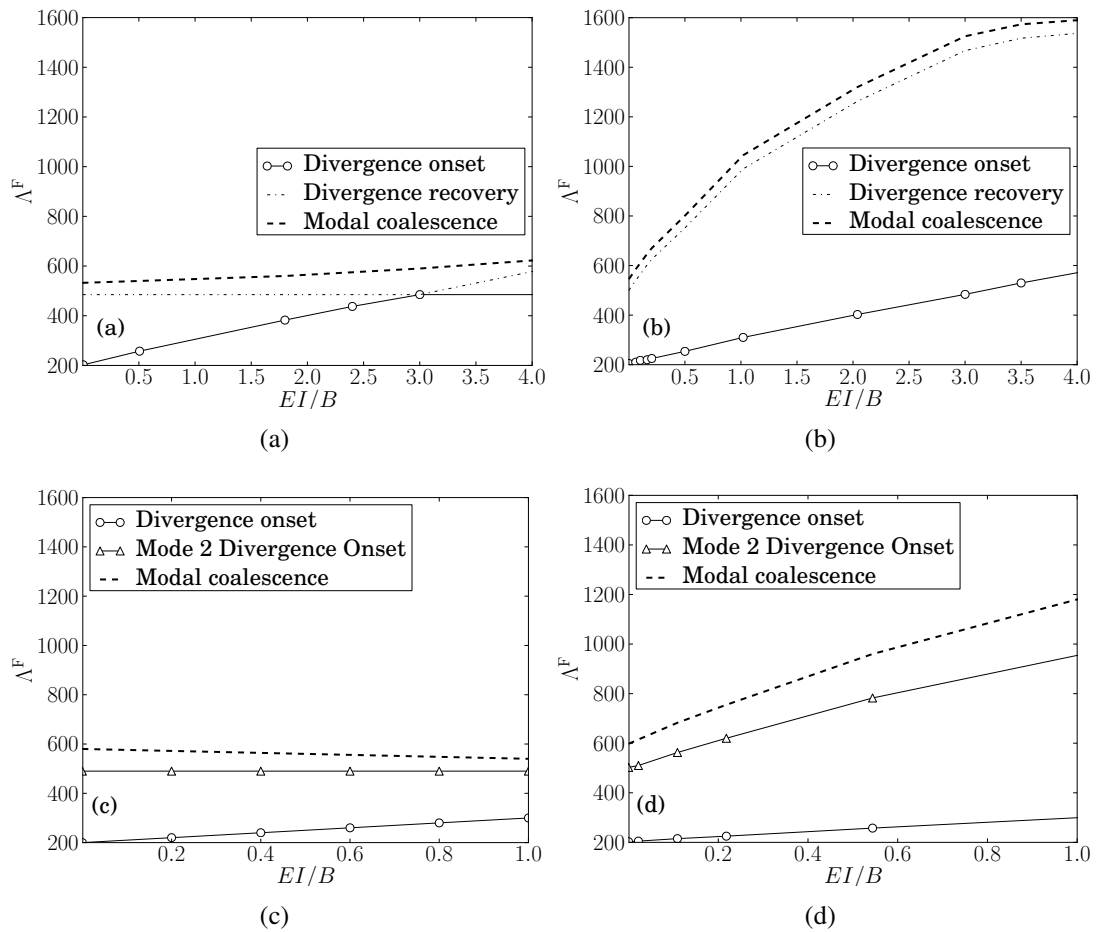


Figure 3.11: Variation of critical speeds with stiffness of (a) and (c) transverse and (b) and (d) streamwise stiffening strips: (a) and (b) for a high mass-ratio system typical of water flow applications and (c) and (d) for a low mass-ratio system typical of air flow applications.

Chapter 4

Optimization by a Multi-objective Genetic Algorithm

Application of a Multi-objective Genetic Algorithm in a Stabilisation Strategy for Flexible Panels in a Mean Flow *3rd Symposium on Fluid-Structure-Sound Interactions and Control*, 5-9 July 2015, Perth, Australia, pp. 195-196.

B.H. Tan, A.D. Lucey & R.M. Howell

Application of a Multi-objective Genetic Algorithm in a Stabilisation Strategy for Flexible Panels in a Mean Flow

B.H. Tan, A.D. Lucey and R.M. Howell

Abstract The stability-control of a fluid-loaded flexible panel has been studied to determine the effectiveness of adding localized stiffening to control or postpone instability. In our previous work for the 2-D system a stabilisation strategy has been demonstrated by localised stiffening with a spring support. Similarly for the 3-D system, the effectiveness of the stabilisation method has also been shown by adding a transverse or streamwise stiffening strip. The most important goal for such stabilisation methods, for both 2-D and 3-D systems, is to refine the localised stiffening strategy to achieve the best use of multiple springs and stiffeners. In this paper we build upon our previous 2-D and 3-D work to develop and apply multi-objective genetic algorithm tools that are able to optimise the stabilisation strategy of added localised stiffness for different design problems: full solution spaces are presented for these problems from which optimal points are readily located.

1 Introduction

This study considers the application of a multi-objective genetic algorithm in the classical aero/hydro-elastic system comprising a flexible panel with a single-side exposed to incompressible uniform flow; linear studies of this system can be found in (Weaver and Unny 1971; Lucey and Carpenter 1993). The fluid-flow is at a high Reynolds number typical of situations encountered in many engineering problems such as the hydrodynamic loading of the hull panels of fast ferries and the strong wind loading on glass/aluminium panels of curtain walls on modern high-rise buildings. In such applications, a design concern is that the panel loses stability at some critical speed due to divergence that can lead to a buckled non-linearly saturated state (Ellen 1977; Lucey et al. 1997) and to dangerous flutter instability at higher flow speeds. Strategies for instability-free design are usually based upon material

B.H. Tan · A.D. Lucey (✉) · R.M. Howell
Fluid Dynamics Research Group, Department of Mechanical Engineering,
Curtin University of Technology, GPO Box U1987, Perth, WA 6845, Australia
e-mail: a.d.lucey@curtin.edu.au

© Springer-Verlag Berlin Heidelberg 2016
Y. Zhou et al. (eds.), *Fluid-Structure-Sound Interactions and Control*,
Lecture Notes in Mechanical Engineering,
DOI 10.1007/978-3-662-48868-3_55

345

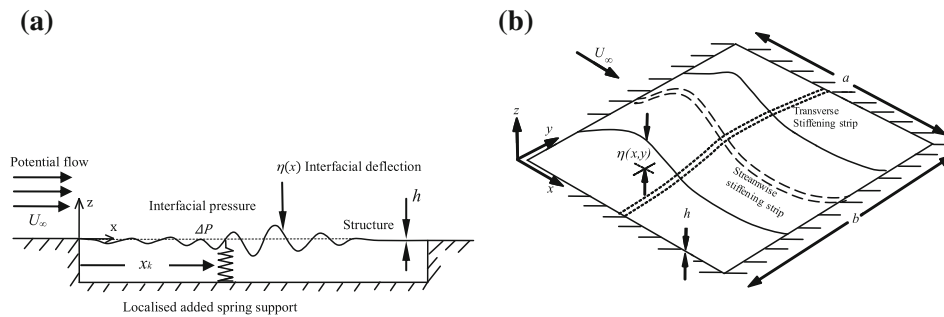


Fig. 1 Schematics of the **a** two-dimensional (*side view*), **b** three-dimensional (*isometric view*) problems studied wherein a uniform flow interacts with a flexible panel that has localised stiffening; in **(a)** a spring support is added while in **(b)** a stiffening strip, that may be in either the transverse or streamwise direction, is bonded to the underside of the panel

selection or uniform thickening of a panel to achieve a higher critical flow speed. However, this increases cost and dead weight. In contrast, our previous 2-D work represented schematically Fig. 1a Tan et al. (2013b), has demonstrated a stabilisation strategy by localised stiffening with a spring support. For the 3-D system of Fig. 1b we have shown in Tan et al. (2013a) the effectiveness of the stabilisation method by adding a transverse or streamwise stiffening strip. The most important goal for such stabilisation methods, for both 2-D and 3-D systems, is to refine the localised stiffening strategy to achieve the best use of multiple springs and stiffeners in that aero-/hydro-elastic instability can be postponed to higher critical speed with least ‘cost’ in terms of added material mass. Clearly, combinations of location, orientation (in 3-D) and spring/strip stiffness of either single or multiple additions creates a complicated parametric space over which optimisation must be conducted. In this paper we develop and apply multi-objective genetic algorithm tools that are able to optimise the stabilisation strategy of added localised stiffness.

2 Overview of Methods

The Fluid-Structure interaction (FSI) system is modelled by fully coupling a finite-difference representation of the structural mechanics with a boundary-element solution for the ideal-flow fluid mechanics. An Euler-Bernoulli beam is used for the 2-D model and classical thin-plate mechanics is used for the 3-D model. Our methods extend the hybrid of theoretical and computational approach of Pitman and Lucey (2009) to conduct an eigen-analysis of the governing wall-flow matrix equation for both 2-D and 3-D systems. Instead of solving the resulting second-order matrix differential equation for the temporal evolution of wall displacements in the coupled system, we use the fact that instability first sets in, with increasing flow speed, at divergence onset. We then use this to define the critical speed for instability in the

optimisation process. The merit of this approach is that at divergence onset, the wall velocity and acceleration are zero and therefore the critical speed can be determined directly from the eigenvalues of the steady system matrix.

The 3-D homogeneous fluid-structure system is controlled by three parameters, namely the fluid-to-solid mass and stiffness ratios, respectively defined by $L' = L_1 L_2$ and $\Lambda^F = Ca L_1^3$, where $L_1 = a/h$, $L_2 = \rho/\rho_m$ and $Ca = \rho U_\infty^2/E^*$ is the Cauchy number where $E^* = E/(12(1 - \nu^2))$; the final control parameter is the aspect ratio of the plate, $A = b/a$. For the plate, the properties a , b and h are respectively the length (in the flow direction), width and thickness of the plate that has density, Young's modulus, Poisson's ratio and flexural rigidity ρ_m , E , ν and $B = E^* h^3$ respectively; the fluid has density ρ and speed U_∞ . In the 2-D case $a = L$ and $A = \infty$. The results presented herein are for water flow over an aluminium panel ($L_2 = 0.4$) typical of that for a thin hull panel of a high-speed ferry, i.e. at high L' . Finally, spring stiffness k is non-dimensionalised as $k'_s = k/E^*$.

The multi-objective genetic algorithm used is a standard function in MATLAB the derivation of which is fully detailed in (Deb 2001). It has a fitness function comprised of two objective functions, $goal(1)$ and $goal(2)$: $goal(1)$ is to search the control parameters to achieve the non-dimensional design critical speed or *design stiffness ratio* Ca_d ; $goal(2)$ minimises the weight of the added stiffening component(s) that is equivalent to minimising stiffness k of the spring or stiffening strip as these are assumed proportional to weight. The aim is to find the minimum of $goal(1)$ and $goal(2)$: $goal(1) = 0$ when the algorithm has searched for $goal(2)$ successfully.

3 Results and Discussion

To demonstrate the integrity and implementation of the genetic algorithm approach, Fig. 2a, b respectively show typical results for the effect on Ca —the quantity on the vertical axis—of different stiffening strategies that have been validated against previous known results.

The result in Fig. 2a is for a 2-D case that shows the effect on Ca of adding an isolated spring: the horizontal axis on the left-hand side are values of k'_s and the right-hand side axis details the location x/L of the spring along the plate. Selecting individual results from this graph at specific values of Ca_d allow comparisons with previous results in Tan et al. (2013b): good agreement is found and thus confirms that the multi-objective genetic algorithm correctly minimises $goal(1)$ and $goal(2)$. As in Tan et al. (2013b), the results herein show that the maximum effectiveness of stiffening occurs at the panels' mid-chord because this location is the anti-node of the fundamental mode that yields the critical mode for divergence-onset of such panels.

The result in Fig. 2b is for a 3-D case that shows the effect on Ca of adding a streamwise stiffening strip for $A = 1$: the system is structurally inhomogeneous and the horizontal axis on the left-hand side is the stiffness of the added strip described

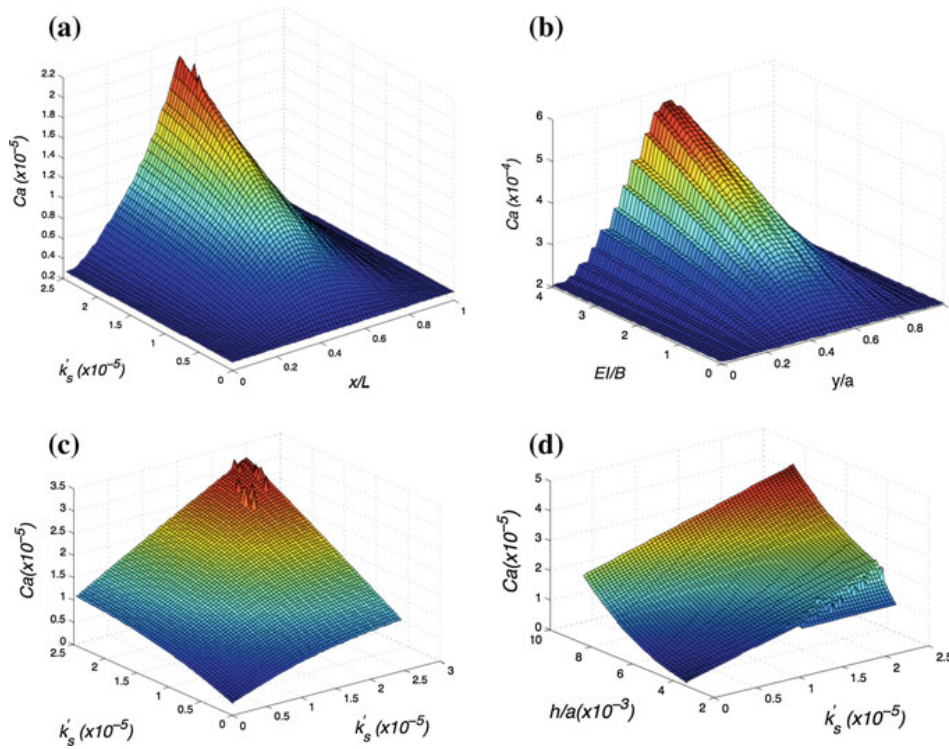


Fig. 2 Variation of a flexible panel's Ca value at $L_2 = 0.4$ with the magnitude and location of added localised stiffening for **a** 2-D model with an isolated spring, **b** 3-D model with a streamwise stiffening strip, **c** 2-D model with an upstream spring located at $L/3$ and a downstream spring located at $2L/3$ and **d** 2-D model with an isolated spring and variable panel thickness. The colours on the surface are proportional to the magnitude on the y -axis that they relate to, *blue* being the lowest y value and *red* the highest

relative to the flexural rigidity of the plate, i.e. EI/B ; the right-hand side axis is the transverse position y/a of the strip. Selecting individual results from this figure at specific values of Ca_d again show good agreement with the values in Tan et al. (2013a), where the maximum effectiveness of stiffening occurs at the panel's mid-width.

We now show how the multi-objective genetic algorithm can be used for two more advanced 2-D problems. First, the optimal weight at fixed locations of two springs for a specified Ca_d is analysed: the control variables are the spring stiffnesses $k(1)$ and $k(2)$ and these are plotted on the horizontal axes in Fig. 2c. When individual results are compared to the single-spring support at mid point in Tan et al. (2013b), the two spring supports are not as effective as the single spring support at mid point: for example at Ca_d values of 0.88×10^{-5} and 1.71×10^{-5} , the increase in spring weight is 31 and 25 % respectively to achieve the same effectiveness as a single spring.

Second, the optimal weight of one spring located at the mid-point of a variable thickness panel for a specified Ca_d is analysed. The control variables are the spring

stiffness k'_s and the panel thickness h and these are plotted on the horizontal axes in Fig. 2d. The graph clearly shows that as h and k'_s are increased, the system stabilises. Also, considerable weight savings are found by using a thinner panel with a spring whilst maintaining the same divergence-onset flow speed $Ca_d = 3 \times 10^{-6}$. For example, if a 2.5 mm plate is replaced by a 2.2 mm plate, the spring stiffness required is $k'_s = 0.86 \times 10^{-5}$: this corresponds to an overall (plate plus springs) weight reduction of 11.81 %.

4 Conclusions

A hybrid of computational and theoretical methods has been developed to form a structural function where divergence-onset stiffness ratio is a function of localised stiffening arrangement. Two problems have been analysed for illustration and design criteria are optimised by the application of a multi-objective genetic algorithm. The optimisation yields a configuration such that the divergence-onset stiffness ratio meets the design requirement as well as minimising the total weight of added spring or stiffening strips.

However, the cases presented herein could have been studied without the use of the GA albeit at much greater computational expense. The optimisation methods developed will confer an even greater advantage for complex multi-stiffener configurations.

References

- Deb, K. 2001 Multi-Objective Optimization Using Evolutionary Algorithms. (John Wiley & Sons, first edition)
- Ellen CH (1977) The non-linear stability of panels in incompressible flow. *Journal of Sound and Vibration* 54:117–121
- Lucey AD, Cafolla GJ, Carpenter PW, Yang M (1997) The nonlinear hydroelastic behaviour of flexible walls. *Journal of Fluids and Structures* 11:717–744
- Lucey AD, Carpenter PW (1993) The hydroelastic stability of three dimensional disturbances of a finite compliant wall. *Journal of Sound and Vibration* 165:527–552
- Pitman MW, Lucey AD (2009) On the direct determination of the eigenmodes of finite flow-structure system. *Proceedings of the Royal Society A* 465:257–281
- Tan BH, Lucey AD, Howell RM (2013a) The effect of localised stiffening on the stability of a flexible panel in uniform flow. 2nd Symposium on Fluid-Structure-Sound Interactions and Control, 20th-23rd May 2013, Hong Kong & Macau, pp. 325–330
- Tan BH, Lucey AD, Howell RM (2013b) Aero-/hydro-elastic stability of flexible panels: Prediction and control using localised spring support. *Journal of Sound and Vibration* 332:7033–7054
- Weaver DS, Unny TS (1971) The hydroelastic stability of a flat plate. *ASME. Journal of Applied Mechanics* 37:823–827

Chapter 5

Conclusions and recommendations for further work

5.1 Conclusions

By using a hybrid of theoretical and computational methods, we have solved 2-dimensional flexible panel problem and 3-dimensional flexible panel problem. Furthermore, combining the hybrid method with Genetic algorithm, we also have solved optimization problems. The hybrid method has been developed and deployed to compare and contrast the effectiveness of transverse and streamwise stiffening strip for the control of hydro- and aero-elastic instabilities of an otherwise homogeneous elastic panel.

The ideal flow model is used throughout this thesis to test the improvement of 2-D model, 3-D model and Genetic algorithm. Actually, in real flow, there has boundary layer affected the flow pattern. It hence therein produces the skin resistance due to viscosity and non-slip boundary.

5.2 Recommendations for further work

A hybrid of theoretical and computational methods has been used in the thesis to solve fluid-flow panel interaction. Replacement of 2-D model and 3-D model and Genetic algorithm with real flow model is investigated the effect of viscosity. From the works of this thesis, there have several possible studies into fluid-flow panel interaction.

The application of a multi-objective genetic algorithm on a flexible panel stability in a mean flow has good and reasonable result. In the future, different configurations and stiffening arrangements will be tested. At the same time, it explores the optimisation of different structural functions.

References

- [1] Dugundji, J., Dowell, E. & Perkin, B., Subsonic flutter of panels on a continuous elastic foundation. *AIAA Journal* **1**, pp. 1146-1154, 1963.
- [2] Weaver, D.S. & Unny, T.S., The hydroelastic stability of a flat plate. *ASME: Journal of Applied Mechanics* **37**, pp. 823-827, 1971.
- [3] Ellen, C.H., The stability of simply supported rectangular surfaces in uniform subsonic flow. *ASME: Journal of Applied Mechanics* **95**, pp. 68-72, 1973.
- [4] Lucey, A.D. & Carpenter, P.W., The hydroelastic stability of three-dimensional disturbances of a finite compliant panel. *Journal of Sound and Vibration* **165**, pp.527-552, 1993.
- [5] Guo, C. Q. & Paidoussis, M. P., Stability of rectangular plates with free side-edges in two-dimensional inviscid channel flow. *Journal of Applied Mechanics* **67**, pp. 171-176, 2000.
- [6] Benjamin, T.B., The threefold classification of unstable disturbances in flexible surfaces bounding inviscid flows. *Journal of Fluid Mechanics* **16**, pp. 436-450, 1963.
- [7] Carpenter, P.W. & Garrad A.D., The hydrodynamic stability of flows over Kramer-type compliant surfaces. Part 2. Flow-induced surface instabilities. *Journal of Fluid Mechanics* **170**, pp. 199-232, 1986.
- [8] Lucey, A.D. & Carpenter, P.W., On the difference between the hydroelastic instability of infinite and very long compliant panels. *Journal of Sound and Vibration* **163**(1), pp. 176-181, 1993.
- [9] Peake, N., On the unsteady motion of a long fluid-loaded elastic plate with mean flow. *Journal of Fluid Mechanics* **507**, pp. 335-366, 2004.

- [10] Brazier-Smith, P.R. & Scott, J.F., Stability of fluid flow in the presence of a compliant surface. *Wave Motion* **6**, pp. 436-450, 1984.
- [11] Crighton, D.G. & Oswell, J.E., Fluid loading with mean flow. I. Response of an elastic plate to localized excitation. *Philosophical Transactions of the Royal Society of London A* **335**, pp. 557-592, 1991.
- [12] Peake, N., On the behaviour of a fluid-loaded cylindrical shell with mean flow. *Journal of Fluid Mechanics* **338**, pp. 387-410, 1997.
- [13] Abrahams, I.D. & Wickham, G.R., On transient oscillations of plates in moving fluids. *Wave Motion* **33**, pp. 7-23, 2001.
- [14] Lucey, A.D., The excitation of waves on a flexible panel in a uniform flow. *Philosophical Transactions of the Royal Society of London A* **356**, pp. 2999-3039, 1998.
- [15] Pitman, M.W. & Lucey, A.D., On the direct determination of the eigenmodes of finite flow-structure systems. *Proceedings of the Royal Society A* **465**, pp. 257-281, 2009.
- [16] Lucey, A.D. & Carpenter, P.W., A numerical simulation of the interaction of a compliant wall and inviscid flow. *Journal of Fluid Mechanics* **234**, pp. 121-146, 1992.
- [17] Lucey, A.D., Cafolla, G.J., Carpenter, P.W. & Yang, M., The nonlinear hydroelastic behaviour of flexible walls. *Journal of Fluids and Structures* **11**, pp. 717-744, 1997.
- [18] Garrad, A.D. & Carpenter, P.W., A theoretical investigation of flow-induced instabilities in compliant coatings. *Journal of Sound and Vibration* **84**(4), pp. 483-500, 1982.

- [19] Lucey, A.D., Sen, P.K. & Carpenter, P.W., Excitation and evolution of waves on an inhomogeneous flexible wall in a mean flow. *Journal of Fluids and Structures* **18**, pp. 251-267, 2003.
- [20] Carpenter, P.W. & Garrad A.D., The hydrodynamic stability of flows over Kramer-type compliant surfaces. Part 1. Flow instabilities. *Journal of Fluid Mechanics* **155**, pp. 465-510, 1985.
- [21] Landahl, M.T., On the stability of a laminar incompressible boundary-layer over a flexible surface. *Journal of Fluid Mechanics* **13**, pp. 609-632, 1962.
- [22] Huerre, P. & Monkewitz, P.A., Local and global instabilities in spatially developing flows. *Annual Review of Fluid Mechanics* **22**(1), pp. 473-537, 1990.
- [23] Lucey, A.D. & Peake, N., Wave excitation on flexible walls in the presence of a fluid flow. In *IUTAM: Flow through collapsible tubes and past other highly compliant boundaries* (eds. P.W. Carpenter & T.J. Pedley), Kluwer Academic Publishers, pp. 118-145, 2003.
- [24] Ishii, T., Aeroelastic instabilities of simply supported panels in subsonic flow. *Meeting of the American Institute of Aeronautics and Astronautics, Los Angeles* Paper AIAA-65-752, 1965.
- [25] Doaré, O. & De Langre, E., Local and global instability of fluid-conveying pipes on elastic foundations. *Journal of Fluids and Structures* **16**(1), pp. 1-14, 2002.
- [26] Ellen, C.H., The non-linear stability of panels in incompressible flow. *Journal of Sound and Vibration* **54**(1), pp. 117-121, 1977.
- [27] Tan, B.H., Lucey, A.D. & Pitman, M.W., Stability of a structurally inhomogeneous flexible plate in uniform axial flow. In *Proc. of the 10th International Conference on Flow Induced Vibration & Flow-Induced Noise* (eds. C. Meskell & G. Bennett), pp. 203-210, 2012.

- [28] Peake, N., Nonlinear stability of a fluid-loaded elastic plate with mean flow. *Journal of Fluid Mechanics* **434**, pp. 101-118, 2001.
- [29] Reynolds, R.R. & Dowell, E.H., Nonlinear aeroelastic response of panels. *Collection of Technical Papers – AIAA/ASME Structures, Structural Dynamics and Materials Conference Part 5*, pp. 2566-2576, 1993.
- [30] Pitman, M. W. & Lucey, A. D., Linear dynamics of the flow-structure interaction of compliant walls having complex boundary conditions. In *FIV2008, Jun 30, 2008, Prague, Czech Republic: Institute of Thermomechanics, Academy of Sciences of the Czech Republic*.
- [31] Pitman, M. W. & Lucey, A. D., The hydro-elastic behaviour of flexible panels with inhomogeneous material properties and added restraints. *International Conference on Innovation in High Speed Marine Vessels, Jan 28 2009, pp. 113-120. Fremantle, Australia: The Royal Institution of Naval Architects*.
- [32] Tan, B.H., Lucey, A.D. & Pitman, M.W., Hydroelastic stability of flexible panel: eigen-analysis and time- domain response. In: *Proceedings of ASME 2010 3rd Joint US - European Fluids Engineering Summer Meeting*, 1-5 August 2010, Montreal, Canada, Paper no. FEDSM-ICNMM2010-30057.
- [33] Tan, B.H., Lucey, A.D. & Pitman, M.W., Controlling hydroelastic instability of hull panels through structural inhomogeneity. In: *RINA, Royal Institution of Naval Architects - International Conference, High Speed Marine Vessels*, 2-3 March 2011, Fremantle, pp. 51-60.
- [34] Tan, B.H., Lucey, A.D. & Pitman, M.W., Controlling aero-elastic instability of curtain wall systems in high-rise buildings. In: *MODSIM2011, 19th International Congress on Modelling and Simulation*. Modelling and Simulation Society of Australia and New Zealand, December 2011, (Eds. F. Chan, D. Marinova & R.S. Anderssen), pp. 601-607.

- [35] Hess, J.L. & Smith, A.M.O., Calculation of potential flow about arbitrary bodies. Vol. 8 of *Progr. Aeronaut. Sci.*, Pergamon Press, New York pp1-138, 1966.
- [36] Lucey, A.D. & Carpenter, P.W., A study of the hydroelastic stability of a compliant panel using numerical methods. *International Journal of Numerical Methods for Heat and Fluid Flow* **2**, pp. 537-553, 1992.
- [37] Howell, R.M., Lucey, A.D. & Pitman M.W., The effect of inertial inhomogeneity on the flutter of a cantilevered flexible plate. *Journal of Fluids and Structures* **27**(3), pp. 383-393, 1992.
- [38] Tan, B.H., Lucey, A.D. & Pitman M.W., The effect of localised stiffening on the stability of a flexible panel in uniform flow. 2nd Symposium on Fluid-Structure-Sound Interactions and Control, 20th-23rd May 2013, Hong Kong & Macau, pp. 86-87.

Every reasonable effort has been made to acknowledge the owners of copyright material. The author would be pleased to hear from any copyright owner who has been omitted or incorrectly acknowledged.

Appendix A

Statements of Contributions of Others

Statements of Contributions of Others for the following papers

Date: _____

To Whom It May Concern

I, Professor A.D. Lucey, contributed by providing overall project supervision and technical advice and manuscript editing to the following papers/publications entitled

Tan, B.H., Lucey, A.D. and Howell, R.M. 2013. Aero-/hydro-elastic stability of flexible panels: Prediction and control using localised spring support. *Journal of Sound and Vibration*, Vol.332(26), pp.7033-7054.

Tan, B.H., Lucey, A.D. and Howell, R.M. 2015. Application of a multi-objective genetic algorithm in a stabilisation strategy for flexible panels in a mean flow. In: *3rd Symposium on Fluid-Structure-Sound Interactions and Control*, 5-9 July 2015, Perth, Australia, pp. 195-196.

Undertaken with Ben Hoes Tan

Signature of Co-Author

A.D. Lucey

Signature of First Author

Ben Hoes Tan

Statements of Contributions of Others for the following papers

Date: _____

To Whom It May Concern

I, Dr. R.M. Howell, contributed by providing technical advice and manuscript editing to the following papers/publications entitled

Tan, B.H., Lucey, A.D. and Howell, R.M. 2013. Aero-/hydro-elastic stability of flexible panels: Prediction and control using localised spring support. *Journal of Sound and Vibration*, Vol.332(26), pp.7033-7054.

Tan, B.H., Lucey, A.D. and Howell, R.M. 2015. Application of a multi-objective genetic algorithm in a stabilisation strategy for flexible panels in a mean flow. In: *3rd Symposium on Fluid-Structure-Sound Interactions and Control*, 5-9 July 2015, Perth, Australia, pp. 195-196.

Undertaken with Ben Hoes Tan

Signature of Co-Author

R.M. Howell

Signature of First Author

Ben Hoes Tan